Theses and Dissertations

5-2018

Fabrication and Characterization of Graphene based 2D Materials for Supercapacitors

Anishkumar Manoharan
University of Arkansas, Fayetteville

Follow this and additional works at: http://scholarworks.uark.edu/etd

Part of the Electrical and Electronics Commons, Metallurgy Commons, and the Power and Energy Commons

Fabrication and Characterization of Graphene based 2D Materials for Supercapacitors

A dissertation submitted in partial fulfillment
of the requirements for the degree of
Doctor of Philosophy in Engineering with a concentration in Electrical Engineering

by

Anishkumar Manoharan
University of Arkansas
Master of Science in Microelectronics-Photonics, 2011

May 2018
University of Arkansas

This dissertation is approved for recommendation to the Graduate Council.

_____
Simon S. Ang, PhD
Dissertation Director

_____
Z. Ryan Tian, PhD
Co-Dissertation Director

_____
Shui-Qing Yu, PhD
Committee Member

_____
Juan Carlos Balda, PhD
Committee Member

Abstract

Supercapacitors have attracted a lot attention due to their efficient energy storage. In comparison to batteries, supercapacitors have high capacitance, energy, and power densities per unit mass than conventional capacitors. Carbon based materials are most promising in supercapacitor application due to their outstanding physical and electrochemical behavior. In this work, a facile method to synthesize a nanocomposite electrode consisting of annealed carbon from carbon ink and MoS_2 was demonstrated. Effects of various aqueous and solid electrolytes were studied. It was found that the nanocomposite electrode with 10% MoS_2 and 1M Na_2SO_4 as the aqueous electrolyte tested using the three electrode method exhibited a capacitance of 207.5 F/g at a current density of 0.5 A/g. However, with the influence of K^+ ions, the 10% MoS_2 nanocomposite electrode based electric double layer (EDL) capacitor displayed a comparatively higher capacitance of 10.1 F/g at a current density of 1 A/g with 0.5 M K_2SO_4 as the aqueous electrolyte. The button cell EDL capacitor performance was further improved up to 50% using 1 M Na_2SO_4 aqueous electrolyte (15.2 F/g at a current density of 1 A/g) in comparison to using 0.5 M Na_2SO_4 aqueous electrolyte (4 F/g at a current density of 1 A/g). Pouch cell supercapacitors were fabricated using both aqueous and solid electrolytes which had almost similar overall performance. A MoS_2/annealed carbon nanocomposite based supercapacitor with solid electrolyte which possesses capacitance and energy density of 10.6 F/g and 5.9 Wh/Kg, respectively, was demonstrated. A cylindrical cell supercapacitor was fabricated using 1M Na_2SO_4 as the aqueous electrolyte and yielded capacitance and energy density of 6.7 F/g and 4.9 Wh/Kg, respectively, at a current density of 1 A/g.

Dedication

I dedicate this dissertation to my Father Dr. N. Manoharan and to rest of my Family members.

Table of Contents

List of Figures

List of Tables

Abbreviations

SOHIO	Standard oil company Cleveland Ohio
EDLC	Electric double layer capacitor
NEC	Nippon electric company
LIB	Lithium ion battery
CV	Cyclic voltammetry
ESR	Equivalent series resistance
SWCNT	Single walled carbon nanotube
HOPG	Highly ordered pyrolytic graphite
CVD	Chemical vapor deposition
GO	Graphene oxide
FTIR	Fourier transform infrared spectroscopy
AC	Activated carbon
2-D	Two dimensional
TMDC	Transition metal dichalcogenides
MoS_2	Molybdenum disulfide
NMP	N-methylpyrrolidinone
EIS	Electrochemical impedance spectroscopy
rGO	Reduced graphene oxide
AAO	Anodic aluminum oxide
SEM	Scanning electron microscopy
XRD	X-ray diffraction
MRG	Molybdenum disulfide/ reduced graphene oxide
HER	Hydrogen evolution reaction
MCG	Molybdenum disulfide/Annealed carbon
CCD	Cyclic charge-discharge

1. Chapter 1: Motivation and Objectives

1.1 Motivation

An increase in demand for fossil fuels had resulted due to consumption of energy worldwide with an ever increasing global population [1]. The primary sources of fossil fuels is predicted to deplete in many countries due to continuous emission of greenhouse gases, water and air pollution that cause environmental degradation and pose a threat to human life. So, For continuous usage of uninterrupted electricity, reliable and efficient energy storage systems are necessary [2]. Since the 21st century, a deep interest in renewable energy sources such as hydropower, geothermal, wind and solar energy has acquired a great interest that helps in fossil resource conservation, limiting CO_2 emission and increasing the energy efficiency [3]. Consumption of these energy resources has doubled during the years 2000 to 2016 mainly because of the incentives they provide [4] But, propitious renewable resources are mainly located only at remote areas, and so building power lines that extend till the cities become expensive. Renewable energy resources if available in a concentrated form can be easily stored and transported. To address these issues, developing cutting edge renewable energy storage devices that are scalable, cheap, and environment friendly will help in far reaching benefits with promising solutions [5]. In this regard, supercapacitor is considered one of the futuristic energy storage devices because of their long cycle life, high power density, and with the capability of achieving high energy densities.

1.2 Objectives

The main objectives of this dissertation are categorized into four main parts which are as follows:

a. Develop a 2-D nanocomposite based supercapacitor by integrating molybdenum disulfide along with reduced graphene oxide for boosting the energy density.

b. Synthesize a novel molybdenum disulfide/carbon nanocomposite electrode using a simple process that will be cheap without compromising performance.

c. Explore the effects of various electrolyte solutions that help in enhancing the performance even further by using the high performance nanocomposites.

d. Fabricate flexible supercapacitors with the formulated high performance nanocomposite and electrolyte solution.

1.3 Outline of Dissertation

Chapter 2 provides a brief overview on the background about batteries and the classifications of capacitors and supercapacitors. The basic concepts of different electrochemical characterization techniques are explained in-depth followed by explanation on the theoretical concepts of supercapacitor parameters that were used for evaluating the performance of supercapacitor.

Chapter 3 provides literature review on different types of nanomaterials that are used for fabricating supercapacitors in our work. These basic insights provide information on how these materials began to evolve as a potential candidate for energy storage applications followed by current trends and techniques that are used to synthesize them. Three different research articles are discussed in brief which are in close association with our major work.

Chapter 4 begins with of our initial work on synthesis molybdenum disulfide/ reduced graphene oxide for use in electrochemical double layer capacitor. The results and discussion part show the physical characterization of the nano-material using SEM and XRD. The electrochemical characterization of the materials was done to evaluate the performance of the supercapacitor in terms of capacitance, energy and power density.

Chapter 5 continues with our further approach in synthesis of nano-composite material using molybdenum disulfide/ annealed carbon. Physical and electrochemical performances of different combinations of materials were evaluated using a three electrode setup. The high performance nano-composite material was then assembled in a button cell and tested with different electrolyte solutions. At the end of the work, high performance electrode material and electrolyte solution were identified.

Chapter 6 deals with different types of flexible supercapacitors ranging from aqueous electrolyte, solid electrolyte, and cylindrical cell based supercapacitors. The aqueous electrolyte based supercapacitors were assembled in a pouch cell with the high performance nano-composite material and electrolyte solution using flexible stainless steel current collectors. The solid electrolyte based supercapacitors were also assembled and tested with the high performance nanocomposite. Finally, the cylindrical supercapacitor was assembled using a 12 inch stainless steel current collector and successfully tested for its performance.

Chapter 7 concludes the dissertation research and highlights the major contributions. Suggestions for future work are also listed.

1.4 References

1.1 Chenyang Zhao, Xu Wang, Junhua Kong, Jia Ming Ang, Pooi See Lee, Zhaolin Liu, Xuehong Lu, "Self-Assembly-Induced Alternately Stacked Single-Layer MoS_2 and N-doped Graphene: A Novel van der Waals Heterostructure for Lithium-Ion Batteries", ACS. Appl. Mater. Interfaces, 8 (3), 2372 (2016).

1.2 Su Y, Zhitomirsky I, "Electrophoretic nanotechnology of composite electrodes for electrochemical supercapacitors", The Journal of Physical Chemistry B, 117, 1563-70 (2012).

1.3 Christian Martin, "Driving change in the battery industry", Nature Nanotechnology 9, 327-328 (2014).

1.4 https://www.eia.gov/energyexplained/?page=renewable_home

1.5 Meirong Wang, Huaihao Zhang, Chengyin Wang, Xiaoya Hu, Guoxiu Wang, "Direct electrosynthesis of poly-*o*-phenylenediamine bulk materials for supercapacitor application", Electrochimica. Acta., 91, 144 (2013).

2. Chapter 2: Background

2.1 Batteries

Although the device is termed as "battery", it is often a basic electrochemical cell unit consisting of electrochemical cells connected in parallel or series or both providing the required potential and current [2.1]. Gaston Plante was the first person to invent secondary lead acid battery in 1859 [2.2]. In battery, electrical energy is directly converted into chemical energy by means of electrochemical reaction called redox (reduction-oxidation) process [2.3]. An important parameter for the battery is the standard potential E^o of a battery cell, which is in association with redox reactions can be calculated using the formula:

$$E° = \frac{-\Delta G°}{zF} \tag{2.1}$$

F is the Faraday constant, ΔG^o, and z is the number of electrons is the standard Gibbs free energy. The overall theoretical cell voltage can be obtained by subtracting the positive electrode potential $E^{o(+)}$ and the negative electrode potential $E^{o(-)}$:

$$\Delta E° = E^{o(+)} - E^{o(-)} \tag{2.2}$$

For several decades, batteries have been more prevalent in portable electronics applications due to their capability of storing high energy density [2.4]. But it takes a long time to charge and discharge resulting in degradation of chemical compounds present inside the battery. In addition to the material damage, the ability to deliver power is also limited. Overcoming this problem has been very difficult even in technologies like lithium ion and lead-acid batteries which have limiting isolated power generation and the short lifespan [2.5, 2.6]. Because of these shortcomings, various research works are being proposed for hybridization of batteries along

5

with supercapacitor to attain a better performance. Battery chemistries in association with sodium-ions are turning out to be promising for future renewable applications but still face certain technical limitations.

2.2 Classification of classic capacitors

Based on the choice of electrode and electrolyte, capacitors are divided into three major categories. They are further classified into a few subgroups depending on specific kinds of materials used as electrodes and electrolytes.

2.2.1 Electrostatic capacitors

In an electrostatic capacitor, energy is stored electrostatically under an electric field using two passive electrical plates. These kinds of capacitors typically have electric conductors (aluminum or copper) that are separated by an insulator (mica, paper, air, glass, ceramic or polymer film). They can be operated at very high voltages for a lifetime and their volumetric and gravimetric energy densities are on the order of 2mWh/L and 1.5mWh/Kg, respectively.

2.2.2 Electrolytic capacitors

In contrast to usage of bulk insulators in conventional electrostatic capacitors, thin metal oxide layers are used as dielectric in electrolytic capacitors. For example, in an aluminum electrolytic capacitor, a thin layer of aluminum oxide gets formed on the aluminum sheet surface acting as a dielectric which helps in improving the capacitance values even higher. Sodium borate or boric acid mixed with aqueous solutions is typically used as electrolyte solutions. The potential of electrolytic capacitors are comparatively lower than that of electrostatic capacitors, but their volumetric energy density (120mWh/L) and gravimetric energy density (30mWh/kg) are higher due to the high capacitance values they possess.

2.3   Supercapacitor

2.3.1 History of Supercapacitor

With the term coined as "supercapacitors", these devices can store energy higher than the

capacity of conventional capacitors and high amount of power than the conventional batteries.

Due to the reason that it is a relatively new storage device, supercapacitor necessitates a small

historical introduction. In the year 1957, high capacity electrochemical capacitor was patented

(US Patent 2800616) [2.7]. Later, Howard Becker of General Electric Company developed a

basic construction of the device that consisted of porous carbon electrodes [2.8]. "Becker was

able to describe the large capacitive phenomena of the device but was not able to explain the

reason behind the exceptionally large capacitance value that was being obtained. Consequently, a

double layer capacitor was introduced by Robert Rightmire of Standard Oil Company Cleveland

Ohio (SOHIO) utilizing porous carbon with non-aqueous electrolyte in the year 1966 (US Patent

3288641). After four years, another employee of SOHIO, carbon paste soaked in an electrolyte

(US Patent 3536963) based device was patented by Donald Boos which was the first company to

manufacture high capacitance devices. Conway performed extensive research in the area of

electric double layer capacitor (EDLC) and ruthenium oxide type electrochemical

supercapacitors [2.9]. The word "supercapacitor" was first used by Conway, found in Conway's

scientific monograph with a detailed description of it. Yet, Nippon electric company (NEC),

were the first to produce a capacitance device that was commercially successful under the same

name "supercapacitor". G.L. Bullard [2.10, 2.11] suggests that the double layer capacitor

produced by Pinnacle Research Institute Inc. has a very good performance. In accordance with

the Helmholtz model, this capacitor has positive and negative charges aligned along the interface

representing a simple parallel plate capacitor. Later, after a decade of proposing this model, these

EDLCs were integrated into several applications [2.12]. Figure 2.1 (a), (b) shows the modern day

construction of EDLC. A very high power density and fast-rising time were obtained using this

device due to its low resistance and inductance. As seen in dielectric capacitors, the double layer

capacitors do not have such constraints or limitations.

(a)   (b)
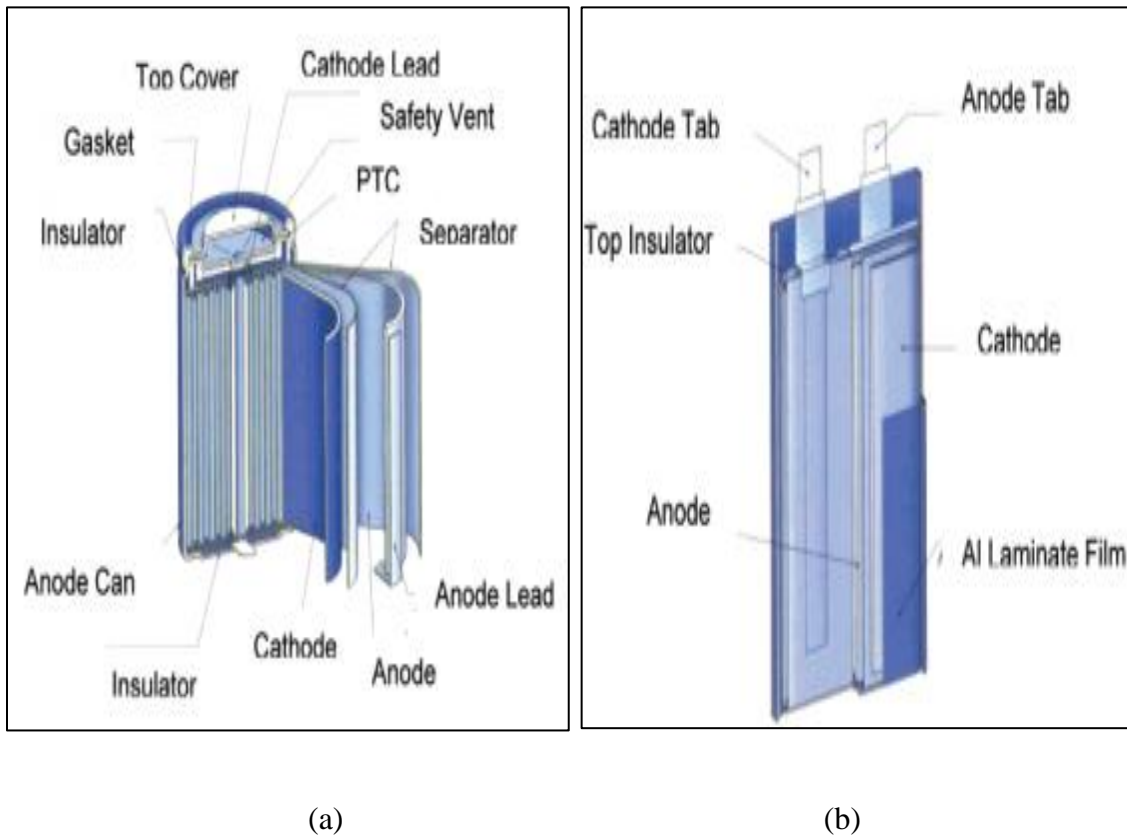
Figure 2.1 (a), (b) Modern day construction of EDLC [Reprinted with permission from 2.24]

2.3.2 Need for Supercapacitor

There is an increasing demand for high-quality energy supplies for portable, stationary and

mobile applications. Different types of electrochemical energy storage applications such as fuel

cells [2.13, 2.14], batteries [2.15, 2.16] and supercapacitors [2.17, 2.18] have received a great

attention in the past decade due to mounting concerns about environmental protection and energy

saving. In the past, lithium-ion batteries (LIBs) were widely used in various applications such as

cell phones, laptops, computers etc. But in general, electrochemical devices have a great aptitude for large-scale applications such as hybrid electric vehicles and smart grids [2.19, 2.20] and the requirements differ depending on the applications in terms of scale, energy and power supply.

Currently, modern day electrical and electronic device demand high current, energy and power requirements with extreme safety precautions. Capacitors are one of the solutions to meet these extreme requirements of high power density, emitting a large amount of energy in a short time period. And at ideal conditions, capacitors can replace batteries satisfying power requirements in electric vehicle systems combining both high power density of capacitors and high energy density of batteries. When in need of rapid acceleration, capacitors can dispense large amounts of power, batteries could help in electrically charging the capacitors and to power the vehicle. These capacitors require a high recyclability, high energy and power densities higher than the batteries under the same operating potential and reliable discharge characteristics [2.21]. But, in practice, traditional electrolytic capacitors are short in persistent energy density as can be seen in Table 1, which can be used only for a very short time, while electric vehicles are in need of acceleration. So, instead, supercapacitors could be used to greatly enhance the energy density of the capacitor for a sufficient time period to attain high powered output. This high energy density, in supercapacitors, is stored in a small unit volume of carbon based materials that has vast surface area bearing no dielectric materials.

Table 1: Basic comparison of battery, electrolytic capacitor and supercapacitor parameters

Parameters	Supercapacitor	Electrolytic Capacitor	Battery
Energy density (Wh/Kg)	1-10	<0.1	20-100
Power density (W/Kg)	~1000-2000	>10000	~50-200
Charge time	1-30 seconds	10^{-6}-10^{-3} seconds	0.3 -3 hours
Discharge time	1-30 seconds	10^{-6}-10^{-3} seconds	1-5 hours
Operating Voltage(V)	2.5 to 3 per cell	6 to 800	1.25 to 4.2 per cell
Cycle life	>100000	>500000	~500-2000
Charge/discharge efficiency	~0.9-0.95	~1.0	~0.7-0.85
Operating temperature (^{o}C)	-40 to 85	-20 to 100	-20 to 65

2.3.3 Basics of Supercapacitor

Supercapacitors (also known as ultra-capacitors or electric double layer capacitor) are energy storage devices that have low internal resistivity and very high capacitance behavior. The energy storage mechanism here involves the separation of charges between the interface of the electrode and the electrolyte [2.22, 2.23]. This device, in particular, can store and deliver energy at a relatively high capacity in comparison to batteries [2.24]. A supercapacitor model comprises of a separator, two electrodes and an electrolyte but the electrode material plays the major role in determining its performance [2.25, 2.26]. Major benefits of using a supercapacitor are its flexible packaging, high power, long life cycle, wide operational ranges (-40°C to 77°C), lightweight and low maintenance [2.27].

A supercapacitor can be best used in applications that require short load cycle and high

reliability. Some of the examples of these types of devices are electric vehicles, load cranes, and

forklifts [2.28]. In addition, some of the most promising applications of supercapacitors are low

emission hybrid vehicles and fuel cell vehicles [2.29, 2.30]. Although, the energy density of a

supercapacitor have high energy density than conventional capacitors, but still they are not up to

the mark of fuel cells and batteries as can be seen in Figure 2.2. So, in such devices,

supercapacitors can be used along with fuel cells or batteries serving as a temporary storage

energy device with high power capacity to store energy while braking [2.31].
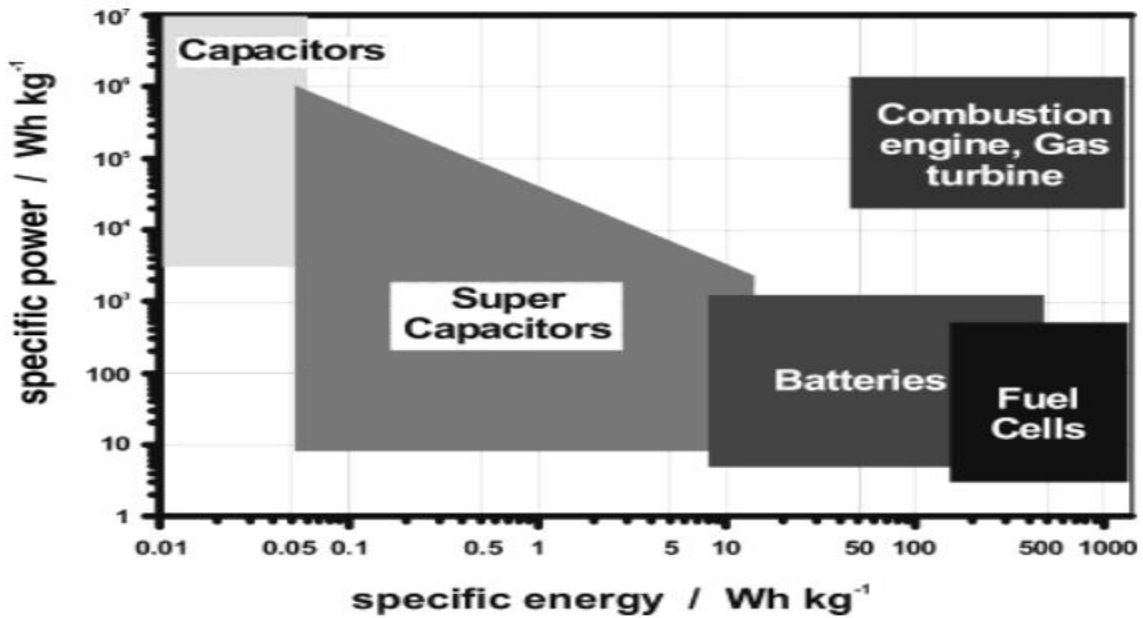
Figure 2.2: Energy vs power plot of different energy storage devices [Reprinted with permission from 2.24]

2.4   Classification of Supercapacitors

The operation principle of a supercapacitor is based on the amount of energy stored as ions

between the electrolyte and the electrode. Based on different types of storage mechanisms, as

shown in Figure 2.3, supercapacitors are classified into three major types: electrochemical double layer capacitor, pseudo-capacitor, and hybrid supercapacitor [2.32].
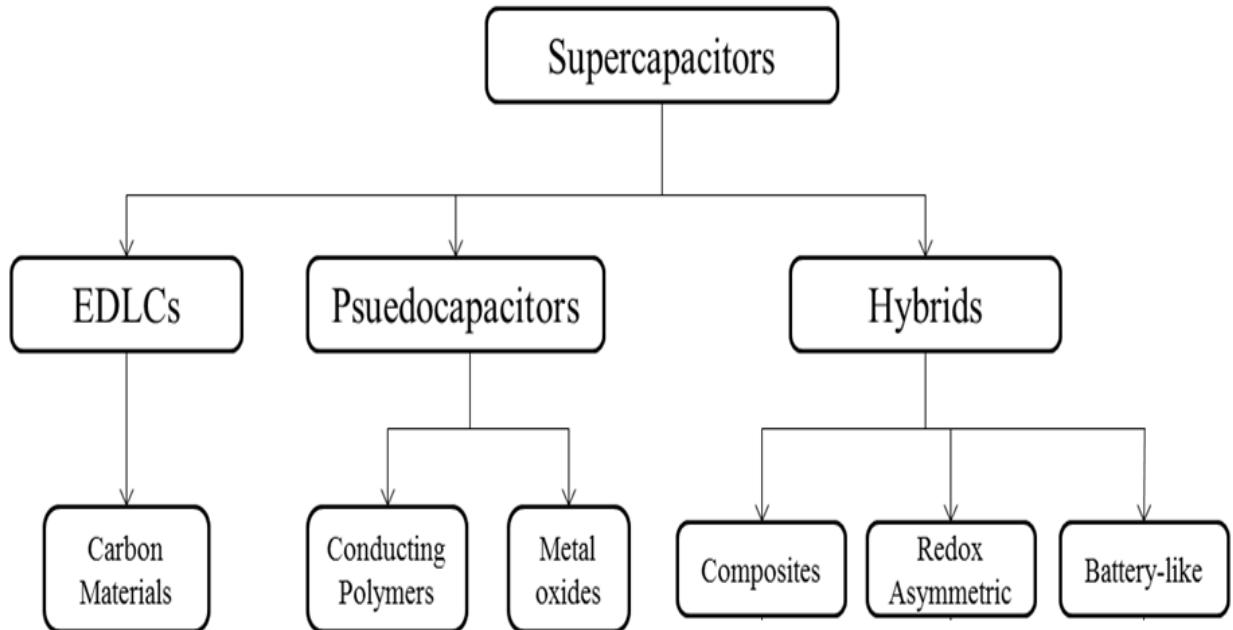
Figure 2.3: Classification of Supercapacitors [Reprinted with permission from 2.32]

2.4.1 Electric double layer Capacitor

An electric double layer capacitor (EDLC) is structured with two carbon-based electrodes on either side, a separator between the electrodes and an electrolyte that completes the electrical connection by filling in the gap between electrodes and the separator very tightly. In an EDLC device, energy can be either stored electrostatically or by a non-faradaic process involving no charge transfer between electrolyte and electrode [2.33, 2.34]. EDLCs are widely used due to their high degree of reversibility, long-term self-discharge, high power density, and energy density that are somewhere between the rechargeable batteries and conventional electrostatic/electrolytic capacitors. Initially, when the supercapacitor is in discharge state, the ions float freely. After a voltage is applied, a nanometer-sized electrostatic charge separation

occurs between the electrolyte and the large surface area carbon electrodes [2.35-2.37] as two layers, and thus, the name electric double layer capacitor. When an electrode material is immersed into an electrolyte solution, this electric double layer is the one responsible for charge storage in an EDLC. The free electrons moves towards the electrolyte side from the metal surface and the cations in the electrolyte moves away from the metal surface.

As it can be seen in Figure 2.4 (a) that an overall negative charge is aligned along the electrode surface with an equal amount of opposite charges aligned along the electrolyte side. The first layer that gets formed on the metal/electrolyte interface is termed as the Helmholtz plane which comprises of anions, cations, and neutral solvent molecules. Past the tightly held Helmholtz layer, the diffusion layer as seen in Guoy-Chapman model in Figure 2.4 (b) is responsible for the thermal fluctuations of ions in the solution. The capacitance is then determined by smallest of Helmholtz and Guoy-Chapman models that contributes to the double layer. But later it was discovered that the Guoy-Chapman model overestimates the capacitance of high concentration electrolyte and the interface change. Stern-graham model as shown in Figure 2.4 (C) recommends that each electrolyte possess ionic radius, and therefore, would not be able to move closer to electrode surface than what the ionic radius allows [2.38, 2.39]. So, a zone that is depleted of ionic changes will appear near the electrode surface as an additional contribution to the total capacitance. Chmiola et.al [2.40] proved that the energy storage of an EDLC, that widely poses a challenge for charge storage mechanism [2.41, 2.42], can be drastically improved by using a sub-nanometric pore sized material (tungsten carbide) which has a pore size smaller than that of solvated ions.
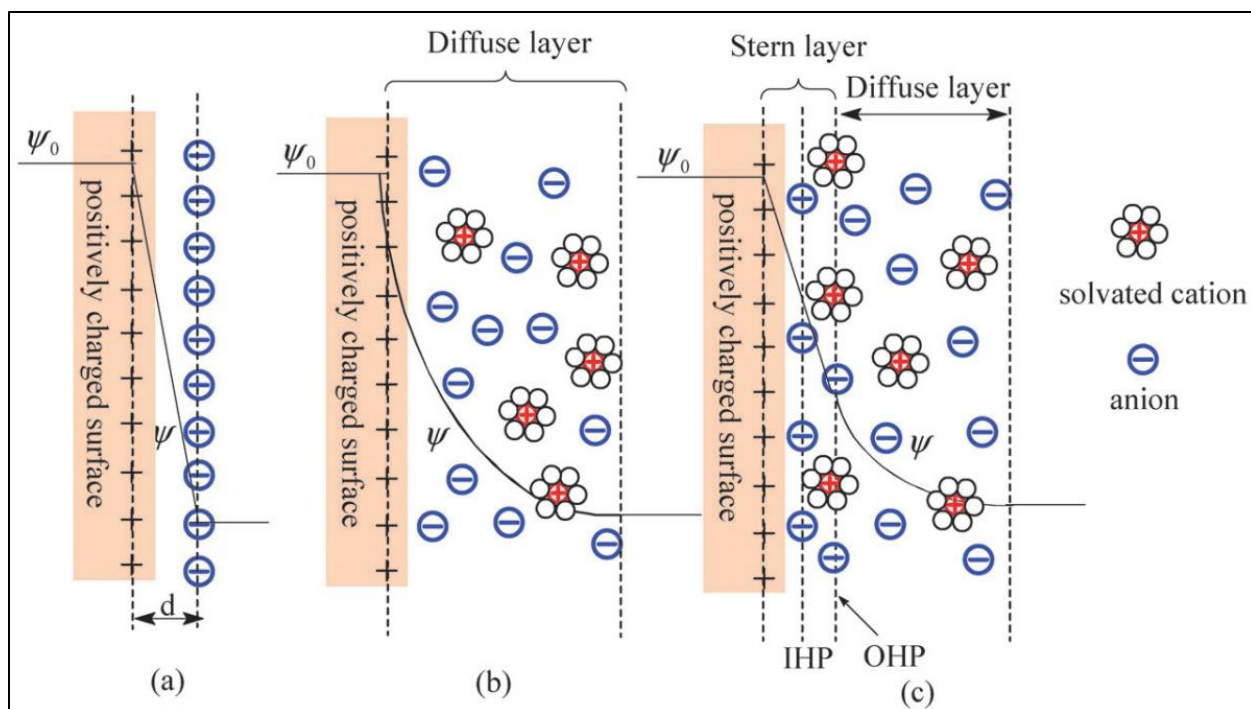
Figure 2.4: Schematic of a) Helmholtz, b) Gouy-Chapman and C) Stern-Graham models
[Reprinted with permission from 2.39]

2.4.2 Pseudo-capacitor

In efforts to produce EDLCs with high energy density, the surface area of the material has been widely researched. But, unfortunately, the highest energy density of supercapacitor was only 10% than that of lithium ion batteries and needed major improvements before making it commercially available for several applications. So materials that exhibit pseudo-capacitive behavior is used which helps in enhancing the energy density and specific capacitance compared to EDLC. An intercalation of pseudo-capacitance can be recognized when a fast ion transport strikes at the near surface. A material is said to be "near surface" when its grain size is small enough (tens of nanometers) for transport. Several parameters, including, "small diffusion distances compared to the diffusion constant of the material; interconnectivity between the grains for easy electron transport; sufficient space between grains to allows for ample surface access for

14

the electrolyte; and a suppression of the typical phase transition" must be satisfied in order for a pseudo-capacitance to occur. Materials that possess these desired parameters would have to be porous and nano-structured. In general, synthesizing nanoporous structured materials require mixing precursors along with active materials in solution phase leading to self-assembly upon evaporation.

One of the approaches to enhance the energy density is to limit the rate step and improve the charging time in lithium ion battery. This can be done by reducing the grain size of the electrode materials [2.43, 2.44]. By successfully reducing the grain size of the electrochemically active materials, an improved reversibility of the process and increased redox was noticed. These changes, in turn, led to improvement in charge/discharge rates and cyclability of the supercapacitors bearing these electrode materials. The process of fast redox in electrochemically active materials is referred to as pseudo-capacitance [2.45, 2.46]. The redox reactions change in par with the rate of charging and discharging since they are dependent on the electrode potential. So based on this mechanism, the capacitance and energy density of the pseudo-capacitor becomes superior than the carbon based EDLCs as shown in Table 2. Although they have comparatively better performance, but still they have poor life cycle. This happens due to the fact that the pseudo-capacitive material gets damaged after multiple cycles inducing morphological changes, and therefore, leading to reduction in performance. So to resolve this issue, carbon-based materials are integrated along with pseudo-capacitive materials to form as hybrid nanocomposites.

Table 2: Advantages and disadvantages of EDLC and Pseudo capacitor

Pseudo capacitor	Electric double layer capacitor
High specific energy	Low specific energy
Phase angle is a function of frequency typically showing transmission line behavior	~90 degree phase angle
Highly reversible	Indefinitely reversible
Capacitance not constant with voltage	Capacitance constant with voltage
Kinetic limitations for high charge/discharge rates and hence power is limited by kinetic factors	High charge/discharge rate and very high power

2.4.3 Hybrid Supercapacitor

As mentioned earlier, EDLCs possess good power performance and life cycle whereas pseudo-capacitors exhibit comparatively higher capacitance and energy density. But still they lack in cyclic performance and also the material gets deteriorated with time. So in hybrid capacitors a combined performance characteristics is demonstrated which was formerly unattainable. By combining the features of both, that is by combining the power density of supercapacitor electrodes and the energy source of pseudo capacitive materials, they were able to outperform EDLCs and pseudo-capacitors [2.47-2.51]. But technically, an increase in energy density occurs still at the expense of good cyclic stability which poses as a drawback of hybrid supercapacitors [2.52]. So recently, a lot of research works have been reported testing hybrid supercapacitor with several combinations of different electrode materials along with inorganic and organic

electrolytes with the interest of improving the energy and power density and still having a good life cycle [2.53-2.57].

2.5 Electrochemical Characterization Techniques

Electrochemistry knowledge can help in selecting an appropriate oxidizing agent in order to put a metal complex in intermediate oxidation state. The electrochemical methods have also taken advantage by removing blocking agents and introducing functional groups. Some of the widely used electrochemical techniques for testing supercapacitor are cyclic charge/discharge, CV and EIS.

2.5.1 Cyclic Voltammetry

Cyclic voltammetry (CV) has become one of the most common tools for the past few decades to evaluate the electrochemical reactions taking place in an experiment. Using this technique we can perform qualitative and pseudo-quantitative studies to determine the voltage range of the device or the electrodes and perform a kinetic analysis of the device over a wide range of scan rates. In fundamental research, commonly three electrode setups are used for electrochemical measurements. The three electrodes are: a) *Working Electrode*, b) *Reference Electrode*, and C) *Counter Electrode*. But, the packaged capacitors can also be tested using two electrode connection by simply connecting the counter and reference electrodes together. The primary principle of a CV is to apply a potential sweep across an electrochemical cell and measure the amount of current flowing. The current created during the sweep can be measured by

$$I = \frac{dQ}{dt} = C\frac{dV}{dt} \qquad\qquad (2.3)$$

where, C is the capacitance in Farads, I is the current in amperes, and $\frac{dV}{dt}$ is the scan rate of voltage sweep.

2.5.2 Chronopotentiometry

The mechanism of a process and the kinetics of the chemical reactions can be studied using chronopotentiometry test. The system operates in galvanostatic mode, where the current is kept in control and the voltage is measured. The current can either be applied in a single or double step. The experiments are usually performed in an unstirred solution or solid devices. Using this technique, redox mechanism of the device can be realized. A potential is applied to the electrode which ramps up from an open circuit voltage to a fixed constant potential to a level until which the concentration of redox substance at the electrode gets depleted. The voltage rapidly shifts to a level where the applied current gets sustained, when the substance gets depleted at the surface of the electrodes. This immediate shift in voltage is called the transition time. For systems having only one type of redox substance, the voltage shifts to a level where the solvent or the supporting electrolyte would be oxidized/ reduced [2.58]. The chronopotentiometry techniques are mainly used during the charging/ discharging of energy storage devices like supercapacitors and batteries.

2.5.3 Electrochemical Impedance Spectroscopy

In general, impedance spectroscopy is a linear electrical response of a material subsuming small signal measurements and analyzing the subsequent response of the physio-electrochemical properties of the system. The measurements are commonly done in frequency domain, but sometimes they are converted by Fourier transform to frequency domain after measuring them in the time domain. An ideal resistor follows Ohm's law, according to which resistance (R) of any electrical device is defined as the ratio of voltage (V) and current (I).

$$R = \frac{V}{I} \qquad\qquad (2.4)$$

However, in the real world, there are some limitations for an ideal resistor exhibiting some

complex behavior in terms of circuit elements. Electrochemical impedance spectroscopy (EIS) is

an electrochemical characterization technique where the response of electrodes is in the form of

AC signals at different frequencies. At any particular frequency, the expected result for a

sinusoidal voltage will be a sinusoidal current response but with a shifted phase as shown in

Figure 2.5. If there is a phase shift experienced at different frequencies, a separate set of data set

would be created that will be in relation to the electrochemical process within the

electrochemical device. The EIS tool will be able to differentiate different electrodes, solution

capacitance by phase shift, resistive and magnitude of current responses at different times [2.59-

2.62]. Although, EIS will require an equivalent circuit model in order to understand the obtained

data, nyquist plot is a graph plotted with real (x-axis) and imaginary (y-axis) part at a particular

frequency.
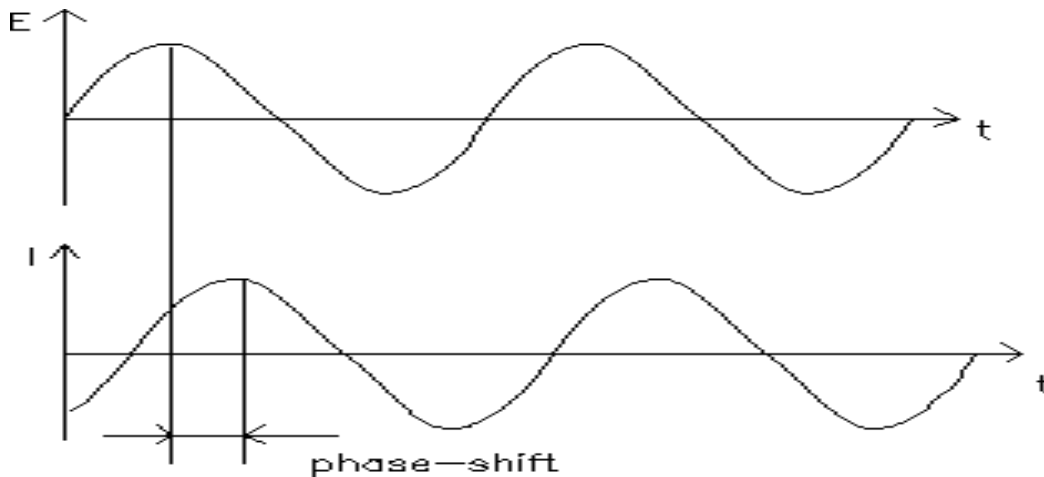
Figure 2.5: Sinusoidal response of current in a system [Reprinted with permission from 2.62]

The excitation signal as function of time can be expressed as

$$E_t = E_o \sin(\omega t) \qquad\qquad (2.5)$$

where, E_o is the amplitude of the signal, E_t is the potential at time t and ω is the radial frequency.

In a linear system, the response signal, I_t is shifted in phase (Φ) than I_o.

$$I_t = I_o \sin(\omega t + \Phi) \qquad\qquad (2.6)$$

We calculate the impedance according to Ohm's law, allowing us to determine the terms of magnitude Z_o and Phase shift (Φ),

$$Z = \frac{E_t}{I_t} = \frac{E_o \sin(\omega t)}{I_o \sin(\omega t + \Phi)} = Z_o \frac{\sin(\omega t)}{\sin(\omega t + \Phi)} \qquad\qquad (2.7)$$

2.6 Supercapacitor Parameters

2.6.1 Capacitance

Although there have been a lot of research works done with conventional capacitors, the measurement methods to determine the main parameters like internal resistance, capacitance, energy density, and power density have not been standardized yet [2.63, 2.64]. When a certain amount of voltage is applied across the electrodes, the capacitor will act as a voltage source in the form of connected circuit for a short period of time. Capacitance of this device will be equivalent to the ratio of electric charge on each electrode (Q) and the voltage (V) among them.

$$C = \frac{Q}{V} \qquad\qquad (2.8)$$

In a conventional EDLC where energy is stored in the form of electrostatic charges by reversible desorption and adsorption of electrolyte ions, capacitance of high surface area active carbon based materials is denoted as

$$C = \frac{\varepsilon_o \varepsilon_r A}{d} \qquad\qquad (2.9)$$

20

where d is effective thickness of the double layer, A is surface area of interface, ε_o is the permittivity of vacuum, and ε_r is the relative dielectric constant of the electrolyte. Estimation of standardized capacitance parameters seen in impulse and steady-state electroanalytical methods [2.65, 2.66] can be generally found in formulas adapted from ideal capacitors. A transient voltage response of a system obtained from a galvanostatic charge/discharge response applied with a stepping current, I_{cc} has an average capacitance calculated as

$$C = \frac{I_{cc}}{dV/dt} \qquad (2.10)$$

with dV/dt acting as the slope of the time-voltage curve. Capacitance is usually measured with different values of I_{cc}. But with cyclic voltammetry curves, the integral capacitance of a target electrode can be measured from both the terminals of the device via a linearly changing voltage between them using the formula

$$C = \frac{1}{\Delta V(\frac{dV}{dt})} \int I dV \qquad (2.11)$$

where, ΔV is the potential window and (dV/dt) is the voltage scan rate. In cyclic voltammetry tests, capacitance depends on the sweep rates at which the rate of device is charged/ discharged at different current levels. Universally, specific capacitance is the term used for identifying the gravimetric capacitance, C_G of the active materials in an EDLC.

$$C_G = C_{int} . SA \qquad (2.12)$$

where C_{int} is the intrinsic capacitance and SA is the ionically accessible surface area. Apart from these factors, pore volume and volumetric capacitance; C_V must also be given serious considerations since the volume of the EDLCs must be reduced if they need to be considered for rechargeable energy storage applications. In EDLCs, the mass of the electrolytes are not taken

21

into account whereas, C_G accounts the mass of active material in the device [2.67]. Electrodes

having high pore volume and low volumetric capacitance will require large amounts of

electrolyte solutions which will thereby increase the weight of the device for the given

capacitance. Overall, the above mentioned parameters imply that an electrode material having

room for highest ion-accessible surface area would be the best for the technologically significant

device applications but still there are few factors that still have to be given some serious

considerations.

2.6.2 Energy density and Power density

For an EDLC, evaluating the performance of energy and power density is the most important

yardstick in comparison to other energy storage devices. Formula mentioned below depicts the

state of charge (Q) as a function of potential difference (E) in an EDLC and compares its

performance obtained in a battery. Gibbs Free energy ΔG of both the devices can be calculated

by:

$$\Delta G = \int E \, dQ = \int \frac{Q}{C} dQ = \frac{1}{2} \frac{Q^2}{C} = \frac{1}{2} C . E^2 \qquad (2.13)$$

In EDLC, at the same potential, the Gibbs free energy is half that of a battery charged since the

voltage between cathode and anode does not significantly change in response with charge.

Consequently, operating at higher voltages improves the performance of EDLC which is

indicated by square dependence of ΔG in the above equation. Main advantage an EDLC possess

over other energy storage devices is that the energy density does not change at high rates of

charge/discharge capacity.

The power density (P) of a device is mainly dependent on the equivalent series resistance (ESR)

and the operating voltage of the device. ESR is the overall effective resistance which includes

membrane resistance, electronic and ionic resistances. But ESR changes in response to the time

scale due to its distributed nature. However, if the charging/discharging of an EDLC is modeled

as a simple RC circuit [2.68], then the operating voltage of the device can be approximated to

maximum power (P_{max}). From this supposition, voltage (E) can be calculated in accordance with

the ESR resistance (R_s) as:

$$E = E_i - iR_s \qquad\qquad (2.14)$$

So, power density is just a multiple of current and voltage (P=i.E):

$$P = iE = iE_i - i^2 R_s \qquad\qquad (2.15)$$

The maximum power (P_{max}) takes advantage from the above derivative to find the current and

voltage by setting i to zero.

$$P_{max} = \frac{E_{max}^2}{4R_s} \qquad\qquad (2.16)$$

2.7 References

2.1 Otto Haasa, Elton J. Cairns, "Electrochemical energy storage", *Annu. Rep. Pro. Chem., Sect. C*, 95, 163-197 (1999).

2.2 G. Plante, "The Storage of Electrical Energy", *MT Publisher Kessinger Publishing* ISBN: 9781154857726 (2007).

2.3 Anthony R. West, "Solid State Chemistry and its applications", *John Wiley Sons* (2005).

2.4 Gielen. D, "Electricity Storage and Renewables for Island Power: A Guide for Decision Makers," *International Renewable Energy Agency* (2012).

2.5 Lambert. T, Gilman. P, Lilienthal. P, "Micropower system modeling with HOMER," *Integration of Alternative Sources of Energy*, New York: John Wiley & Sons (2006).

2.6 Coppez. G, Chowdhury. S, Chowdhury. S. P, "Review of battery storage optimisation in Distributed Generation," *Power Electronics, Drives and Energy Systems (PEDES)*, 1-6 (2010).

2.7 Kotz. R, Carlen. M, "Principles and applications of electrochemical capacitors," Electrochimica Acta - Pergamon -Elsevier Science, 45, 2483–2498 (2000).

2.8 Miller. J. M, Smith. R, "Ultra-capacitor assisted electric drives for transportation," presented at IEEE International Electric Machines and Drives Conference, 2003.

2.9 Conway. B. E, "Electrochemical Supercapacitors: Scientific Fundamentals and Technological Applications", Springer, ISBN 0306457369 (1999).

2.10 Bullard. G. L, Sierra-Alcazar. H. B, Lee. H. L, Morris. J. L, "Operating Principles of the Ultracapacitor," IEEE Transactions on Magnetics, 25, 102-106 (1989).

2.11 http://shodhganga.inflibnet.ac.in/bitstream/10603/133431/11/11_chapter2.pdf

2.12 Burke. A. F, "Prospects for Ultracapacitors in Electric and Hybrid Vehicles," presented at 11th Annual Battery Conference on Applications and Advances (1996).

2.13 Sukhvinder P. S. Badwal, Sarbjit S. Giddey, Christopher Munnings, Anand I. Bhatt, Anthony F. Hollenkamp, "Emerging electrochemical energy conversion and storage technologies", *Front Chem.*, 2, 79 (2014).

2.14 Hyun Deog Yoo, Elena Markevich, Gregory Salitra, Daniel Sharon, Doron Aurbach, "On the challenge of developing advanced technologies for electrochemical energy storage and conversion", *Materials Today*, Volume 17, Issue 3, 110-121 (2014).

2.15 https://www.seas.ucla.edu/~pilon/EES.html.

2.16 Rujia Zou, Muk Fung Yuen, Li Yu, Junqing Hu, Chun-Sing Lee, Wenjun Zhang, "Electrochemical Energy Storage Application and Degradation Analysis of Carbon-Coated Hierarchical NiCo$_2$S$_4$Core-Shell Nanowire Arrays Grown Directly on Graphene/Nickel Foam", Nature, 6, 20264 (2016).

2.17 Fei Liu, Dong Feng Xue, "Electrochemical energy storage applications of pristine graphene produced by non-oxidative routes, Volume 58, Issue 11, 1841–1850 (2015)

2.18 Ali Eftekhari, Zhaoyang Fan, "Ordered mesoporous carbon and its applications for electrochemical energy storage and conversion, *Mater. Chem. Front.*, 1, 1001-1027 (2017)

2.19 Maria R. Lukatskaya, Bruce Dunn, Yury Gogotsi, "Multidimensional materials and device architectures for future hybrid energy storage", *Nature Communications,* 7, 12647 (2016).

2.20 Xing Luo, Jihong Wang, Mark Dooner, Jonathan Clarke, "Overview of current development in electrical energy storage technologies and the application potential in power system operation", *Applied Energy*, 1, 511-536 (2015).

2.21 Obreja V. N. Vasile, "On the performance of supercapacitors with electrodes based on carbon nanotubes and carbon activated material-A review", *Physica E: Low-dimensional Systems and Nanostructures*, Volume 40, Issue 7, 2223-2648 (May 2008).

2.22 Stoller. M. D, Park. S, Zhu. Y, An. J, Rouf. R. S, "Graphene-based ultracapacitors", *Nano lett.*, 8 (2008) 3498- 3502.

2.23 Shaoping Shen,"Analysis of stability for the controlled spacecraft with a deployable and retractable flexible appendage", *IEEE International Conference on Control and Automation*, 465-470(2010).

2.24 Martin Winter, Ralph J. Brodd, "What Are Batteries, Fuel Cells, and Supercapacitors?", Chem. Rev. 104, 4245 (2004).

2.25 Matthew H. Ervina, Benjamin S. Miller, Brendan Hanrahan, Benjamin Mailly, Tomas Palacios, "A comparison of single-wall carbon nanotube electrochemical capacitor electrode fabrication methods", *Electrochim. Acta,* 65, 37-43 (2012).

2.26 Michael A. Pope, Sibel Korkut, Christian Punckt, Ilhan A. Aksay, "Supercapacitor Electrodes Produced through Evaporative Consolidation of Graphene Oxide-Water-Ionic Liquid Gels", *J. Electrochem. Soc.*, 160, A1653-A1660 (2013).

2.27 Yan Wang, Zhiqiang Shi, Yi Huang, Yanfeng Ma, Chengyang Wang, Mingming Chen, Yongsheng Chen, "Supercapacitor Devices Based on Graphene Materials", *J. Phys. Chem. C*, 113, 13103-13107 (2009).

2.28 John R. Miller, Patrice Simon, "Electrochemical Capacitors for Energy Management", *Mater. Sci.*, 321, 651-652 (2008).

2.29 Nae-Lih Wu, "Nanocrystalline oxide supercapacitors", *Mater. Chem. Phys.*, 75, 6-11 (2002).

2.30 Ya-meng Cai, Zong-Yi Qin, Long Chen, "Effect of electrolytes on electrochemical properties of graphene sheet covered with polypyrrole thin layer", *Progress Nat. Sci: Mater. Int.*, 21, 460-466 (2011).

2.31 Juan de Santiago, Florian Burmeister, Johan Lundin, Janaina G. Oliveira, "A power buffer in an electric driveline: Two batteries are better than one", *ISRN Automotive Engineering*, 2014, Article ID 525630 (2014).

2.32 Abdul Waheed Anwar, Abdul Majeed, Nadeem Iqbal, Wasi Ullah, Ahmad Shuaib, Usman Ilyas, Fozia Bibi, Hafiz Muhammad Rafique, "Specific capacitance and cyclic stability of graphene based metal/metal oxide nanocomposites: A Review, Journal of materials science and technology, 31, 7, 699-707 (2015).

2.33 Meisam Valizadeh Kiamahalleh, Sharif Hussein Sharif Zein, Ghasem Najafpour, Suhairi Abd Sata, Surani Buniran, *Nano*, 7, 1230002 (2012).

2.34 Jayalakshmi. M, Balasubramanian. K, *Int. J. Electrochem. Sci.*, 3, 1196-1217 (2008).

2.35 Marin S. Halper, James C. Ellenbogen, " Supercapacitors: A brief overview", *Mitre Nanosystems Group*, McLean, Virginia (2006).

2.36 Hojin Choi, Hyeonseok Yoon , "Nanostructured Electrode Materials for Electrochemical Capacitor Applications", *Nanomaterials*, 5 (2), 906-936 (2015).

2.37 Simon. P, Gogotsi. Y, "Charge storage mechanism in nanoporous carbons and its consequence for electrical double layer capacitors", *Philos. Trans. R. Soc. London, Ser. A,* 368, 3457–3467 (2010).

2.38 Gileadi. E, Kirowa-Eisner. E, Penciner. J, "Interfacial Electrochemistry: An Experimental Approach*", Addison-Wesley Publishing Company* (1975).

2.39 Li Li Zhang, X. S. Zhao, "Carbon-based materials as supercapacitor electrodes", *Chem. Soc. Rev.*, 38, 2520-2531 (2009).

2.40 Chmiola. J, "Anomalous increase in carbon capacitance at pore sizes less than 1 nanometer", *Science,* 313, 1760–1763 (2006).

2.41 Skinner. B, Chen. T, Loth. M, Shklovskii. B, "Theory of volumetric capacitance of an electric double-layer supercapacitor", *Phys. Rev. E,* 83, 056102 (2011).

2.42 Skinner. B, Fogler. M, Shklovskii. B, "Model of large volumetric capacitance in graphene supercapacitors based on ion clustering", *Phys. Rev. B,* 84, 235133 (2011).

2.43 Naoki Nitta, Feixiang Wu, Jung Tae Lee, Gleb Yushin, Li-ion battery materials: present and future", *Materials Today*, 18 (5), 252-264 (2015).

2.44   Christian Julien, Alain Mauger, Karim Zaghib, Henri Groult, "Optimization of Layered Cathode Materials for Lithium-Ion batteries", *Materials (Basel)*, 9(7), 595 (2016).

2.45   Zhong Wu, Lin Li, Jun-min Yan, Xin-bo Zhang, "Materials Design and System Construction for Conventional and New-Concept Supercapacitors", *Adv. Sci.*, 4(6), 1600382 (2017).

2.46   Yonggang Wang, Yanfang Song, Yongyao Xia, "Electrochemical capacitors: mechanism, materials, systems, characterization and applications", *Chem. Soc. Rev.*, 45, 5925-5950 (2016).

2.47   Arbizzani, C.; Mastragostino, M.; Soavi, F., "New trends in electrochemical supercapacitors", Journal of Power Sources, 100 (1-2), 164-170 (2001).

2.48   Nanjundan Ashok Kumar, Mushtaq Ahmad Dar, Rukhsana Gul, Jong-Beom Baek, "Graphene and molybdenum disulfide hybrids: synthesis and applications", Materials Today, 18 (5), 286-298 (2015).

2.49   Tianyi Wang, Shuangqiang Chen, Huan Pang, Huaiguo Xue, Yan Yu, "MoS_2-Based Nanocomposites for Electrochemical Energy Storage", Adv. Sci., 4, 1600289 (2017).

2.50   Kulvinder Singh, Sushil Kumar, Kushagra Agarwal, Khushboo Soni, Venkata Ramana Gedela, Kaushik Ghosh, "Three-dimensional Graphene with MoS_2 Nanohybrid as Potential Energy Storage/Transfer Device, *Scientific Reports* 7, 9458 (2017).

2.51   Francesca Clerici, Marco Fontana, Stefano Bianco, Mara Serrapede, Francesco Perrucci, Sergio Ferrero, Elena Tresso, Andrea Lamberti, "*In situ* MoS_2 Decoration of Laser-Induced Graphene as Flexible Supercapacitor Electrodes", *ACS Appl. Mater. Interfaces*, *8* (16), 10459–10465 (2016).

2.52   Patrice Simon, Katsuhiko Naoi, "New Materials and New Configurations for Advanced Electrochemical Capacitors", Electrochem. Soc. interface, 17 (1), 34-37 (2008).

2.53   Naeyoung Jung, Soongeun Kwon, Dongwook Lee, Dong-Myung Yoon, Young Min Park, Anass Benayad, Jae-Young Choi, Jong Se Park, "Synthesis of chemically bonded graphene/carbon nanotube composites and their application in large volumetric capacitance supercapacitors", *Adv. Mater.* 25, 6854–6858 (2013).

2.54   Edney G. S. Firmiano, Marcos A. L. Cordeiro, Adriano C. Rabelo, Cleocir J. Dalmaschio, Antonio N. Pinheiro, Ernesto C. Pereira, Edson R. Leite, "Graphene oxide as a highly selective substrate to synthesize a layered MoS_2 hybrid electrocatalyst", Chem. Commun., 48, 7687–7689 (2012).

2.55   Edney Geraldo da Silveira Firmiano, Adriano C. Rabelo, Cleocir J. Dalmaschio, Antonio N. Pinheiro, Ernesto C. Pereira, Wido H. Schreiner, Edson Robeto Leite, "Supercapacitor Electrodes Obtained by Directly Bonding 2D MoS_2 on Reduced Graphene Oxide", Adv. Energy Mater., 4, 1301380 (2014).

2.56 Lamuel David, Romil Bhandavat, Gurpreet Singh, "MoS$_2$/Graphene Composite Paper for Sodium-Ion Battery Electrodes", *ACS Nano*, *8* (2), 1759–1770 (2014).

2.57 Yuxi Xu, Zhaoyang Lin, Xiaoqing Huang, Yuan Liu, Yu Huang, Xiangfeng Duan, "Flexible solid-state supercapacitors based on three-dimensional graphene hydrogel films", *ACS Nano* 7, 4042–4049 (2013).

2.58 John N. Lalena, David A. Cleary, "Principles of Inorganic Materials Design", *John Wiley and sons* (2010).

2.59 Evgenji Barsoukov, Ross Macdonald. J, "Impedance Spectroscopy: Theory, Experiment, and Application". *Wiley Interscience Publications* (2005).

2.60 Guangchun Li, Peter G. Pickup, "Measurement of single electrode potentials and impedances in hydrogen and direct methanol PEM fuel cells", *Electrochimica Acta*, 49, 4119-4126 (2004).

2.61 Alejandro A. Franco, Pascal Schott, Christian Jallut, Bernhard Maschke, "A dynamic mechanistic model of an electrochemical interface", *Journal of The Electrochemical Society*, 153, A1053-A1061 (2006).

2.62 https://www.gamry.com/application-notes/EIS/basics-of-electrochemical-impedance-spectroscopy/.

2.63 Meryl D. Stoller, Rodney S. Ruoff, "Best practice methods for determining an electrode material's performance for ultracapacitors", *Energy Environ. Sci.* 3, 1294–1301 (2010).

2.64 Sanliang Zhang, Ning Pan, "Supercapacitors performance evaluation", *Adv. Energy Mater.* 5, 1401401 (2015).

2.65 Kierzek. K, Frackowiak. E, Lota. G, Gryglewicz. G, Machnikowski. J, "Electrochemical capacitors based on highly porous carbons prepared by koh activation", *Electrochim. Acta,* 49, 515–523 (2004).

2.66 Arulepp. M, Permann. L, Leis a. J, Perkson. A, Rumma. K, Jänes. A, Lust. E, "Influence of the solvent properties on the characteristics of a double layer capacitor", *J. Power Sources* 133, 320–328 (2004).

2.67 Gogotsi. Y, Simon. P, "True Performance Metrics in Electrochemical Energy Storage", *Science*, 334 (6058), 917-918 (2011).

2.68 John R. Miller, "Electrochemical Capacitor Power Performance: Stability as a Function of Temperature, Voltage, and Operating Time", (1993).

3.   Chapter 3: Literature Review

3.1   Nanomaterials for Supercapacitors

In 1960, a physicist, Richard Phillips Feynman was the first to present about nanotechnology to the world. In an annual meeting of American Physical society he declared, "The principles of physics as far as I can see, do not speak against the possibility of maneuvering things atom by atom, a development which I think cannot be avoided" [3.1]. As per his statement, in recent years, a lot of attention is given to nano-crystalline materials by material scientists due to their unique physical, chemical and mechanical properties. Along the course of time, in technological researches, miniaturizing of devices with the help of nanomaterials has considerably resulted in enhanced performances. Nano-crystalline materials showed great promise even in industrial scale in terms of selectivity and functionality. The properties of the nano-crystalline materials with grain sizes of up to tens of nano-meters are often superior in comparison to conventional coarse grained polycrystalline materials. They exhibit lower resistivity, strength/hardness, diffusivity, thermal expansion, high density and elastic modulus. Synthesizing nano-crystalline based materials, thin films can be formed meriting in applications such as energy storage, photonics, information storage, sensor, non-linear optics etc. Nanotechnology permits the tailoring of these electrode materials as thin film sheets at nano-scale range. The active materials of an EDLC, pseudo capacitor and hybrid supercapacitors are commonly made of activated carbon, transition metal oxides and polymers. The key for maximum energy is high surface area of the material which is a resultant of uniform pore size at nanometer scale.

3.1.1 Graphene

Graphene, which has a honeycomb shaped structure, is bonded by single layer carbon atoms and has grabbed the attention among the scientists and researchers due to its outstanding properties

and wide range of applications [3.2, 3.3]. Graphene has similar surface area as single walled carbon nanotube (SWCNT) of 2630 m^2/g while having a higher conductivity and so is able to outperform SWCNTs and all other carbon materials. The graphene network, due to their quasi 2D nature, has high ionic conduction and facilitates interconnectivity of pore space in templated and nanoporous activated carbons [3.4]. Abundant amount of research have been performed using this as a base material over a short time period. A single sheet of graphene having no functional groups or lattice defect is defined to be pristine graphene. This graphene has high flexibility and mechanical strength due to its strong in plane σ bonds. It is also impermeable, transparent and has good electrical charge and thermal carrying property due to it's out of plane π bonds. This material was first ever discovered by peeling off using a scotch tape from highly ordered pyrolytic graphite (HOPG) [3.5, 3.6] until single atomic layer was reached. Various methods have been developed to attain this pristine graphene, for example, exfoliation of graphite in appropriate solvents using ultra-sonication, Chemical vapor depositions (CVD) [3.7, 3.8]. Materials fabricated using these methods although is porous, has good electrical conduction. But still these methods are time consuming and involve complicated procedures.

Several structures and chemistries have been proposed by many scientists over the past 80 years. Figure 3.1 shows the schematics of some of the structural models. It was projected by Hofmann and Holst that there was presence of epoxides in graphene oxide (GO) that contributes to the stoichiometry of C_2O and Ruess added that there was existence of hydroxides also on its surface [3.9, 3.10]. Scholtz and Beohm [3.11] were the first who suggested that there may be presence of quinoidal species but Lerf and Klinowski [3.12, 3.13] put forth the first detailed nuclear magnetic resonance (NMR) model in regards to chemical reactivity. This is the widely accepted GO model with structures that are in functional groups and not periodic in nature with sp^2

domains distributed randomly across the structure. Szabo-Dakeny's structure [3.14] can be used

to explain the FTIR spectroscopic nature that has the presence of quinines and/or ketones.

Although all these models have been proposed, the final structure is always said to change based

on the oxidation method followed and the extent to which the reaction in the process occurs

[3.15].
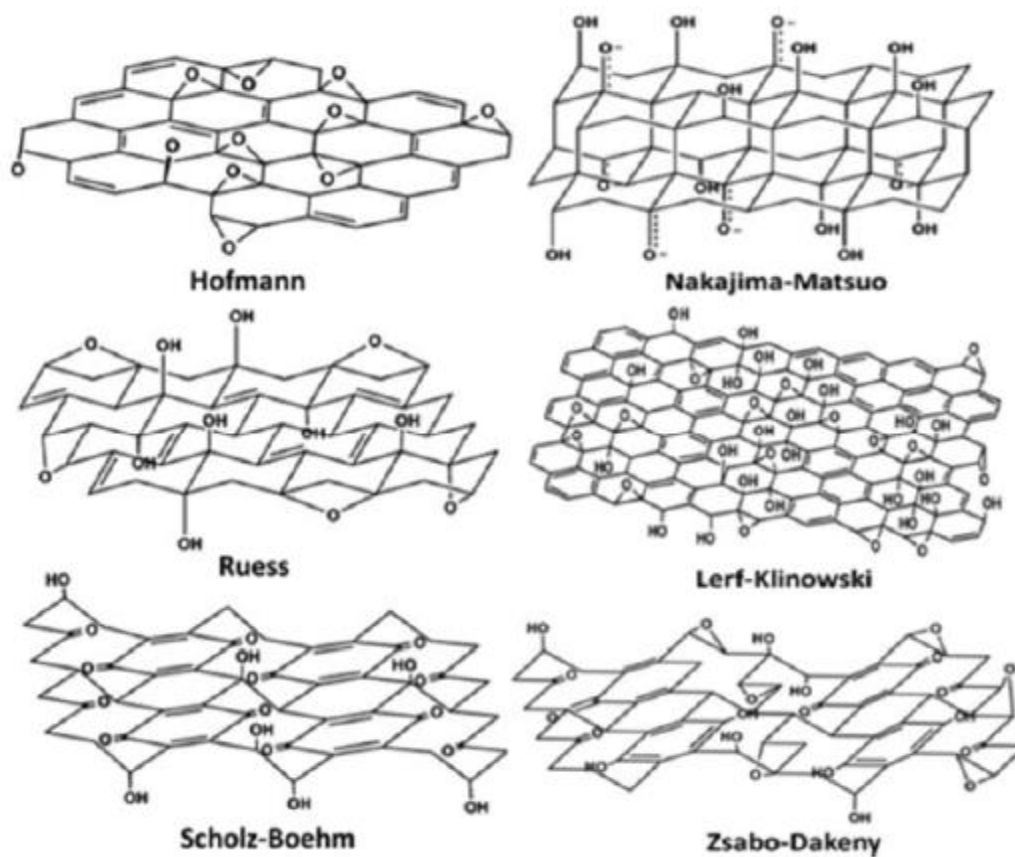
Figure 3.1: Graphene oxide structure proposed by several scientists [Reprinted with permission from 3.9]

3.1.2 Graphene Oxide

Nevertheless possessing all the above mentioned properties, a defect free single layer or few

layer graphene sheets are expensive to be produced in a commercial scale. As an alternative to

graphene, which cannot be dispersed in any organic solvent or in water, graphene oxide (GO)

31

has excellent water solubility, convenient processing method and ease of operation [3.16, 3.17]. It contains carboxyl groups at its edges [3.18, 3.19] and high density oxygen functional groups on its basal plane. They are undeniably of great importance to be developed as an eco-friendly, scalable and economical to be produced as GO [3.20, 3.21]. As widely known, synthesis of GO is done by chemical oxidation of graphite [3.22, 3.23] although some of the reports claim that they use electrochemical oxidation. In 1859, Brodie was the first to synthesize graphite oxide using slurry of graphite and by adding potassium and nitric acid to it [3.24]. After few years, Staudenmaier, advanced the process by replacing nitric acid with sulfuric acid and fed the chlorates in batches [3.25]. Later, in 1958, Hummers and Offeman proposed an alternative oxidation method [3.26] in which sodium nitrate and potassium permanganate was dissolved in concentrated sulfuric acid for oxidizing graphite into graphite oxide. Their reaction took almost 2 hours but yielded GO at low temperature settings. Throughout the years, a lot of modification has been done to this process to ease the operation and to produce GO that would be viable for mass production [3.27-3.31]. As an example, most recently, Marcano et.al [3.32] replaced sodium nitrate with more of potassium permanganate and concentrated sulfuric acid which led to ease of control in process and resulted in high yield.

Graphene oxide produced after oxidation of graphite is an insulator and is mostly stacked as multiple sheets one on top of the other with a range of size from 1 to 100μm [3.33]. These aggregates can be deoxygenated to form as conductive reduced graphene oxide (rGO) and exfoliated as single sheets. This can be done using thermal reduction at a temperature above 200°C [3.34]. And in order to get single sheets of functionalized and disordered reduced graphene oxide sheets, ultra-sonication was done in an appropriate solution. Through characterizations, it was proven that during thermal reduction, CO/CO_2 and water vapor gets

32

liberated. Figure 3.2 (a) shows the basic schematic of graphene, graphene oxide and reduced graphene oxide [3.35].

It was suggested that the exfoliation of sheets were going through because of the building up of these gases [3.36, 3.37]. So for a complete exfoliation to occur, the gases must diffuse through each sheets and the rate of decomposition must be high during the heating process. Increase in conductivity of films varies in order with change in temperature. If the heating process is slow (0.1-1°C/min), an effective exfoliation might not have happened throughout the sheets and also may lead to vacancy defects by removal of CO/CO_2 and partial restoration of conductive sheets [3.38]. GO can also be reduced using solvo-thermal reduction process where the graphene oxide sheets are dispersed in water and in other solvents [3.39, 3.40]. It can also be reduced electrochemically using electrolytes inside which the GO electrodes are cycled to negative potentials [3.41, 3.42]. Chemical exfoliation with strong reducing agents like sodium borohydride [3.43] and hydrazine hydrate [3.44] has proved to be an effective method to partially restore the conductive lattice and to remove the functional groups to a significant level. Figure 3.2 (b) shows an overall process by which graphite can be synthesized as graphene oxide and can be transformed into reduced graphene oxide. Regardless of progress discussed above, two main problems outstand in all the modifications done: (1) The unavoidable high consumption of intercalating agents and oxides, (2) it is a lengthy process and consumes a lot of time to prepare the end product. These drawbacks result in poor scalability and high cost for practical applications.
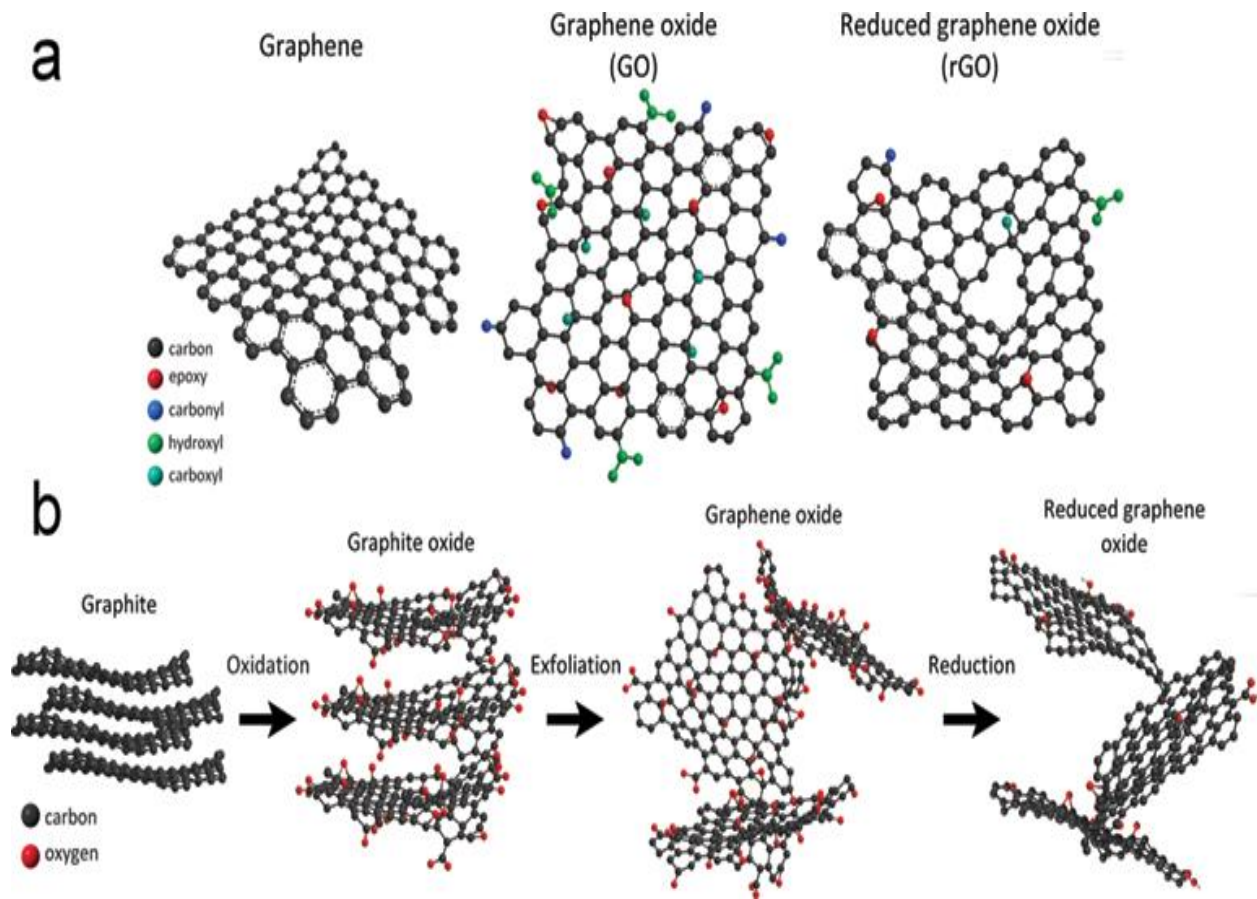
Figure 3.2: (a) Schematics of graphene, GO and rGO. (b) Synthesis of rGO from graphite. [Open access journal, 3.35]

3.1.3 Activated Carbon

Due to the reasons that it is less expensive, possess a high surface area than other carbon materials, have good electrical properties, activated carbon (AC) is used in EDLCs as an electrode material [3.45]. The ACs can be produced from different types of carbonaceous materials (nutshell, wood etc) either by chemical or physical activation. During chemical activation, the material is treated at lower temperature (400-700°C) with the help of activating agents such as potassium hydroxide, sodium hydroxide, phosphoric acid, and zinc chloride [3.46]. Based on activation methods and carbon precursors, AC has a surface area of up to 3000 m^2/g possessing various physiochemical properties. The activation process creates pores in AC

structures and the pore distribution is comprised of micropores (<2nm), mesopores (2-50nm), and macropores (>50nm) [3.47]. Lot of research works has been done to test the discrepancy between surface area and specific capacitance of AC. Although both the parameters are directly proportional to each other, it has been proven that the exhibited capacitance of the device is not an inclusion of all of the high surface area [3.48, 3.49]. This inconsistency is believed to be caused by electrolyte ions which has large pore size and is not able to diffuse completely with the electrode material thereby preventing it from contributing towards the capacitance of the device [3.50-3.52]. In theory, a counteracting relationship surfaces among pore size, power and energy density. Smaller pore size results in higher energy density and large pore size contributes to a higher power density. This variability has led researchers to focus more on the pore sizes of the given material to improve the overall performance of the device [2.53, 3.54]. Efforts also have been made for usage of different kinds of electrolytes to improve the capacitance of AC [3.55].

3.1.4 Molybdenum di-sulfide

The physics of two dimensional (2-D) materials has opened up the possibilities to research materials similar to single layer graphene. These materials can be fashioned as atomic thick layers using state of the art equipment and tools. And the understating of these materials has led the way to explore a wide range of research interests in to these transition metal dichalcogenides (TMDCs) based 2-D materials. In general, TMDCs has a generalized MX_2 compound (M = Transition metal bearing the elements of groups IV, V and VI from the periodic table [3.56-3.58]. The unsaturated d-orbitals present in the transition metals contribute to material's band structure and thereby imploring an array of properties such as magnetism, superconductivity and charge density waves and [3.59, 3.60]. Recently, among TMDCs, Molybdenum disulfide (MoS_2)

has attracted a lot of attention in electrochemical storage applications [3.61] due to their vast availability in nature, high surface area, unique electronic structure, and stable semiconducting properties. In spite of its high catalytic activity and being an efficient hydrogen evolution catalyst [3.62-3.64], they did not receive much attention in the past. But lately, it has been gaining interest for use in energy storage devices and lithium ion batteries [3.65, 3.66] due to its similar characteristics with graphene [3.67]. The material possesses an indirect band gap of 1.23eV when it is in bulk form and increases up to 1.8eV when prepared as monolayer sheets [3.68]. As a monolayer structure, Mo (+4) and S (-2) arranged in a trigonal prismatic arrangement of S-Mo-S atoms [3.69] to form as a sandwiched hexagonal structure, although the sandwich layers are interconnected by relatively weak Van der Waals force as shown in Figure 3.3 (a) and (b). In theory, thickness of each layer is ~0.65 nm with a bond length of 0.24 nm and distance between the sulfur atoms of 0.31 nm [3.70-3.72]. It has a Young's modulus higher than steel because of which the crystal layers could be deformed up to 11% without fracture. As explained earlier, porous carbon materials such as graphene is widely used for several applications due to their high surface area, electronic, and thermal conductivity.

Although bulk materials have been known to exist for several years, scientists predicted that these materials would be too unstable in single layer crystalline form. The "scotch-tape method" serves as a base for fabrication of atomic thick 2-D layered graphene material. Later, other 2-D layered materials such as MoS_2, tungsten sulfide, boron nitride have been fabricated using several methods as one atom thick layer. Mechanical exfoliation of natural bulk MoS_2 was done by sticking the material to a stretched adhesive tape and exfoliating repeatedly by peeling it off of the surface layer by layer. These few layers MoS_2 were investigated through an optical microscope by laying the material on top of a dielectric layer coated substrate. MoS_2 flakes

prepared using this method has pristine crystal structures that can be used only for research

purposes. The yield obtained using this process is very less and the flake sizes vary from few

micrometers to tens of micrometers. Another class of exfoliation named chemical exfoliation is

currently being researched a lot for exfoliating and separating crystalline MoS_2 layers. This

method is being preferred due to its unique physical nature and the range of applications that it

possesses.
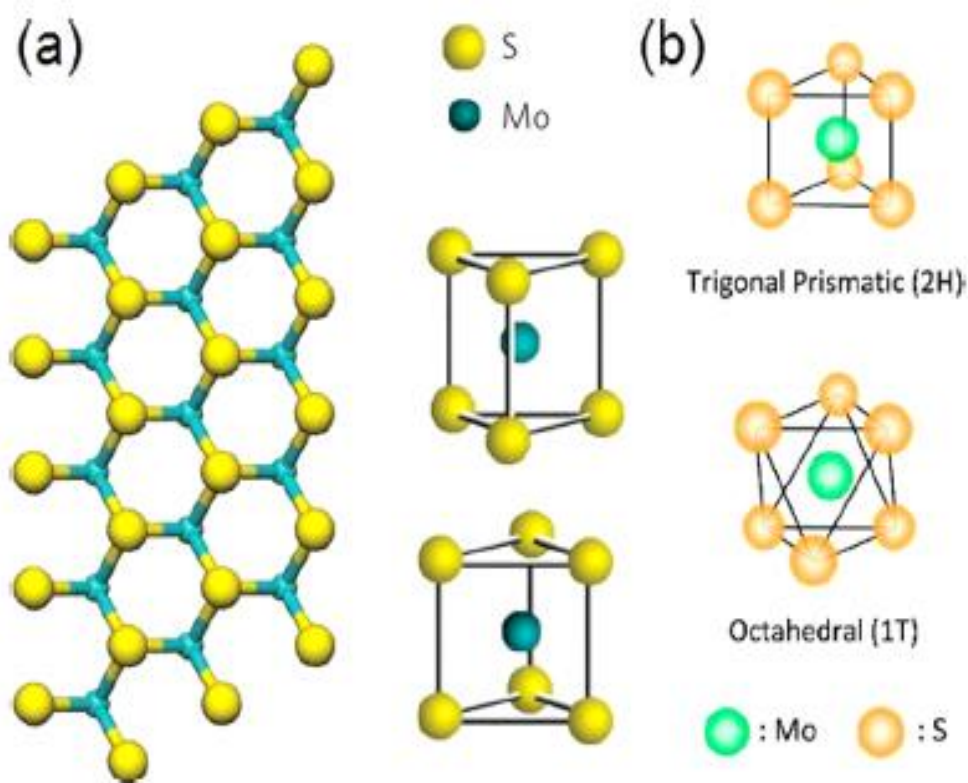
Figure 3.3: Structure of crystal MoS_2 [Reprinted with permission from 3.72].

There are two basic types of exfoliation methods that are widely used now namely solvent based

exfoliation and ion intercalation. In 1986, ion intercalation method [3.73] was proposed in which

insertion of ions between MoS_2 was done to widen the layer gaps as seen in Figure 3.4. N-butyl

lithium in hexane which is a common source of lithium ions was used due to its small ion sizes.

Water was introduced after the lithium ion intercalation, inducing a vigorous reaction which resulted in formation of hydrogen between the MoS_2 layers. But this process is lengthy (up to 3 days) and also the extent to which the intercalation happens cannot be controlled. Zeng et. al.'s exfoliation process [3.74] helped in improving the chemical exfoliation process in which a galvanic cell was setup with MoS_2 as the cathode instead of n-butyl lithium in hexane and lithium foil as anode. Using this technique, a good control over the lithiation process was attained and it yielded high amount of single layer MoS_2 sheets. This process could be completed in few hours instead of days. So, a highly controlled and fast process was reported in to exfoliate a series of TMDC nanosheets. But Coleman et. al. [3.75] was the first to propose a solvent based exfoliation method for $2H$-MoS_2 where the bulk MoS_2 was mixed in organic solvents like isopropyl alcohol and N-methylpyrrolidone (NMP). The reason for using organic solvents is that it will reduce the amount of energy necessary for layer separation. After mixing with these solvents, the mixture was sonicated which resulted in exfoliation of suspended flakes into single or few layer sheets of MoS_2. This process was further enhanced by Coleman later with high power sonication with aqueous surfactant leading to high suspension of flakes (92%) in the solvent [3.76]. This technique can be used for preserving 2-H MoS_2, metallic MoS_2 crystal structure using organic solvents. Chemical exfoliation, in liu with mechanical exfoliation helps in large production of 2-D materials. But the sonication process would affect the 2D lattice structure and break down the flake sizes to a few thousands of nanometers thereby limiting the applications to large scale electronic and integrated circuits.
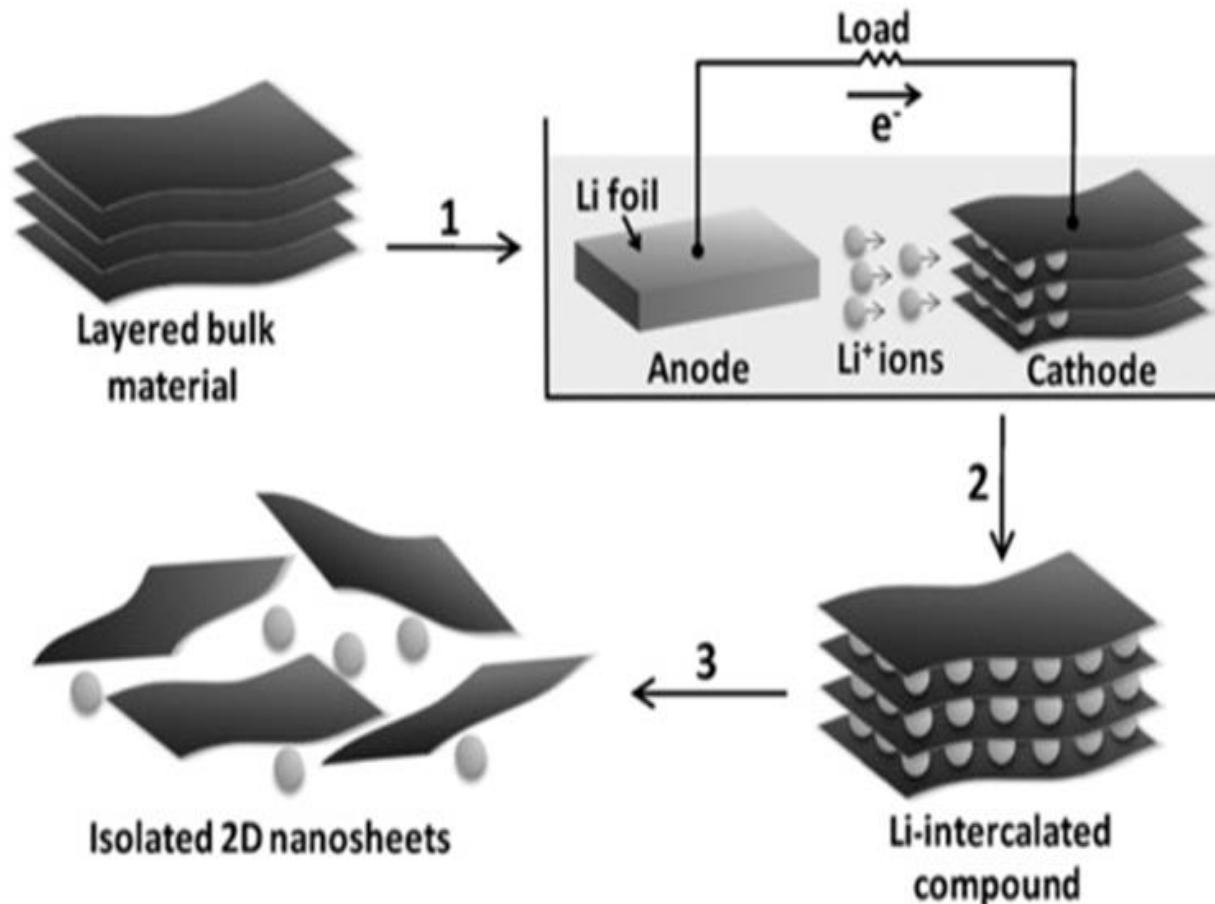
Figure 3.4: Electrochemical lithiation of 2D MoS$_2$ nanosheets [Reprinted with permission from 3.74].

3.2 High performance MoS2−Graphene Composites based Coin Cell Supercapacitors

Two dimensional (2-D) materials, mainly graphene and MoS$_2$ can greatly help in increasing the electrochemical energy storage devices performance by combining the high electrical conductivity and wide surface area. In [3.77], Bisset et. al. has reported the investigation of exfoliated MoS$_2$ for use as electrodes in supercapacitor application with aqueous electrolyte (Na$_2$SO$_4$) solution. By inducing a little of graphene material into the MoS$_2$ network and forming a nanocomposite, resistivity of the material decreased in order leading to increase in specific capacity. In brief, MoS$_2$ dispersion was prepared by liquid exfoliation process using MoS$_2$ powder and N-methyl-2-pyrrolidone (NMP) that was purchased commercially. Both of them

39

were mixed to a certain concentration and sonicated at 20°C. MoS_2 prepared this way is claimed to be stable for months without any sedimentation as shown in Figure 3.5. Later, commercially available graphene powder exfoliated by sonicating it again with NMP solution was mixed along with MoS_2 to form as a composite. This mixture was filtered using a PVDF filter to form membrane sheets with a pore size of 1μm.
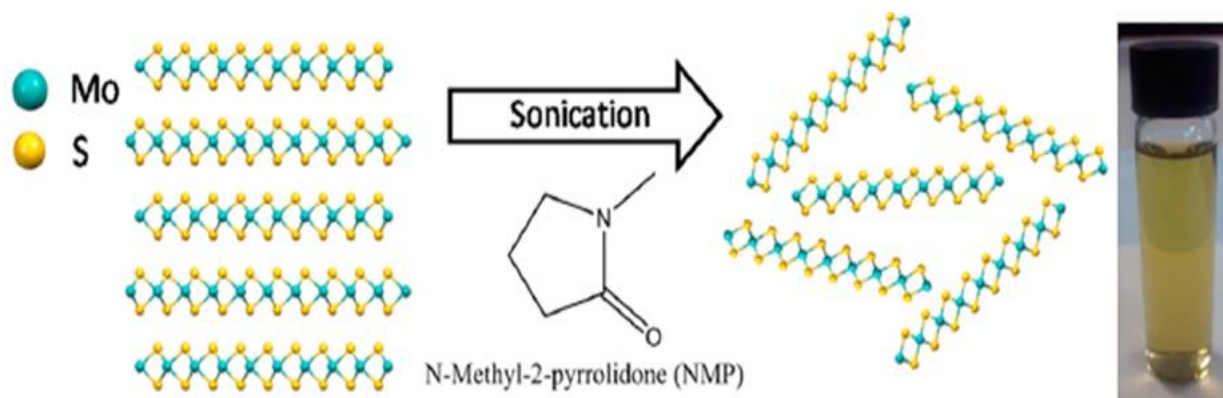
Figure 3.5: Illustration of stable MoS_2 dispersed in NMP using centrifugation process [Reprinted with permission from 3.77].

The composite membranes were prepared in three different ratios of MoS_2/graphene (1:1, 1:3 and 3:1). 1M Na_2SO_4, a neutral electrolyte solution was used in spite of other acid, base and organic electrolytes to avoid hydrogen evolution reaction and increase the stability of the supercapacitor. The main goal of this research is the continued increase in charge/discharge cycles (up to 800%) which is claimed to be a result of ion intercalation of the partially re-exfoliated layered materials. Figure 3.6 shows the percentage of specific capacitance retained during continuous charge/discharge cycles for MoS_2, graphene and the composite membrane for over 10, 000 cycles. Any electrochemical cell requires an initial "preconditioning" where the electrolyte permeates through the pores of the electrode structure and stabilizes. So before the actual test, these membranes were preconditioned up to 200 cycles. As can be seen in Figure 3.6

(a), after preconditioning the MoS_2 membrane, instead of degradation there was an initial large

increase in capacitance for over next 3000 cycles and stabilized gradually for the other 7000

cycles. In the case of graphene, in Figure 3.6 (b), the performance increased for only the first 500

cycles before attaining the stabilization condition. Finally, the composite membrane, unlike other

individual membranes, showed a steady increase in cycling for up to 250% as seen in Figure 3.6

(c), which is claimed to exhibit a good performance in commercial devices.
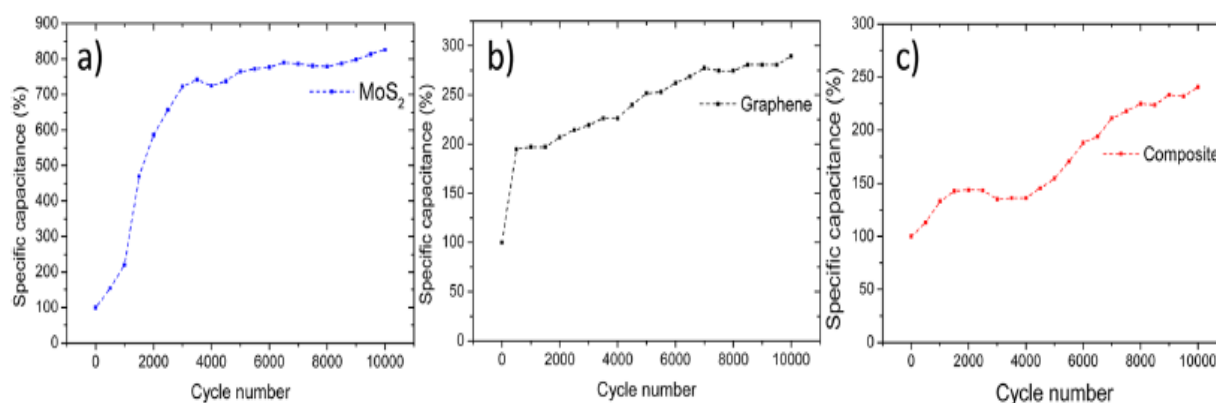
Figure 3.6: Specific capacitance plot that changes during continuous charge/discharge cycles for MoS_2 (a), graphene (b), and composite (1:3) membrane (c) [Reprinted with permission from 3.77].

The Figure 3.7 (a) shows the comparison of cyclic voltammetry (CV) curves for all the three

membranes. CV curves have been used for electrochemical characterization. The capacitive

behavior of a device can be determined using the loop size of the CV curve. The wider the

hysteresis loop of the CV curve, the higher will be the capacitance. In this study, the CV curve of

the composite is much wider in comparison to individual electrodes indicating an improved

capacitive behavior. The calculated specific capacitance in response to increasing scan rates were

measured during pre and post charge/discharge cycles as shown in Figure 3.7 (b). It can be seen

that before cycling, capacitance has reduced for both MoS_2 and graphene membranes by 80 and

43%, respectively, as the scan rate increases from 5mV/s to 1000mV/s. The composite

membrane also has about 80% decrease in capacitance at the end of 1000mV/s scan rate, but the overall capacitance always remained higher than the individual membranes accrediting to prevention of restacking and continuous physical interaction between MoS_2 and graphene. Attributing to "electroactivation", the capacitance of all the membranes were found to increase during post cycling. The composite membrane had retained more than 37% and 25% capacitance in comparison to individual graphene and MoS_2 membranes, respectively.
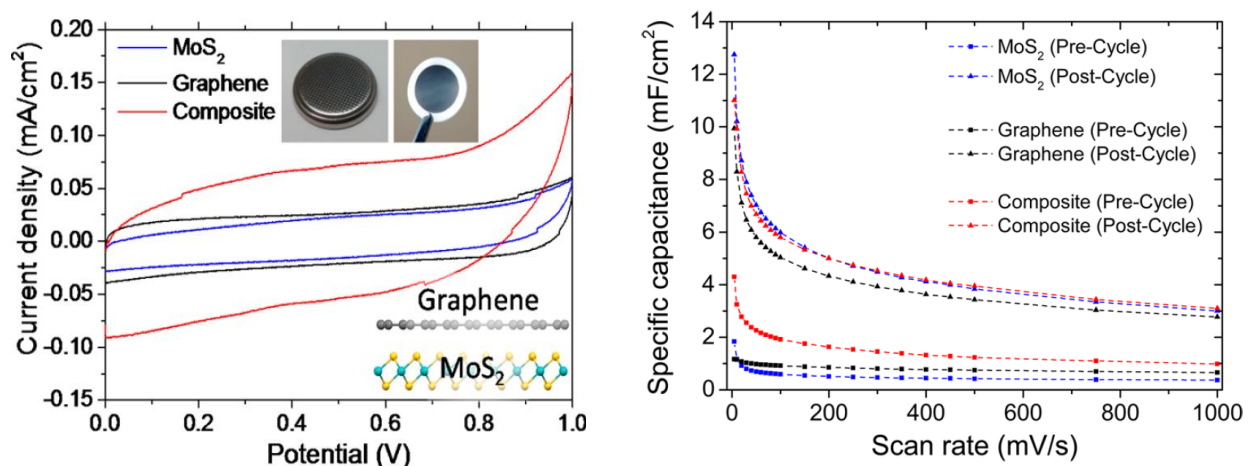
Figure 3.7: Plot showing (a) cyclic voltammograms (CVs) and (b) specific capacitance of coin cells at different scan rates having MoS_2, graphene, and composite membranes (1:3) [Reprinted with permission from 3.77].

3.3 Synergistic energy storage of MoS2 based nanocomposite for supercapacitor application

The two dimensional transition metal dichalcogenide MoS_2/graphene nanocomposites has attracted a lot of attention due to its unique tailoring of materials, high faradaic activity, and electronic properties. In this study, a facile one step process of highly uniform MoS_2/graphene composite and its electrochemical performances are discussed [3.78]. In brief, graphene oxide was synthesized using modified Hummer's method from natural graphite. After synthesizing, the material was reduced with citric acid using hydrothermal method to obtain graphene sheets. The synthesis of multilayer MoS_2/graphene nanocomposite is shown in Figure 3.8 where a mixture of

0.6g thioactetamide, 0.98g of ammonium heptamolybdate tetrahydrate and 0.38g of citric acid was dissolved in 40ml deionized (DI) water and stirred continuously. After stirring and sonicating for 30mins, the solution was poured in to a Teflon-lined stainless steel autoclave and heated up to 180°C for 24 hours. After cooling down, the black precipitate that was formed was collected using centrifuge and the final nanocomposite was obtained as a powder by drying at 60°C for 24hours.
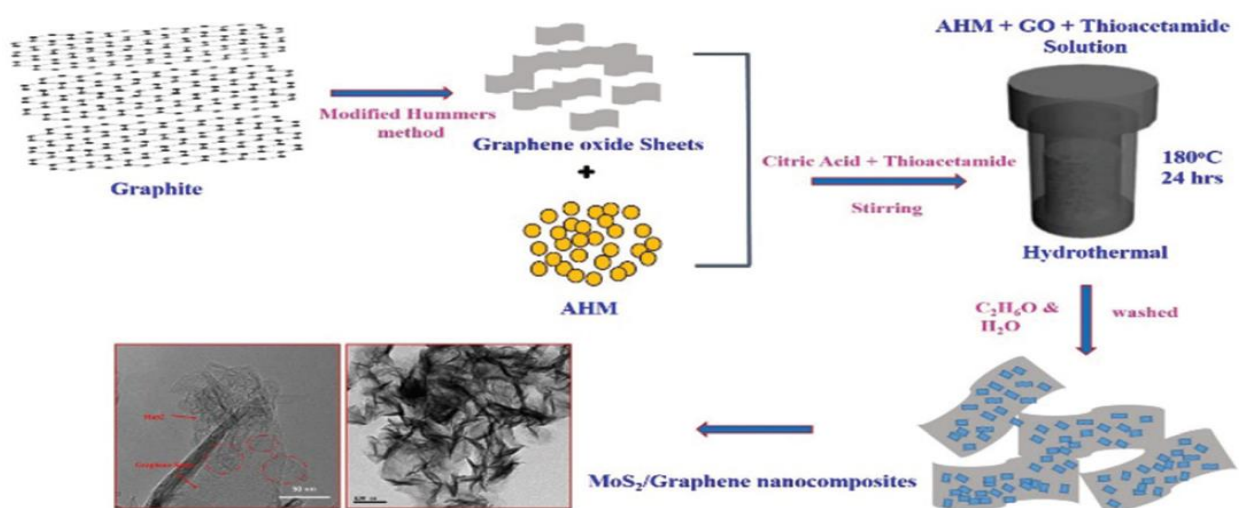
Figure 3.8: Schematic of layered MoS$_2$/Graphene nanocomposite synthesis [Reprinted with permission from 3.78].

A three electrode setup was used for investigating the electrochemical performance of electrodes where the active material was the working electrode, platinum foil acted as the counter electrode, and Ag/Agcl as the reference electrode. According to this study, synergistic effect of metal oxide and graphene helped in enhancing the specific capacitance of the material. To analyze the prospective of the electrode materials and the nanocomposite, galvanostatic charge/discharge measurements were done. As seen in Figure 3.9 (a) and (b), in charging and discharging steps, the charging curve is in symmetry with the discharge curve for the GO material but for the

nanocomposite there is a slight curvature at the end of the discharge curve which indicates high reversibility of the material.

The specific capacitances of the nanocomposite measured at different current densities (0.1 to 1 A/g) with intervals of 0.1 A/g were 270, 240, 180, 155, 126 and 90 F/g. All the measurements were done using 1M Na_2SO_4 as electrolyte solution. The maximum specific capacitance of 270 F/g was obtained at 0.1 A/g for the composite is comparatively higher than the capacitance measured with MoS_2 nanosheets (162.5 F/g). The capacitances decreased gradually for both kinds of electrodes in response to increasing current densities, At all recorded current densities, the capacitances of MoS_2 nanosheets were found to be less than the composite as shown in Figure 3.9 (c). The boosting of capacitance value for the composite is attributed to graphene's electrical conductivity in the material. Graphene is responsible for the fast electron transfer owning to a good electronic conductive channel throughout the electrodes and further leading to high electrochemical performance [3.79, 3.80].

Ragone plot is the most resourceful way to determine the supercapacitive nature of every individual electrode materials. It has been reported that the energy and power density of the composite were found to be in the range of 1 to 15Wh/Kg and 200 to 1500W/Kg, respectively as shown in Figure 3.9 (d). Some of the disadvantages of this particular study is that the process followed to synthesize all the electrode materials (GO and MoS_2) and the composite involves complex chemical process methods and also is time consuming. In spite of all the process done, the maximum current density at which the material can be charged/ discharged is very less (only a maximum of 1 A/g). And also the maximum power density was only reported to be 2500 W/Kg at the highest current density for the composite material. From this we can conclude that a less

complicated process involving less toxic chemicals for the synthesis of the electrode materials can be designed and still attain a comparatively better electrochemical performance.

(a)

(b)

(c)

(d)
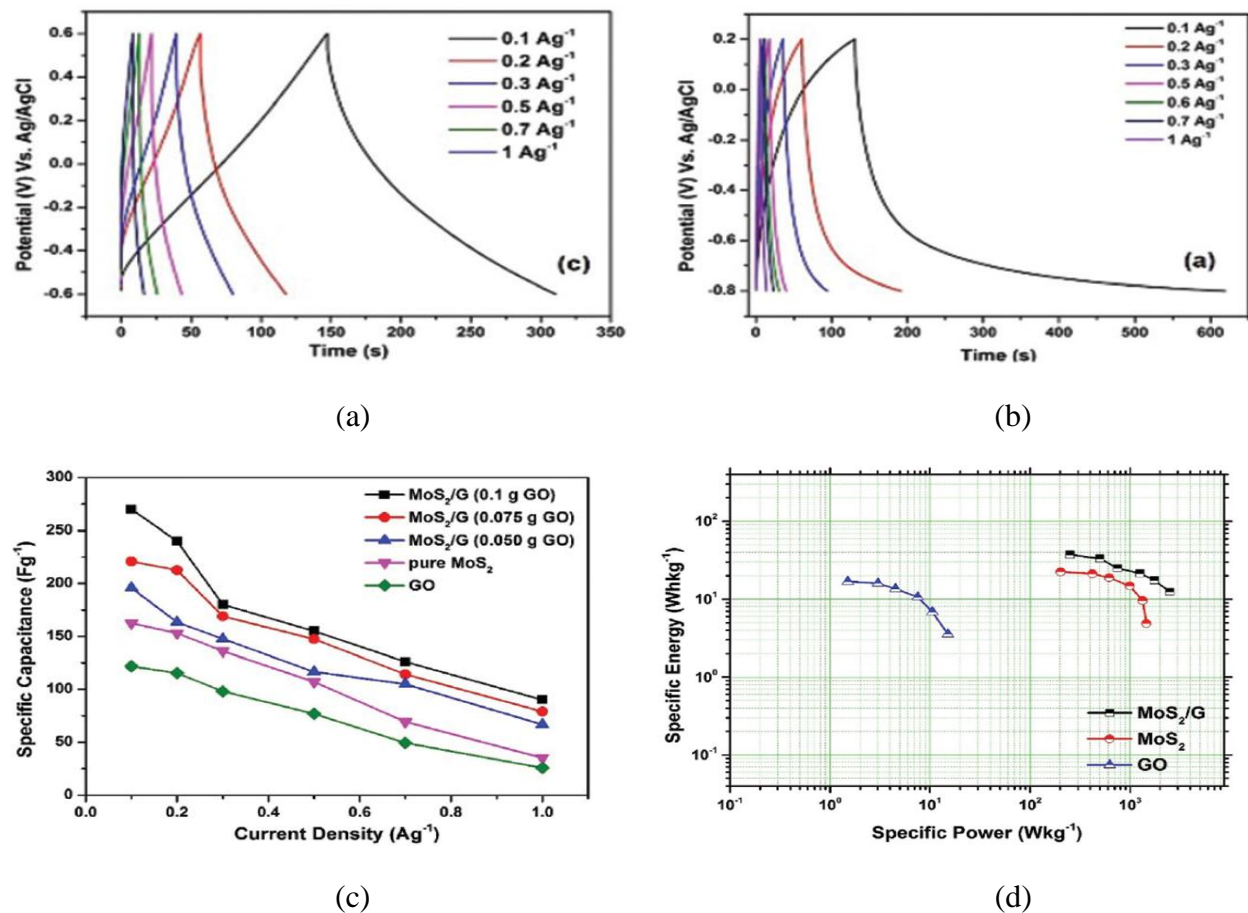
Figure 3.9: Galvanostatic charge/discharge curves of (a) GO and (b) MoS_2/Graphene composite, (c) Specific Capacitance and (d) Ragone plot of MoS_2/Graphene, pure MoS_2 and GO [Reprinted with permission from 3.78].

3.4 Electrochemical performance of activated carbon using various aqueous electrolyte solutions

In a supercapacitor, apart from depending on the surface area of the electrodes, the electrochemical behavior is also bound on solvated ion sizes of the electrolytes and pore distribution of the electrodes. In this study, electrochemical performances of electrodes are investigated based on three electrolyte solutions namely, lithium sulfate, sodium sulfate and potassium sulfate with different ion sizes. Theoretically, the equivalent series resistance (ESR)

45

can be determined with the help of output power. But, in practical, electrochemical impedance spectroscopy (EIS) can be used to assess the ESR of the electrodes [3.81]. Nyquist plot in Figure 3.10 (a) and (b) shows the comparison of ESR evaluated using EIS techniques for the above mentioned three electrolytes with activated carbon as the electrode. For all the samples, with different electrolytes, the Nyquist plot is nearly vertical at low frequency and is a semicircle at high frequencies. In most cases, the nearly vertical lines at low frequencies indicate that the sample is highly capacitive with low transfer resistance existing between the carbon electrode and the electrolyte.

(a)   (b)
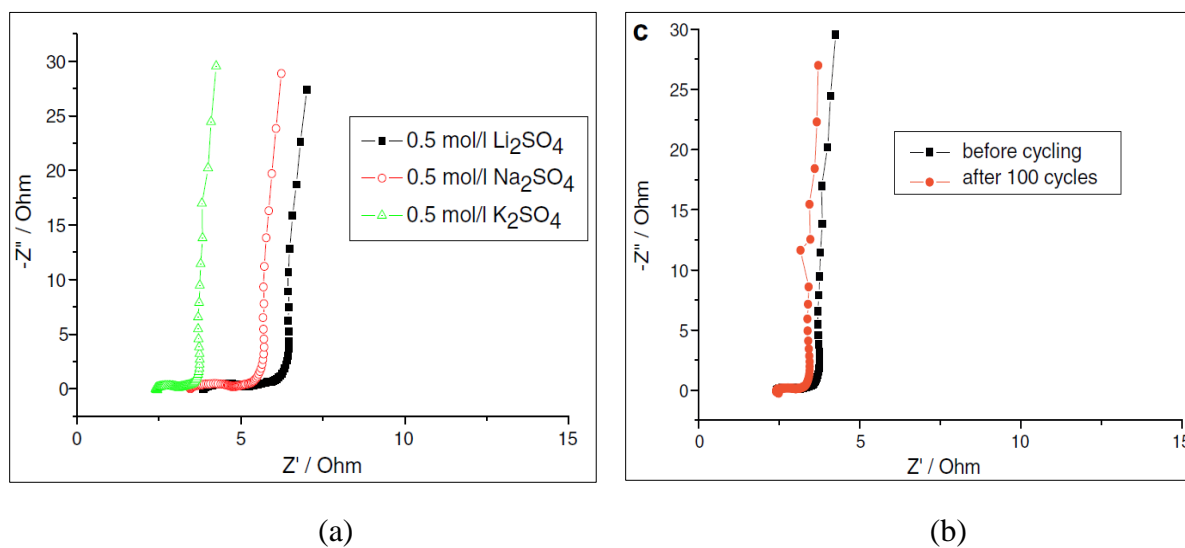
Figure 3.10: Nyquist plots at open-circuit voltage (a) in 0.5 M aqueous Li_2SO_4, Na_2SO_4 and K_2SO_4 electrolyte and (b) before and after 100 cycles in 0.5 M K_2SO_4 aqueous electrolyte [Reprinted with permission from 3.81].

At high frequencies, the capacitive behavior can be identified by the diameter size of the semicircle, the smaller the diameter of the semicircle, the higher the capacitance. Based on the impedance curve, the capacitance is in the order of $K_2SO_4 > Na_2SO_4 > Li_2SO_4$. This result indirectly reflects on the fact that for all the three electrolytes, the ESR value decreases in the order of $K_2SO_4 < Na_2SO_4 < Li_2SO_4$. Figure 3.11 shows the change in specific capacitance at different scan rates. As can be observed, the capacitance decreases with an increase in scan rate

for electrodes with all three kinds of electrolytes. Among all the electrolytes, capacitance of

Li_2SO_4 based supercapacitor fades away faster as scan rate increases and fades away slowly

while using K_2SO_4. The reason behind this kind of a behavior is attributed to the particle size of

the electrolytes. K_2SO_4 electrolyte has smaller particle size than that of the other two electrolytes

comparatively. This helps in interactions of the electrolytes easily with active spots of the

electrodes thereby leading to an increase in the conductivity of the supercapacitor.
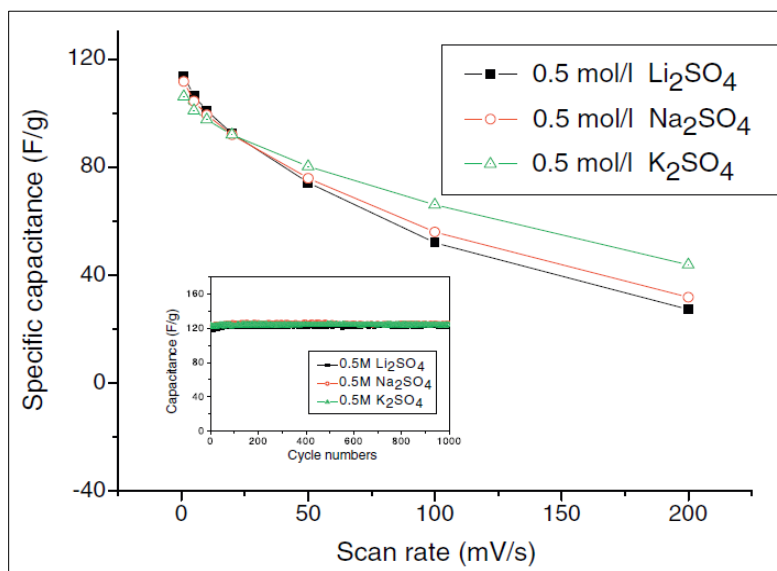
Figure 3.11: Capacitance variations of AC in 0.5 M aqueous Li_2SO_4, Na_2SO_4 and K_2SO_4 electrolytes [Reprinted with permission from 3.81].

3.5 References

3.1 Doran. N. J, "Electronic Structure and Band Theory of Transition Metal Dichalcogenides", Physica BþC, 99, 227–237 (1980).

3.2 Wonbong Choi, Jo-won Lee, "Graphene: Synthesis and Applications", CRC Press, Taylor & Francis Group, Boca Raton (2012).

3.3 Siegfried Eigler, Andreas Hirsch, "Chemistry with Graphene and Graphene Oxide – Challenges for Synthetic Chemists", Angew Chem Int Ed., 53, 2–21 (2014).

3.4 Vineyard. G. H, Dienes. G. J, "The Theory of Defect Concentration in Crystals", Physical Review, 93(2), 265-268 (1954).

3.5 Novoselov. K. S, Geim. A. K, Morozov. S. V, Jiang. D, Zhang. Y, Dubonos. S. V, Grigorieva. I. V, Firsov. A. A, "Electric Field Effect in Atomically Thin Carbon Films", Science, 306(5696), 666-669 (2004).

3.6 Novoselov. K. S, Jiang. D, Schedin. F, Booth. T. J, Khotkevich. V. V, Morozov. S. V, Geim. A. K, "Two-dimensional atomic crystals", Proceedings of the National Academy of Sciences of the United States of America, 102(30), 10451-10453 (2005).

3.7 Alfonso Reina, Xiaoting Jia, John Ho, Daniel Nezich, Hyungbin Son, Vladimir Bulovic, Mildred S. Dresselhaus, Jing Kong, "Large Area, Few-Layer Graphene Films on Arbitrary Substrates by Chemical Vapor Deposition", Nano Letters, 9(1), 30-35 (2008).

3.8 Jonathan N. Coleman, "Liquid Exfoliation of Defect-Free Graphene", *Acc. Chem. Res.*, *46* (1), 14–22 (2013).

3.9 Shun Mao, Haihui Pu, Junhong Chen, "Graphene oxide and its reduction: modeling and experimental progress", RSC Advances, 2(7), 2643-2662 (2012).

3.10 Ulrich Hofmann, Rudolf Holst, "Über die Säurenatur und die Methylierung von Graphitoxy", *Berichteder deutschen chemischen Gesellschaft (A and B Series),* 72(4), 754-771 (1939).

3.11 Scholtz. W, Boehm. H. P, "Untersuchungen am Graphitoxid. VI. Betrachtungen zur Struktur des Graphitoxids", Anorg. Allg. Chem, 369, 327-340 (1969).

3.12 Anton Lerf, Heyong He, Michael Forster, Jacek Klinowski, "Structure of Graphite Oxide Revisited", The Journal of Physical Chemistry B, 102(23), 4477-4482 (1998).

3.13 Heyong He, Thomas Riedl, Anton Lerf, Jacek Klinowski, "Solid-State NMR Studies of the Structure of Graphite Oxide", The Journal of Physical Chemistry, 100(51), 19954-19958 (1996).

3.14 Tamás Szabó, Ottó Berkesi, Péter Forgó, Katalin Josepovits, Yiannis Sanakis, Dimitris Petridis, Imre Dékány, "Evolution of Surface Functional Groups in a Series of

Progressively Oxidized Graphite Oxides", Chemistry of Materials, 18(11), 2740-2749 (2006).

3.15 Lee, D.W, Seo. J. W, "sp2/sp3 Carbon ratio in graphite oxide with different preparation times", The Journal of Physical Chemistry C, 115(6) 2705-2708 (2011).

3.16 Seiji Obata, Koichiro Saiki, Takaaki Taniguchi, Toshihiro Ihara, Yusuke Kitamura, Yasumichi Matsumoto, "Graphene Oxide: A Fertile Nanosheet for Various Applications", J Phys Soc Japan. 84, 121012 (2015).

3.17 Ruiguang Xing, Yanan Li, Huitao Yu, "Preparation of fluoro-functionalized graphene oxide via the Hunsdiecker reaction", Chem Commun. 52, 390–393 (2016).

3.18 Zdenko Spitalsky, Martin Danko, Jaroslav Mosnacek, "Preparation of functionalized graphene sheets", Curr Org Chem, 15, 1133–1150 (2011).

3.19 Daniel R. Dreyer, Sungjin Park, Christopher W. Bielawski, Rodney S. Ruoff, "The chemistry of graphene oxide", Chem Soc Rev. 39, 228–240 (2010).

3.20 Ayrat M. Dimiev, James M. Tour, "Mechanism of Graphene Oxide Formation" ACS Nano. 8, 3060–3068 (2014).

3.21 Sajjad Shamaila, Anum Iqbal, "Modifications in development of graphene oxide synthetic routes", Chem Eng J. 294, 458–477 (2016).

3.22 Adriano Ambrosi, Martin Pumera, "Electrochemically Exfoliated Graphene and Graphene Oxide for Energy Storage and Electrochemistry Applications", Chem Eur J. 22, 153–159 (2016).

3.23 Arshad Hussain Wazir, Imran Waseem Kundi, "Synthesis of Graphene Nano Sheets by the Rapid Reduction of Electrochemically Exfoliated Graphene Oxide Induced by Microwaves", J Chem Soc Pak. 38, 11–16 (2016).

3.24 Brodie, B. C, "The Atomic Weight of Graphite", Philos Trans R Soc London 14, 249–259 (1859).

3.25 Staudenmaier, L.Verfahren zur Darstellung der Graphitsäure. Ber Dtsch Chem Ges. 31, 1481–1487 (1898).

3.26 William S. Hummers Jr., Richard E. Offeman, "Preparation of Graphitic Oxide", J Am Chem Soc. 80, 1339 (1958).

3.27 Ji Chen, Bowen Yao, Chun Li, Gaoquan Shi, "An improved Hummers method for eco-friendly synthesis of graphene oxide", Carbon, 64, 225–229 (2013).

3.28 Huitao Yu, Bangwen Zhang, Chaoke Bulin, Ruihong Li, Ruiguang Xing, "High-yield preparation of graphene oxide from small graphite flakes via an improved Hummers method with a simple purification process", Carbon, 81, 826–834 (2015).

3.29 Jiaojiao Sun, Ningxin Yang, Zhe Sun, Mengqi Zeng, Lei Fu, Chengguo Hu, Shengshui Hu, "Fully Converting Graphite into Graphene Oxide Hydrogels by Preoxidation with Impure Manganese Dioxide", ACS Appl Mater Interfaces, 7, 21356–21363 (2015).

3.30 Liou Yan-Jia, Tsai Bo-Da, Huang Wu-Jang, "An economic route to mass production of graphene oxide solution for preparing graphene oxide papers" Mater Sci and Eng B, 193, 37–40 (2015).

3.31 Li Peng, Zhen Xu, Zheng Liu, Yangyang Wei, Haiyan Sun, Zheng Li, Xiaoli Zhao, Chao Gao, "An iron-based green approach to 1-h production of single-layer graphene oxide", Nature Comm., 6, 5716 (2015).

3.32 Daniela C. Marcano, Dmitry V. Kosynkin, Jacob M. Berlin, Alexander Sinitskii, Zhengzong Sun, Alexander Slesarev, Lawrence B. Alemany, Wei Lu, James M. Tour, "Improved synthesis of graphene oxide", ACS Nano, 4, 4806–4814 (2010).

3.33 Shuyang Pan, Ilhan A. Aksay, "Factors Controlling the Size of Graphene Oxide Sheets Produced via the Graphite Oxide Route", ACS Nano, 5(5), 4073-4083 (2011).

3.34 Boehm. H.P, Clauss. A, Fischer. G, Hofmann. U, "Surface Properties of Extremely Thin Graphite Lamellae", Proceedings of the Fifth Conference of Carbon (1961).

3.35 Edgar Jimenez-Cervantes Amieva, Juventino López-Barroso, Ana Laura Martínez-Hernández and Carlos Velasco-Santos, "Graphene-Based Materials Functionalization with Natural Polymeric Biomolecules", Recent Advances in Graphene Research, Dr. Pramoda Nayak (Ed.), InTech, (2016).

3.36 Hannes C. Schniepp, Je-Luen Li, Michael J. McAllister, Hiroaki Sai, Margarita Herrera-Alonso, Douglas H. Adamson, Robert K. Prud'homme, Roberto Car, Dudley A. Saville, Ilhan A. Aksay, "Functionalized single graphene sheets derived from splitting graphite oxide", Journal of Physical Chemistry B, 110(17), 8535-8539 (2006).

3.37 Michael J. McAllister, Je-Luen Li, Douglas H. Adamson, Hannes C. Schniepp, Ahmed A. Abdala, Jun Liu, Margarita Herrera-Alonso, David L. Milius, Roberto Car, Robert K. Prud'homme, Ilhan A. Aksay, "Single sheet functionalized graphene by oxidation and thermal expansion of graphite" Chemistry of Materials, 19(18), 4396-4404 (2007)

3.38 Konstantin N. Kudin, Bulent Ozbas, Hannes C. Schniepp, Robert K. Prud'homme, Ilhan A. Aksay, Roberto Car, "Raman spectra of graphite oxide and functionalized graphene sheets", Nano Letters, 8(1), 36-41 (2008).

3.39 Yong Zhou, Qiaoliang Bao, Lena Ai Ling Tang, Yulin Zhong, Kian Ping Loh, "Hydrothermal Dehydration for the "Green" Reduction of Exfoliated Graphene Oxide to Graphene and Demonstration of Tunable Optical Limiting Properties", Chemistry of Materials, 21(13), 2950-2956 (2009).

3.40 Hailiang Wang, Joshua Tucker Robinson, Xiaolin Li, Hongjie Dai, "Solvothermal Reduction of Chemically Exfoliated Graphene Sheets", Journal of the American Chemical Society, 131(29), 9910-9911 (2009).

3.41 Yuyan Shao, Jun Wang, Mark Engelhard, Chongmin Wang, Yuehe Lin, "Facile and controllable electrochemical reduction of graphene oxide and its applications", Journal of Materials Chemistry, 20(4), 743-748 (2010).

3.42 Zhijuan Wang, Xiaozhu Zhou, Juan Zhang, Freddy Boey, Hua Zhang, "Direct Electrochemical Reduction of Single-Layer Graphene Oxide and Subsequent functionalization with Glucose Oxidase", Journal of Physical Chemistry C, 113(32), 14071-14075 (2009).

3.43 Hyeon-Jin Shin, Ki Kang Kim, Anass Benayad, Seon-Mi Yoon, Hyeon Ki Park, In-Sun Jung, Mei Hua Jin, Hae-Kyung Jeong, Jong Min Kim, Jae-Young Choi, Young Hee Lee, "Efficient Reduction of Graphite Oxide by Sodium Borohydride and Its Effect on Electrical Conductance", Advanced Functional Materials, 19(12), 1987-1992 (2009).

3.44 Sasha Stankovich, Dmitriy A. Dikin, Richard D. Piner, Kevin A. Kohlhaas, Alfred Kleinhammes, Yuanyuan Jia, Yue Wu, Son Binh T. Nguyen, Rodney S. Ruoff, "Synthesis of graphene-based nanosheets via chemical reduction of exfoliated graphite oxide", Carbon, 45(7), 1558-1565 (2007).

3.45 Nirwan Syarif, Ivandini Tribidasari. A, Widayanti Wibowo, "Direct Synthesis Carbon/Metal Oxide Composites for Electrochemical Capacitors Electrode", *Int. Transaction J. Eng. managemen & Applied Sci. & Tech*., 3, 21 (2012).

3.46 Pandolfo. A. G, Hollenkamp. A. F, "Carbon properties and their role in supercapacitors", J. Power Sources, 157, 11-27 (2006).

3.47 Ting Lee, Chee-Heong Ooi, Radzali Othman, Fei-Yee Yeoh, "Activated carbon fiber – The hybrid of carbon fiber and activated carbon", Rev. Adv. Mater. Sci., 36, 118-136 (2014).

3.48 Elzbieta Frackowiak, Francois Beguin, "Carbon materials for the electrochemical storage of energy in capacitors." Carbon, 39(6), 937-950 (2001).

3.49 Arbizzani. C, Mastragostino. M, Soavi. F, "New trends in electrochemical supercapacitors", Journal of Power Sources, 100(1-2), 164-170 (2001).

3.50 Deyang Qu, Hang Shi, "Studies of activated carbons used in double-layer capacitors", Journal of Power Sources, 74(1), 99-107 (1998).

3.51 Gamby. J, Taberna. P. L, Simon. P, Fauvarque. J. F, Chesneau. M, "Studies and characterisations of various activated carbons used for carbon/carbon supercapacitors", Journal of Power Sources, 101(1), 109-116 (2001).

3.52 Hang Shi, "Activated carbons and double layer capacitance", Electrochimica Acta, 41(10), 1633-1639 (1996).

3.53 Katarzyna Lota, Agnieszka Sierczynska, Ilona Acznik, "Effect of aqueous electrolytes on electrochemical capacitor capacitance", Chemik, 67, 1138 (2013).

3.54 Lufrano. F, Staiti. P, "Mesoporous Carbon Materials as Electrodes for Electrochemical Supercapacitors", Int. J. Electrochem. Sci., 5, 903 (2010).

3.55 Cheng Zhong, Yida Deng, Wenbin Hu, Jinli Qiao, Lei Zhang, Jiujun Zhang, "A review of electrolyte materials and compositions for electrochemical supercapacitors", Chem. Soc. Rev., 44, 7484 (2015).

3.56 Yoffe. A. D, "Electronic Properties of Low Dimensional Solids: The Physics and Chemistry of Layer Type Transition Metal Dichalcogenides and Their Intercalate Complexes", Solid State Ionics, 39, 1–7 (1990).

3.57 Yoffe. A. D, "Electronic Properties of Two Dimensional Solids: The Layer Type Transition Metal Dichalcogenides", Springer: Berlin, 13, 129 (1973).

3.58 Castro Neto. A. H, "Charge Density Wave, Superconductivity, and Anomalous Metallic Behavior in 2D Transition Metal Dichalcogenides", Phys. Rev. Lett., 86, 4382– 4385 (2001).

3.59 Lieth. R. M. A, Terhell. J. C. J. M, "Transition Metal Dichalcogenides", Springer: Berlin, 141223 (1977).

3.60 Xue Yang, Hao Niu, He Jiang, Qian Wang, Fengyu Qu, "A high energy density all-solid-state asymmetric supercapacitor based on MoS2/graphene nanosheets and MnO2/graphene hybrid electrodes", J. Mater. Chem. A, 4, 11264–11275 (2016).

3.61 Thomas F. Jaramillo, Kristina P. Jørgensen, Jacob Bonde, Jane H. Nielsen, Sebastian Horch, Ib Chorkendorff, "Identification of Active Edge Sites for Electrochemical H2 Evolution from MoS2 Nanocatalysts", Science, 317 (5834), 100−102 (2007).

3.62 Laura Guardia, Juan I. Paredes, José M. Munuera, Silvia Villar-Rodil, Miguel Ayán-Varela, Amelia Martínez-Alonso, Juan M. D. Tascón, "Exfoliated MoS2 Nanosheets as Efficient Catalysts for Electrochemical Hydrogen Evolution", Electrochim. Acta, 109 (0), 269−275 (2013).

3.63 Mark A. Lukowski, Andrew S. Daniel, Fei Meng, Audrey Forticaux, Linsen Li, Song Jin, "Enhanced Hydrogen Evolution Catalysis from Chemically Exfoliated Metallic MoS2 Nanosheets", J. Am. Chem. Soc., 135 (28), 10274−10277 (2013).

3.64 Haotian Wang, Zhiyi Lu, Shicheng Xu, Desheng Kong, Judy J. Cha, Guangyuan Zheng, Po-Chun Hsu, Kai Yan, David Bradshaw, Fritz B. Prinz, Yi Cui, "Electrochemical Tuning of Vertically Aligned MoS2 Nanofilms and Its Application in Improving Hydrogen Evolution Reaction", Proc. Natl. Acad. Sci., 110 (49), 19701−19706 (2013).

3.65 Tyler Stephenson, Zhi Li, Brian Olsen, David Mitlin, "Lithium Ion Battery Applications of Molybdenum Disulfide (MoS_2) Nanocomposites", Energy Environ. Sci., 7 (1), 209−231 (2014).

3.66 Lamuel David, Romil Bhandavat, Gurpreet Singh, "MoS_2/Graphene Composite Paper for Sodium-Ion Battery Electrodes", ACS Nano, 8 (2), 1759−1770 (2014).

3.67 Min-Rui Gao, Yun-Fei Xu, Jun Jiang, Shu-Hong Yu, "Nanostructured Metal Chalcogenides: Synthesis, Modification, and Applications in Energy Conversion and Storage Devices" Chem. Soc. Rev., 42 (7), 2986−3017 (2013).

3.68 Martin Pumera, Zdeněk Sofer, Adriano Ambrosi, "Layered Transition Metal Dichalcogenides for Electrochemical Energy Generation and Storage", J. Mater. Chem. A, 2, 8981−8987 (2014).

3.69 Deep Jariwala, Vinod K. Sangwan, Lincoln J. Lauhon, Tobin J. Marks, Mark C. Hersam, "Emerging Device Applications for Semiconducting Two-Dimensional Transition Metal Dichalcogenides", *ACS Nano*, 8 (2), 1102–1120 (2014).

3.70 Ataca. C, Sahin. H, Ciraci. S, "Stable, Single-Layer MX_2 Transition-Metal Oxides and Dichalcogenides in a Honeycomb-like Structure", J. Phys. Chem. C, 116, 8983–8999 (2012).

3.71 Ataca. C, Topsakal. M, Aktürk. E, Ciraci. S, "A Comparative Study of Lattice Dynamics of Three- and TwoDimensional MoS_2", J. Phys. Chem. C, 115, 16354– 16361 (2011).

3.72 Rudren Ganatra, Qing Zhang, "Few-Layer MoS_2: A Promising Layered Semiconductor", *ACS Nano*, 8 (5), 4074–4099 (2014).

3.73 Per Joensen, FrindtS. R. F, Roy Morrison, "Single-Layer MoS_2", Mater. Res. Bull., 21, 457–461 (1986).

3.74 Zhiyuan Zeng, Zongyou Yin, Xiao Huang, Hai Li, Qiyuan He, Gang Lu, Freddy Boey, Hua Zhang, "Single-Layer Semiconducting Nanosheets: High-Yield Preparation and Device Fabrication", Angew. Chem., Int. Ed., 50, 11093–11097 (2011).

3.75 Jonathan N. Coleman, Mustafa Lotya, Arlene O'Neill, Shane D. Bergin, Paul J. King, Umar Khan, Karen Young, Alexandre Gaucher, Sukanta De, Ronan J. Smith, Igor V. Shvets, Sunil K. Arora, George Stanton, Hye-Young Kim, Kangho Lee, Gyu Tae Kim, Georg S. Duesberg, Toby Hallam, John J. Boland, Jing Jing Wang, John F. Donegan, Jaime C. Grunlan, Gregory Moriarty, Aleksey Shmeliov, Rebecca J. Nicholls, James M. Perkins, Eleanor M. Grieveson, Koenraad Theuwissen, David W. McComb, Peter D. Nellist, Valeria Nicolosi, "Two-Dimensional Nanosheets Produced by Liquid Exfoliation of Layered Materials", Science, 331, 568–571 (2011).

3.76 Ronan J. Smith, Paul J. King, Mustafa Lotya, Christian Wirtz, Umar Khan, Sukanta De, Arlene O'Neill, Georg S. Duesberg, Jaime C. Grunlan, Gregory Moriarty, Jun Chen, Jiazhao Wang, Andrew I. Minett, Valeria Nicolosi, Jonathan N. Coleman, "Large-Scale

Exfoliation of Inorganic Layered Compounds in Aqueous Surfactant Solutions". Adv. Mater., 23, 3944–3948 (2011).

3.77 Mark A. Bissett, Ian A. Kinloch, Robert A. W. Dryfe, "Characterization of MoS2−Graphene Composites for High-Performance Coin Cell Supercapacitors", ACS Appl. Mater. Interfaces, 7, 17388−17398 (2015).

3.78 Thangappan. R, Kalaiselvam. S, Elayaperumal. A, Jayavel. R, Arivanandhan. M, Karthikeyan. R, Hayakawa. Y, "Graphene decorated with MoS2 nanosheets: a synergetic energy storage composite electrode for supercapacitor applications", Dalton Trans., 45, 2637 (2016).

3.79 Jun Yan, Zhuangjun Fan, Tong Wei, Weizhong Qian, Milin Zhang, Fei Wei, "Fast and reversible surface redox reaction of graphene–MnO2 composites as supercapacitor electrodes", Carbon, 48 (13), 3825–3833 (2010).

3.80 Shubin Yang, Xinliang Feng, Sorin Ivanovici, Klaus Müllen, Fabrication of Graphene-Encapsulated Oxide Nanoparticles: Towards High-Performance Anode Materials for Lithium Storage", Angew. Chem., Int. Ed., 49, 8408–8411 (2010).

3.81 Qu. Q.T, Wang. B, Yang. L.C, Shi. Y, Tian. S, Wu. Y.P, "Study on electrochemical performance of activated carbon in aqueous Li2SO4, Na2SO4 and K2SO4 electrolytes", Electrochemistry Communications, 10, 1652–1655 (2008).

4. Synthesis and assembly of MoS2-reduced graphene oxide based supercapacitor to boost the capacitance and energy density.

4.1 Introduction

In this chapter, we report the synthesis of 2-D transition metal dichalcogenide (TMDC) based MoS$_2$/rGO nanocomposite using solution process method for use in electric double layer capacitor (EDLC). This 2-D nanocomposite exhibited a high faradaic activity and good reversibility as an EDLC with unique electronic properties and nano-construction. The physical and electrochemical properties of the individual electrode and the nanocomposite were examined using different characterization techniques. EDLC bearing the nanocomposite showed an improved performance with specific capacitance and energy density of 14.52 F/g and 8.06 Wh/Kg, respectively, in comparison to stand alone rGO based EDLC. These enhancements in performance are mainly due to the synergetic effect and excellent interconnected conductive networks of rGO and MoS$_2$.

4.2 Experimental Methods

4.2.1 Synthesis of reduced graphene oxide solution

Graphene oxide (GO) solution was prepared using Hummers method [4.2]. In short, a measured quantity of graphite and sodium nitrate (NaNo$_3$) were mixed and kept in an ice bath. Concentrated sulfuric acid (H$_2$SO$_4$) was then added slowly by stirring the mixture. Potassium permanganate (KMNO$_4$) was then gradually added to the mixture without altering the setup. The mixture was then stirred at a temperature of 50°C for 2 h, and at end of the process DI water was added. As a next step, 30% H$_2$O$_2$ and additional DI water were added to the mixture. The final solution mixture as shown in Figure 4.1 (a) was washed by centrifuge using HCl solution (up to

two times) to remove the metal residues and washed with DI water until the pH became neutral.

A desired concentration of graphene oxide solution (2mg/ml) was prepared by diluting the

washed GO powder with DI water [4.2]. In order to prepare the GO nanosheets, the GO solution

was drop casted on a watch glass as seen in Figure 4.1 (b) and dried at 60°C overnight. Finally,

rGO nanosheets were obtained by thermally reducing graphene oxide sheets at 350°C for 1 hour.

4.2.2 Synthesis of MoS$_2$/rGO nanocomposite

MoS$_2$ was synthesized using solution phase exfoliation method where the commercially

available MoS$_2$ powder was mixed in N-Methyl-2-pyrrolidone (NMP) solution at a concentration

of 2 mg/ml and sonicated for 12 hours [4.2]. Then, the as prepared GO nanosheets was added to

the exfoliated MoS$_2$ solution in an equivalent wt% (1:1) and sonicated for about 3 hours to obtain

a well dispersed homogenous mixture. Anodic aluminum oxide (AAO) template was used to

filter this mixture and to obtain thin film nanocomposite sheets that were later dried at 100°C for

30mins. Conductive rGO/MoS$_2$ nanosheets were then procured by annealing the nanocomposite

at 350°C as shown in Figure 4.1 (c).

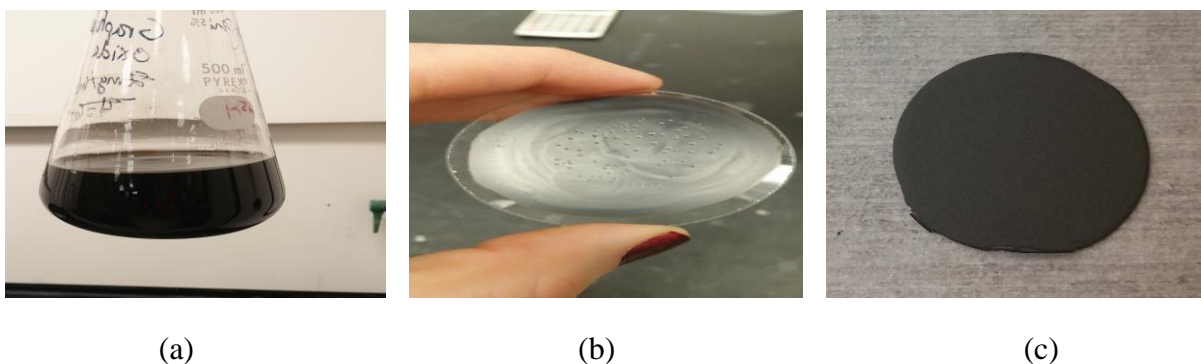| (a) | (b) | (c) |

Figure 4.1: (a) As prepared graphene oxide solution, (b) rGO on a watch glass and (c) standalone MoS$_2$/rGO nanocomposite.

4.2.3 Characterization techniques

The structural properties of individual rGO electrode and the nanocomposite were analyzed using various physical characterization techniques. SEM images were taken using a FEI XL-30 Environmental SEM at an accelerating voltage of 18kV. RIGAKU Miniflex X-ray diffractometer was used for profiling the materials under high intensity Cu Kα radiation in the range of 5°-70°. The electrochemical studies of rGO and MoS_2/rGO EDLCs were done using GAMRY reference 6000 equipment by stacking the materials in a button cell. The active materials are at either edges acting as active electrodes with Celgard membrane serving as a separator between them. Galvanostatic charge/discharge and cyclic voltammetry studies were carried out with 6M potassium hydroxide (KOH) solution as electrolyte introduced between the electrodes and the separator.

4.3   Results and Discussion

4.3.1 Synthesis and morphological studies of active materials

The most prevalent technique used for preparation of reduced graphene oxide is shown in Figure 4.2. Exfoliation of GO was first proposed by Hummers and his coworkers. As explained earlier, the process involves oxidation of natural graphite using $KMnO_4$, $NaNO_3$ and H_2SO_4 and further sonicated in water to exfoliate as GO sheets. The exfoliated GO sheets were further centrifuged in order to remove impurities such as acids and metal ions. Following the above process helped in avoiding formation of N_2O_4 and NO_2 toxic gases. Addition of $KMnO_4$ extremely helped in improving the oxidation efficiency but MnO_4 needs an acidic environment in order to be activated. So sulfuric acid is added along with $KMnO_4$ to create an acidic environment during the process. Mn_2O_7, a subsidiary of MnO_3^+ is highly reactive and releases heat during the reactions which need to be controlled otherwise would result in a devastating explosion. Performing all of

57

the procedural steps needs a deep understanding during the time of its preparation. The reactions happening during chemical feeding releases a lot of heat and might have consequences. So developing a nominal plan to process the reactions would come in handy.

$$KMnO_4 + 3\,H_2SO_4 \rightarrow K^+ + MnO_3 + H_3O + + 3\,HSO_4^- \qquad (4.1)$$

$$MnO_3^+ \rightarrow Mn_2O_7 \qquad (4.2)$$
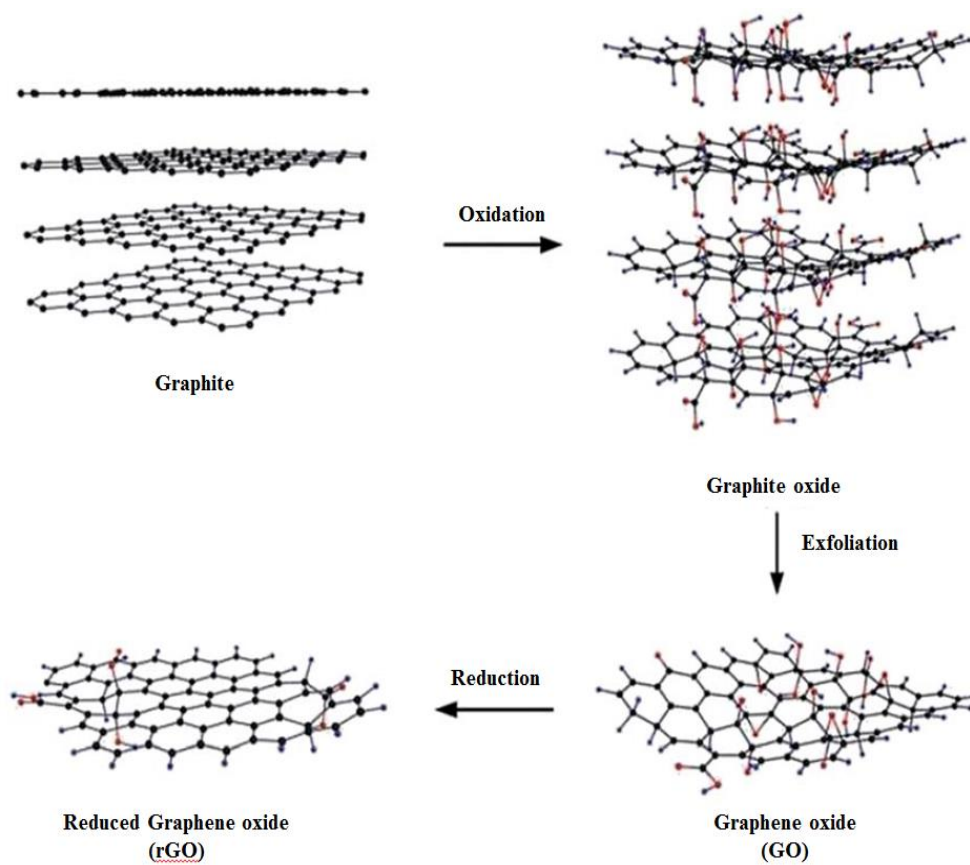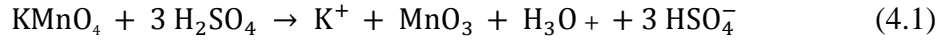
Figure 4.2: Schematic of reduced GO preparation process using solution process method [Reprinted with permission from 4.1].

The dispersion of GO in water was calculated to be approximately 2 mg/ml. The as prepared solution even when formed as sheets using a filtering process was still an insulator. The final step of making this material useful for certain applications involve thermal annealing in a vacuum or inert atmosphere at desired temperature. During this step, intercalated H_2O molecules

and functional groups such as hydroxyl, carboxyl and epoxies are removed from the carbon surface. This rapid annealing of graphite oxide at high temperatures results in sudden expansion of CO and CO_2 gases making the carbon surface to exfoliate into porous carbon structures and form rGO. The heat treatment not only helps in exfoliating the graphite oxide structure but also reduces the functionalities by decomposing the oxygen groups present on the structure. Structural defect and certain damages occurring to the annealed GO sheets due to sudden change in temperature and carbon dioxide release are some of the noticeable effects that cannot be avoided.

A lot of works have reported the synthesis of MoS_2 using hydrothermal process which involves mixing of MoS_2 precursors and transferred to an autoclave and heated at certain temperature. But in our work, MoS_2 was prepared using solution phase exfoliation technique by mixing the powder in a solvent. N-methyl-2-pyrrolidone (NMP) which has similar surface energy as MoS_2 and exfoliated the powder using sonication process. During sonication, thickness of the flakes breaks down to few layers but forms a stabilized solution that is free from re-aggregation. Exfoliated MoS_2 was again mixed along with rGO using sonication process resulting in weak van der Waals interactions binding the layers together. The Scanning electron microscopy (SEM) image of rGO as shown in Figure 4.3 (a) has a nm-scale smooth but μm-scale rippled morphology of the typical multilayered rGO sheets. The inclusion of MoS_2 resulted in formation of rough surface as can be seen in Figure 4.3 (b), logically due to co-stacking of MoS_2 and rGO nanosheets. This stacking of nanosheets helps increase the surface-area of the nanocomposite, and in turn, leads to fast ion charge-transfer throughout the membrane-matrix [4.2].

<center>(a)   (b)</center>
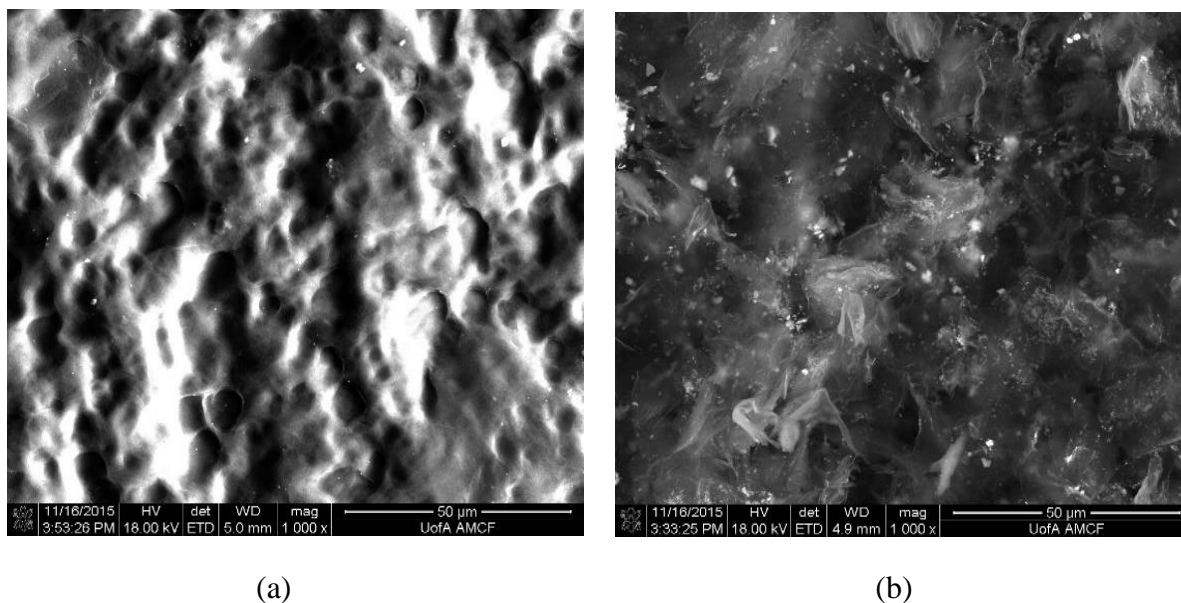
Figure 4.3: SEM of a) reduced graphene oxide and b) MoS$_2$-reduced graphene oxide nanosheets [Reprinted with permission from 4.2].

The structural properties of the as-prepared reduced graphene oxide membrane and the nanocomposite were performed using X-ray diffraction (XRD) analysis as shown in Figure 4.4 (a). Two broad peaks can be seen for rGO at $2\theta = 20^o$ and 43°, relating to the inter-planar spacing of 0.4 nm and 0.2 nm at (002) and (100) planes, respectively. The crystal peak at (002) is very broad, indicating disorderly arrangement along the stacking direction. The XRD pattern of MoS$_2$/rGO nanocomposite has similar trend as rGO, and in addition also has the presence of (105), (103), and (002) diffraction peaks implying layered structure of MoS$_2$. The diffraction peaks indicates the presence of MoS$_2$ in the nanocomposite [4.2].

After physical analysis of the materials, they were assembled as electric double layer capacitors (EDLC) in a CR 2032 button cell with rGO and the composite as the electrode materials, celgard membrane as the separator and 1M Na$_2$SO$_4$ as the electrolyte solution. For easy understanding, rGO based EDLC and MoS$_2$/rGO based EDLCs are labelled as RG-EDLC and MRG-EDLC, respectively. The capacitive nature of an EDLC can be determined using cyclic voltammetry

<center>60</center>

(CV) measurements. The width of the hysteresis loop in a CV spectrum curve indicates a high capacitance value for an EDLC. Figure 4.4 (b) shows the CV plots for RG-EDLC and MRG-EDLC plotted between 0 and 1V. A wide loop area can be observed for the MRG-EDLC compared to that of the RG-EDLC, indicating higher capacitive behavior and the synergistic effect of rGO and MoS_2 in the nanocomposite. Another possible reason might be the pseudo-capacitive nature of MoS_2 present in the nanocomposite with a faradaic charge transfer process. Intercalation of alkali Na^+ metals occurs in the electrolyte solution upon reduction during redox process followed by de-intercalation upon oxidation.

a)   b)
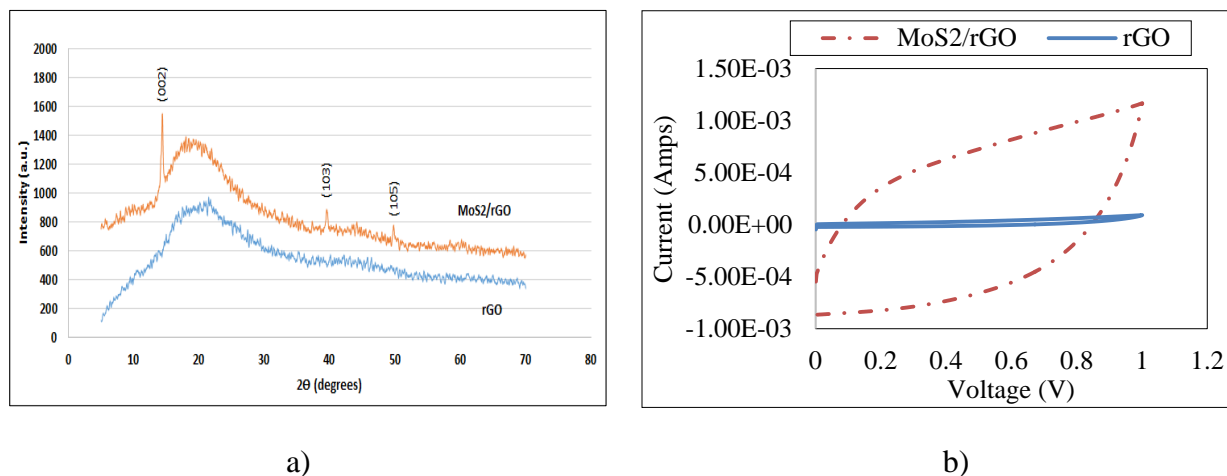
Figure 4.4: (a) XRD and (b) Cyclic voltammetry curve at a current density of 0.5A/g of both RG-EDLC and MRG-EDLC [Reprinted with permission from 4.2].

4.3.2 Electrochemical studies of active materials

The galvanostatic charge-discharge curve shows the electrochemical adsorption and desorption at the interface of electrode and electrolyte with slope variations as a function of time. It can be observed from Figure 4.5 (a), that RG-EDLC has a faster discharging rate compared to charging time at all current densities with a maximum potential of 3.35V. This kind of behavior is attributed to low electrochemical reversibility of the material [4.3]. Reversibility refers to the rate of electron transfer occurs between solution redox species and the working electrode. Assuming

if an electrode material is infinitely stable with the aqueous solution during both the charge and discharge sweeps, an ideal reversible wave response should be observed proving high (fast) electron transfer rate.

A fast rate means that the electron transfer is easy and occurs repeatedly while ions interact with the electrodes. This "easy" electron transfer response can be seen in the MRG-EDLC supercapacitor in Figure 4.5 (b) and (c) which has a charge/discharge curve that is almost symmetrical at all current densities ensuring a nearly ideal reversible EDLC device. Additionally, MRG-EDLC was able to charge and discharge up to a maximum current density of 2.5 A/g.
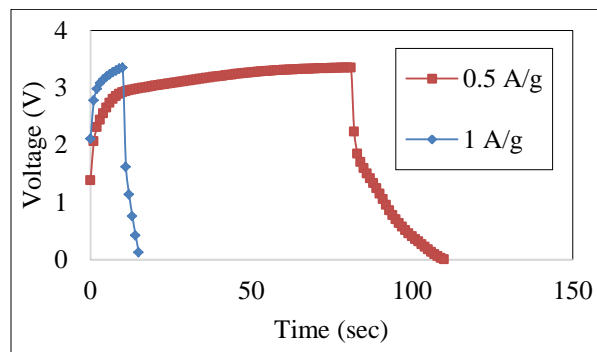
(a)
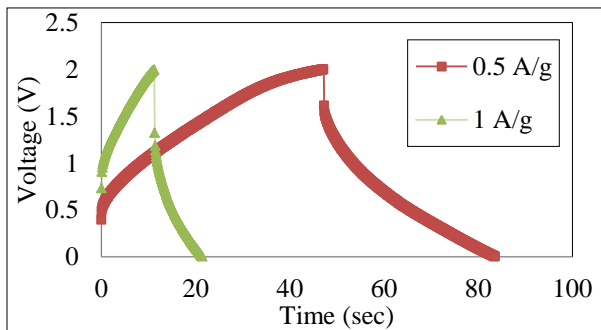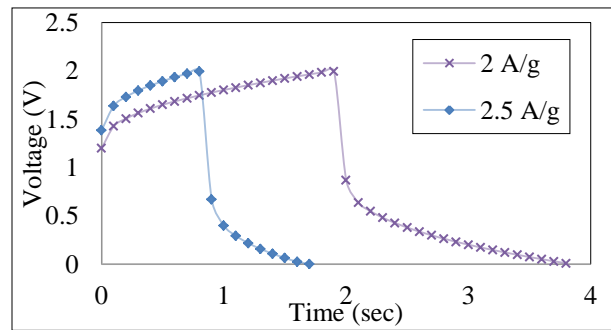
(b)   (c)

Figure 4.5: Galvanostatic charge-discharge curves for (a) RG based EDLC and (b), (c) MRG based EDLC at different current densities [Reprinted with permission from 4.2].

Specific capacitance (Cs) was calculated for both the types of EDLC according to the
relationship:

$$C_S = I\Delta t/m\Delta V \qquad\qquad (4.3)$$

where I is discharge current, t is the discharging time, V is the potential window, and m is the
mass of the active material. The calculated specific capacitances for MRG-EDLC and RG-EDLC
at 0.5 A/g are 14.52 F/g and 2.26 F/g, respectively as shown in Figure 4.6 (a). The specific
capacitance of the EDLC with the nanocomposite is almost seven times higher than that of the
RG-EDLC [4.2]. This kind of an accelerated performance is also due to the fast electron transfer
rate with more active sites of the high surface area material having both MoS_2 and rGO. The
maximum current density at which the MRG-EDLC can operate has increased to 2.5 A/g
comparatively. Because of this boost in current density, the specific capacitance also fades away
slowly taking advantage of accessibility of electroactive sites in the electrode materials. The
ability for a device to operate at higher current densities with a high capacitance level would
benefit commercial device applications.

Ragone plots is an efficient way to study the supercapacitive performance in relation to energy
and power density of an EDLC based supercapacitor where,

$$Energy\ density\ E = \frac{1}{2}CV^2 \qquad\qquad (4.4)$$

$$Power\ density\ P = E * 3600/t \qquad\qquad (4.5)$$

where C is the capacitance, V is the potential window and t is the discharge time. Figure 4.6 (b),
shows the energy-density of MRG-EDLC (8.06 Wh/Kg) that at a current-density of 0.5 A/g,
which has increased double the time than that of RG-EDLC (3.52 Wh/Kg). And the energy-

density has increased almost 3.5 times, at a current density of 1.0 A/g, from 1.28 Wh/Kg in RG-EDLC to 4.53 Wh/Kg for the MRG-EDLC. The maximum power-density of MRG-EDLC calculated at a current-density of 2.5 A/g is 6,940 W/Kg, which is also not compensated much in order of improving the capacitance and energy density of the device [4.2]. Overall, a 2-D nanocomposite material (MoS_2/rGO) was synthesized with carbon as a precursor and improving the material to a stage where it can be used as an EDLC based supercapacitor. The overall performance of the device was scaled up by the usage of MoS_2 material without compensating much on every other parameter comparatively.

(a)   (b)
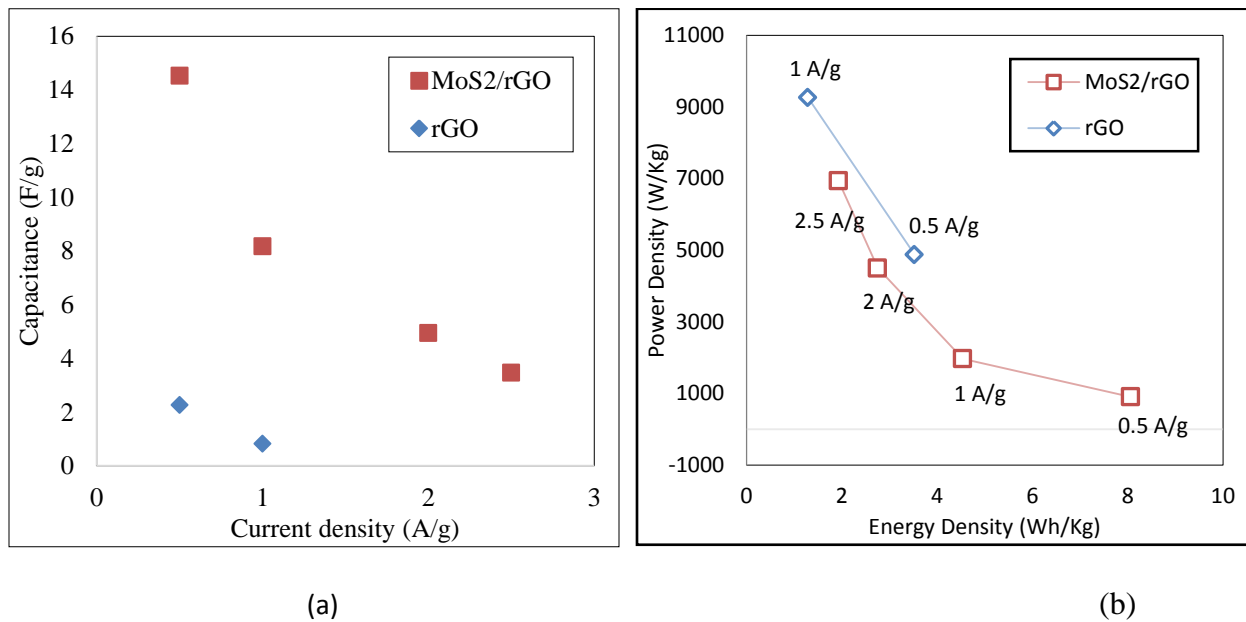
Figure 4.6: (a) Specific capacitance and (b) Energy density Vs Power density curve of rGO and MoS_2/rGO electrode based EDLC at various discharge current densities [Reprinted with permission from 4.2].

4.4   Summary

The main aim at initial stages of the project was to synthesize a nanocomposite based supercapacitor that will help in enhancement of the overall performance. MoS_2, a 2-D material that has properties close enough to graphene was synthesized and mixed along the rGO solution

that was prepared using Hummers method. Due to increase in surface area after addition of MoS$_2$, combined with its synergistic effects, the specific capacitance, and energy density of MoS$_2$/rGO based EDLC was improved more than three times than that of the EDLC with just the rGO material. The maximum attained specific capacitance and energy density of MoS$_2$/rGO based EDLC is 14.52 F/g and 8.1 Wh/kg respectively. This initial achievement of goal motivated to further enhance the performance by altering each individual component of the supercapacitor that includes electrode material, and the electrolyte solution.

4.5 References

4.1 Hua Bai, Chun Li and Gaoquan Shi, "Functional composite materials based on chemically converted graphene", Adv. Mater., 23, 1089–1115 (2011).

4.2 Anishkumar Manoharan, Ryan Tian, Simon S.Ang, "Molybdenum Sulfide/Reduced Graphene oxide 2D material as a High performance Electric double layer capacitor (EDLC)", *MRS Advances,* 1 (22), 1619-1624 (2016).

4.3 Kiran N. Solanki, Bmytro Orlov, Alok Singh, Neale R. Neelameggham, "Magnesium technology", springer (2007).

5.   Chapter 5: Simple and Facile MoS$_2$-Annealed carbon nanocomposite to enhance the overall supercapacitor performance for flexible electronics applications

5.1   Introduction

In the previous chapter, although overall improvement in performance is shown with nanocomposite based EDLC but still the synthesis procedure is too lengthy and time consuming. And also the performance of the supercapacitor, as a whole, can further be improved by altering other parameters in the device particularly the electrolyte solution. In this chapter, we report a nanocomposite material composed of cheap and low resistance carbon paste in the form of annealed carbon (AC) integrated with MoS$_2$ for use in supercapacitor application. The synthesis procedure is a pretty straightforward method of mixing MoS$_2$ with carbon paste in three different weight ratios of 10%, 20% and 30%. The composite that had just 10% MoS$_2$ material exhibited the highest performance comparatively with a capacitance of 207.5 F/g and energy density of about 28.8 Wh/Kg with 1M Na$_2$SO$_4$ aqueous electrolyte solution. Later when these materials were tested for its behavior as a supercapacitor, still the device having nanocomposite with 10% MoS$_2$ displayed the highest performance. Then we kept this material as a base and tested them as a supercapacitor with different electrolyte solutions to explore an electrolyte that would enhance the performance of the device even further. Finally, a flexible supercapacitor was fabricated with the nanocomposite that exhibited the best performance with an electrolyte that helped in the performance ever further.

5.2 Experimental Methods

5.2.1 Synthesis of Annealed Carbon

A low resistance carbon ink consisting mainly of carbon and graphite particles was purchased from Materials Inc. This carbon ink was coated directly on a stainless steel substrate and dried at $100^{o}C$ for 30 minutes and later annealed at $350^{o}C$ for 1 hour with a 45 minutes ramp up and ramp down time. The annealed carbon was formed and analyzed using physical and electrochemical characterization techniques.

5.2.2 Synthesis of MoS$_2$/AC Nanocomposite

MoS$_2$ dispersion was prepared using liquid exfoliation method by mixing the powder with NMP solution and sonicating it for 12 hours. The exfoliated MoS$_2$ solution was centrifuged and cleaned using IPA which up to 2 times and then dried at $60^{o}C$ overnight. This dried powder was mixed with carbon paste at different ratios of 10%, 20% and 30% and were coated on a stainless steel substrate to act as working electrodes. The nanocomposites were labelled as MCG 1.9, MCG 2.8 and MCG 3.7, for mixtures with 10%, 20% and 30% MoS$_2$, respectively, for easy identification. With further concentrations, the mixture became solid during the mixing process, and thereby, not enabling us to prepare them as electrodes for testing.

5.2.3 Characterization techniques

Electrochemical tests such as galvanostatic charge/discharge, EIS and CV were performed for AC and all combinations of nanocomposites using a Gamry Reference 600 potentiostat shown in Figure 5.1 (a). A Three-electrode setup was used for all electrochemical measurements where the active materials acted as the working electrode, platinum sheet as the counter electrode and Ag/AgCl as the reference electrode as shown in Figure 5.1 (b). The studies were carried out with 1M Na$_2$SO$_4$ acting as electrolyte solution at room temperature. The physical characterizations of

AC and the highest performance nanocomposite were done using FEI XL-30 Environmental

SEM at an accelerating voltage of 30kV and RFT-6000 Raman spectrometer.

| (a) | (b) |
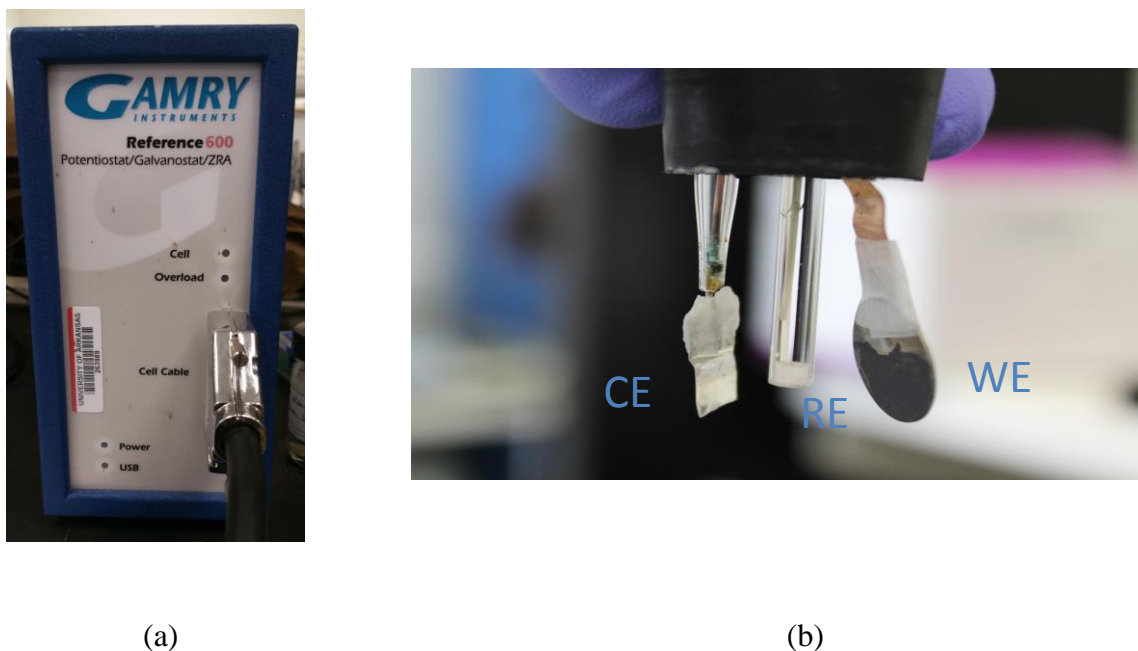
Figure 5.1: (a) Gamry Reference 600 potentiostat and (b) three electrode setup used for electrochemical testing

5.3   Results and discussion

5.3.1 Synthesis and morphological studies of active materials

Commercially available carbon ink which had low resistance was used as the electrode material.

The carbon ink was annealed at $350^{o}C$ and tested using a three electrode method with 1M

Na_2SO_4 as the electrolyte solution. It is known that the lower the resistance of the material, the

higher will be its electrical conductivity. Later, AC was mixed with MoS_2 at difference

concentrations and prepared as a nanocomposite using the procedure explained above. All the

electrodes were tested using a three electrode setup and the results obtained using different ratios

of composites were compared with the "pure" AC electrode. The test performances of all the

composite membranes were superior in comparison to the AC electrode. The composite that had

just 10% MoS$_2$ showed the highest performance even among all the other nanocomposites, so we focused on this ratio. The reason for an enhanced performance is attributed to the linear arrangement of particles in the active material allowing increased contact with most of the electrolyte ions and forming a shorter ion diffusion channels during charging/discharging process which helps in improving the conductivity of the material, and in turn, leads to increase in capacitance. In synthesis of these materials, there is a balance between high concentration of AC with just enough MoS$_2$ material which helps in prevention of coagulation and restacking thereby providing more surface area. But as the concentration of MoS$_2$ increases, the overlapping or coalescing of materials occur which hinders ion travel and leads to degradation in performance. Figure 5.2 (a) shows the SEM image of highly porous carbon particles that can be observed as a result of annealing at a higher temperature. Figure 5.2 (b) shows the SEM of MCG 1.9 which has a rough surface in comparison to the "pure" AC material. Smaller flakes of MoS$_2$ is found to be tailored to AC and stacked in a fashion that provides high surface area.
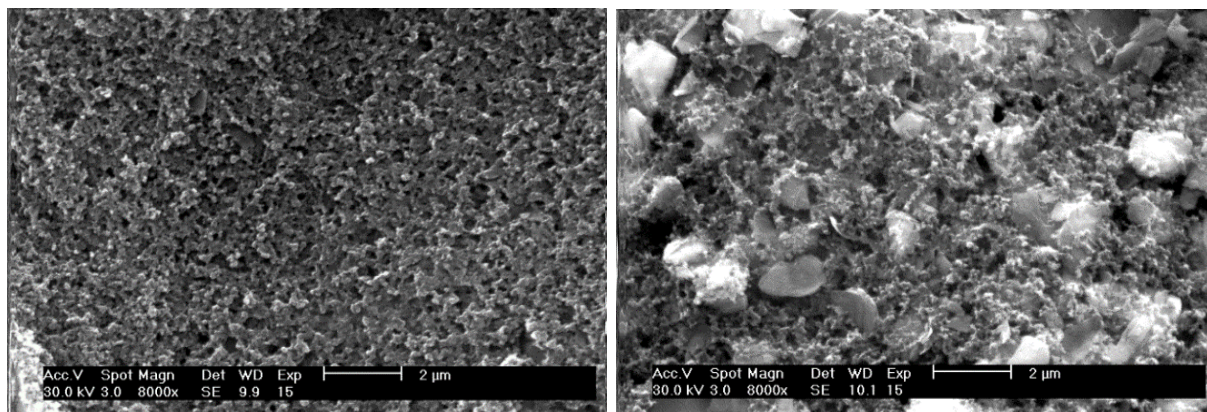
(a)   (b)

Figure 5.2: SEM images of (a) Annealed carbon (AC) and (b) MoS$_2$/AC composite electrode

In order to further characterize AC and the composite material, Raman spectroscopy technique was used. Using this technique, we were able to make sure that the bulk MoS_2 was successfully exfoliated into few layer structure. Raman analysis is an effective tool to characterize the sp^2 carbon based materials because of its unique chemical signatures, highly selective nature, and the distinctive information contained between D and G bands. Figure 5.3 shows the Raman spectroscopy graphs of both AC and the MCG 1.9 composite material. The peak at about 1580 cm^{-1} (G band) corresponds to E_{2g} which is the center mode of the crystalline graphite. The D band at about 1365 cm^{-1} represents the sp3-hybridized carbon [5.1]. The plot for nanocomposite MCG 1.9 shows the peaks of both MoS_2 and AC. The modes A_{1g} and E^1_{2g} are assigned to MoS_2 characteristics peaks at 378 and 403 cm^{-1}. A_{1g} is correlated to the out of plane vibration of Mo and S and E^1_{2g} in correspondence to its in-plane motion [5.2]. From this Raman plot, the composite is indeed comprised of MoS_2 and AC.
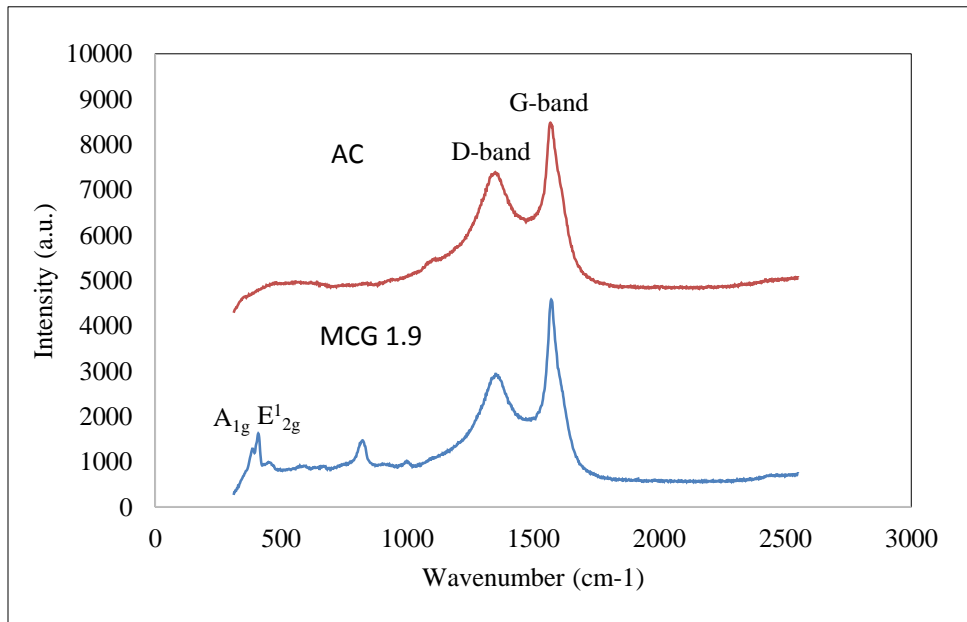

Figure 5.3: Raman shift peaks of annealed carbon and MCG at 350^oC

5.3.2 Electrochemical Studies

After thorough characterization of AC and the composite membrane, electrochemical measurements of the electrodes were done using a three-electrode method. During the test, the active material was coated only on half of the stainless steel substrate and a copper sheet was extended from the stainless steel sheet for electrical connections. A pH neutral solution, 1M Na_2SO_4, was used as the electrolyte instead of an acid or base solution in order to avoid any side reactions and to increase the long term stability of the electrodes. Due to large size of the electrolyte ions, Na_2SO_4 electrolyte results in lower capacitance values in comparison to acids and bases [5.3], a maximum potential of only 2 to 2.5V could be attained due to electrolysis and higher over potential issues [5.4]. Higher potential windows could be attained while using organic electrolytes but still these electrolytes suffer from high material corrosiveness, bulk ion transportation and ionic moisture contamination. While using acid or base solution, when a potential level is reached, hydrogen evolution reaction (HER) occurs. In addition, MoS_2 is also proved to be an excellent hydrogen evolution catalyst [5.5-5.8]. The hydrogen evolution limits the lifetime of supercapacitor by deforming the device with an increasing gas pressure.

Cyclic Voltammetry (CV) and glavanostatic charge/discharge tests were performed to evaluate the electrochemical performance of AC and all combinations of MCG composites. Figure 5.4 (a) shows the CV curves measured at a scanning rate of 100mV/s for all the AC and the composite electrodes. All the materials are said to possess a typical electrical double layer capacitance in regards to the rectangular shape they exhibit.
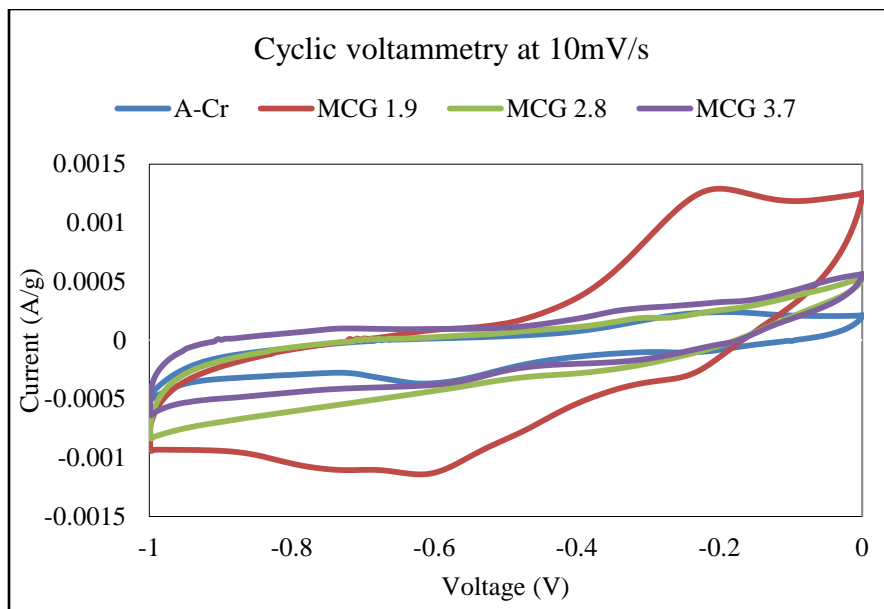
(a)
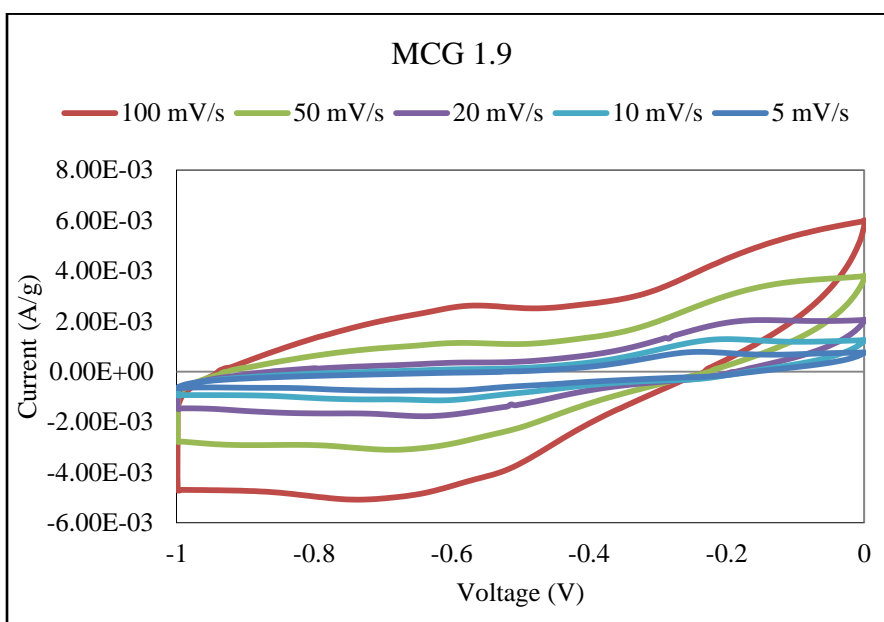
(b)

Figure 5.4: Cyclic voltammetry of (a) AC and all the composite electrode materials at 10mV/sec and (b) MCG 1.9 composite at different scan rates

In general, a CV curve is a reflection of oxidation-reduction reaction that the material experiences and so the wider the loop of the CV curve, the higher the capacitance. It can be observed that MCG 1.9 has a wider loop compared to the AC curve depicting a higher capacitance as a resultant of combined synergistic effects of both metal and the carbon components in the composite. The loop width decreases linearly when tested with further combinations of MCG as the capacitance of the material decreases. This decrease in capacitance again might be due to the fact that the concentration of MoS_2 dominates over the concentration of AC, which results in restacking of materials that leads to lower surface area and further leading to lower conductivity of the material. Figure 5.4 (b) shows the CV curve of MCG 1.9 recorded at different scan rates from 5-100mV/s. The width of the loop here decreases as the scan rate decreases indicating just the reduced interaction between the electrolyte ions and the active material at various scan rates and not due to the decrease in capacitance.

A study of electrochemical impedance spectrum (EIS) of a material is mainly done to determine its various fundamental behaviors. Just by looking at the way the curve appears in an impedance graph, capacitive nature of a material could be understood. In general, capacitance of any material will be high if the curve is vertical at lower frequencies. And as the curve starts to bend into a semicircle, capacitance is also said to reduce. At higher frequencies, the impedance curve is dependent on the resistance between the sheet layers of the active electrode materials and is mostly in a semicircle shape. The lesser the width of the semicircle, the material would be more capacitive. In the Figure 5.5, at lower frequencies, the impedance curve of MCG 1.9 is more vertical than AC and all the other composite materials, proving that this particular composite electrode is more capacitive than the rest of them. And at higher frequencies, the width of the

semicircle is smaller for MCG 1.9 again indicating higher capacitance of the material comparatively. All the impedance measurements were done between 0.1Hz and 100 KHz.
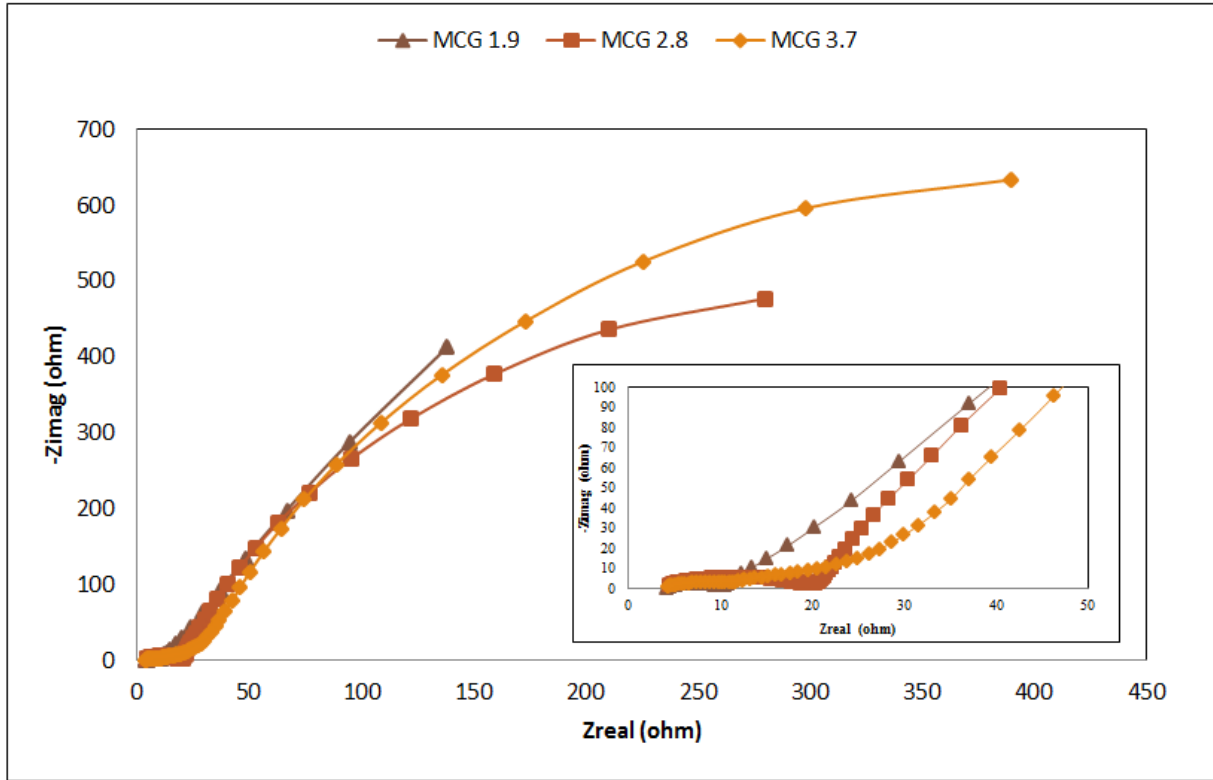
Figure 5.5: Comparison of electrochemical impedance between AC and all combinations of composite electrodes

Galvanostatic cyclic charge-discharge (CCD) is a basic method which is used to determine the life cycle of a material or a device. The repetition of charging and discharging loops is called a cycle. For most of the cases, CCD is tested with a constant charging and discharging current. Before the charge starts, the potential of the material or the device is assumed to be zero. After the charge cycle starts, it reaches a desired potential and switches to discharging mode automatically. During charging process, the electrolyte containing the alkali metal ion (Na^+) gets adsorbed and intercalates between the MoS_2 layers of the electrode surface.

$$MoS_2 + Na^+ + e^- \leftrightarrow MoS - SNa \qquad (5.1)$$
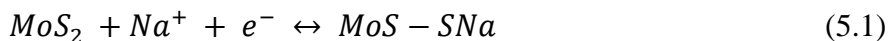
This kind of ion intercalations have been seen to occur in most of the reported works that used

MoS_2 and metal oxide films [5.9-5.11]. Continuous intercalation and de-intercalation of these

sodium ions occurs with MoS_2 present in the electrode surface, exfoliating it layer by layer

which is also one of the reasons for increased surface area and improvement in capacitance of the

material. The higher the interaction between the electrolyte ions and membrane, the higher will

be the capacitance. Although, as the current density increases, there is a reduction in capacitance

since the interaction between the ions and the electrode becomes greatly reduced due to fast

charge transfer. The current density at which a material or device can charge and discharge

depends on these effective interactions. Figures 5.6 (a), (b), (c) and (d) shows the CCD curves of

AC and MCG 1.9 with a maximum current density of 6 A/g and 11 A/g, respectively. It can be

observed from these figures that for both composite and the AC electrodes, at lower current

densities, they have a slow discharging time than the time taken for charging. The time taken to

charge and discharge became more symmetrical as the current density increases. The overall

charge and discharge time also decreases as the current density increases due to insufficient

release or insertion of Na^+ ions during the process.

Tables 3 and 4 show the amount of time taken to charge and discharge the AC and the composite

at different current densities. In both tables, the discharge time is higher than the charging time.

And as the current density increases, they both become symmetrical due to the insertion or

release of Na^+ ions. It can be clearly seen that the charging and discharging times become

symmetrical even up to the range of milliseconds as it tapers down.
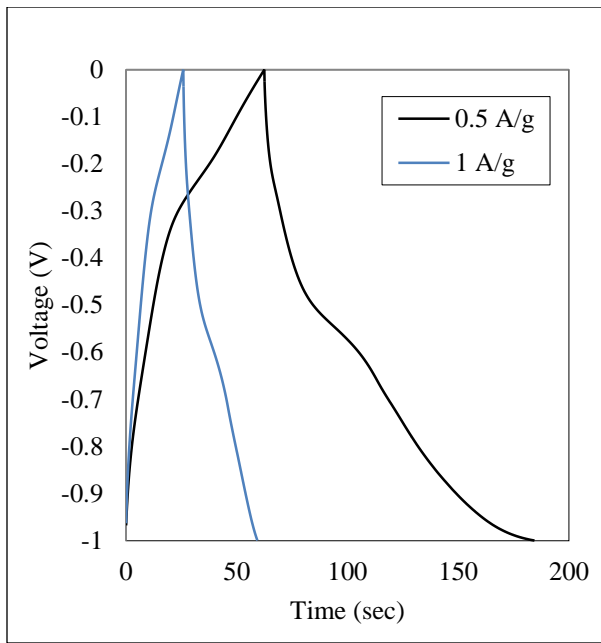
(a)
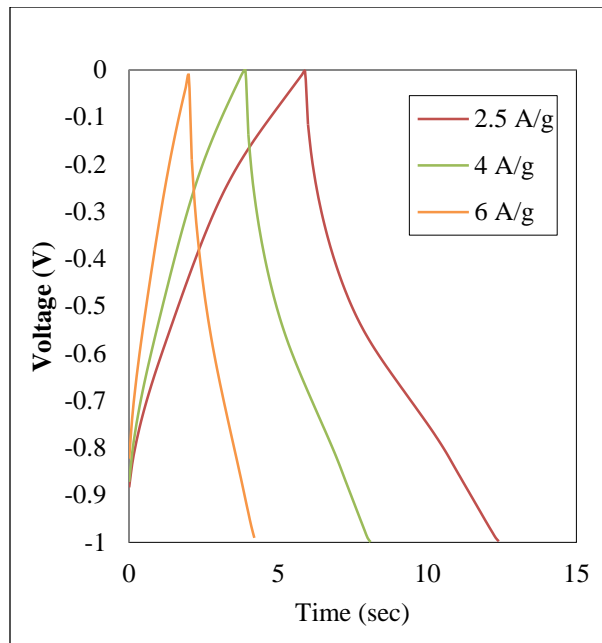
(b)
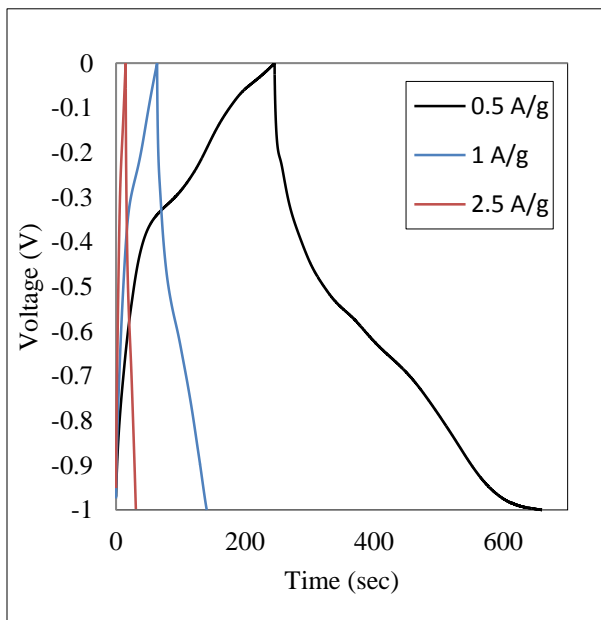
(c)
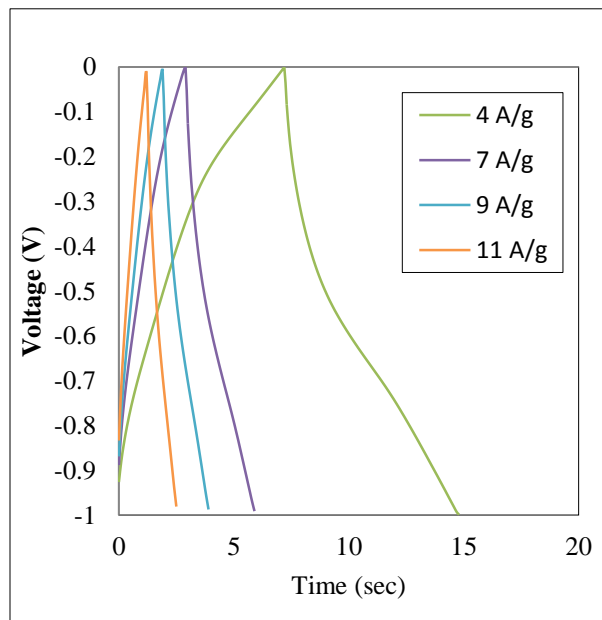
(d)

Figure 5.6: Charge/ discharge profiles of (a), (b) AC electrode and (c), (d) MCG 1.9

Table 3: Time taken to charge and discharge AC electrode at different current densities

Charge Time (s)	Discharge Time (s)	Current density (A/g)
62.4	122	0.5
25.8	33.4	1
8	8.3	2.5
3.9	4.1	4
2.7	2.8	5
2	2.1	6

Table 4: Time taken to charge and discharge MCG 1.9 nanocomposite at different current densities

Charge Time (s)	Discharge Time (s)	Current density (A/g)
246	413	0.5
63.6	76.9	1
14.9	15.7	2.5
7.2	7.5	4
5	5.1	5
3.7	3.8	6
2.9	2.9	7
2.3	2.3	8
1.9	1.9	9
1.6	1.6	10
1.2	1.2	11

Specific capacitance (C_{sp}) of the electrode materials are calculated using the formula

$$C_{sp} = \frac{(I * \Delta t)}{(\Delta V * m)} \qquad\qquad (5.2)$$

where I, Δt, ΔV, and m are the current density at which the material was discharged, discharge time, potential window and mass of active material, respectively. Figure 5.7 shows the specific capacitance calculated at various current densities for AC and all the other composites. A highest capacitance of 61 A/g obtained at 0.5 A/g current density can be observed for the AC electrode. In comparison, MCG 1.9 has a highest capacitance value of 207.5 F/g at 0.5 A/g. Using this material, continuous charge/discharge process can also be conducted up to a maximum current density of 11 A/g whereas, using AC material can reach only a maximum 6 A/g current density as shown in Table 5. This indicates that the composition of both AC and MoS_2 combined will be able to resist the structural changes with much better endurance during the charge and discharge processes and also have effective contact with the electrolyte ions. It has been generally known that weak Van der Waals force between the neighboring sheets hinders the surface area of the material and results in restacking. So a high surface energy and flake dimension difference in the nanocomposite will prevent restacking and formation of disordered heterostructures. Possessing these characteristic might be the reasons for high specific surface area and the boosting of specific capacitance in MCG 1.9 nanocomposite. As the concentration of MoS_2 increases in the composites, the surface energy decreases, restacking of materials occurs leading to a decrease in the specific capacitance. The specific capacitances of MCG 2.8 and MCG 3.7 are 99.25 and 73.2 F/g, respectively which are lower than the capacitance of MCG 1.9 but still higher than those of the AC electrode.

Table 5: Maximum current density and capacitance of AC and all MCG composites

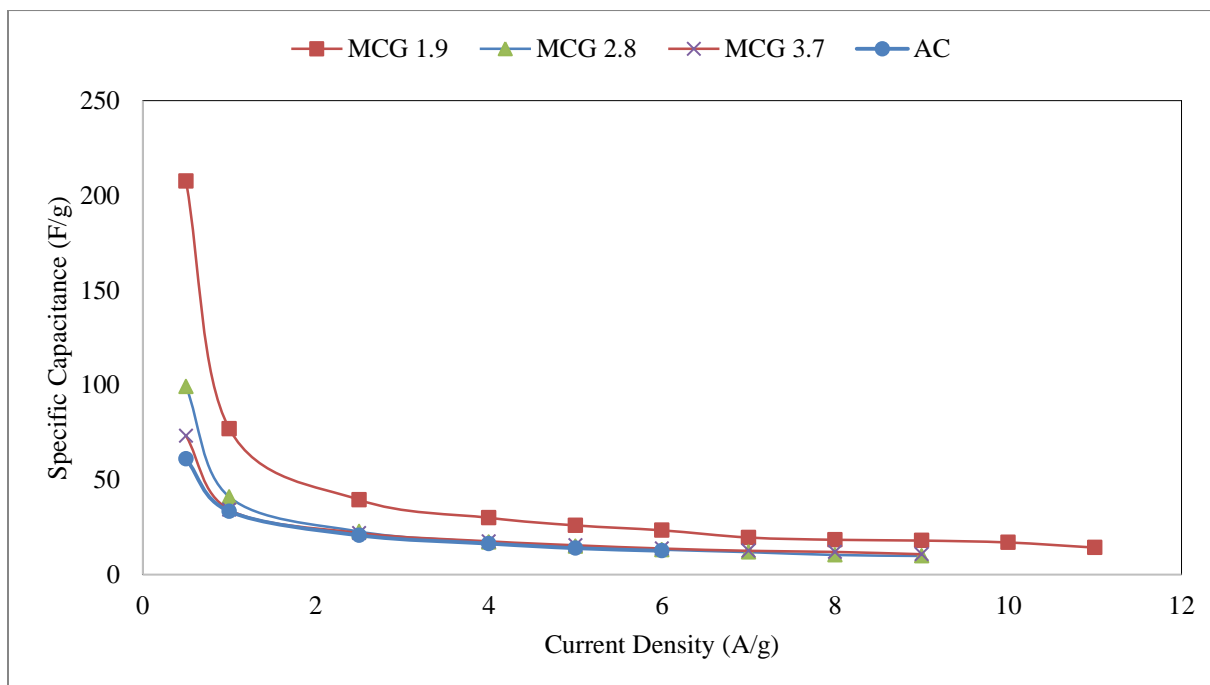|	Max. Current density	Max. Capacitance (at 0.5 A/g)
MCG 1.9	11 A/g	207.5 F/g
MCG 2.8	9 A/g	99.25 F/g
MCG 3.7	9 A/g	73.2 F/g
AC	6 A/g	61 F/g

Figure 5.7: Specific capacitance of AC and all MCG composites at increasing current density

Figure 5.8 shows the plot of energy versus power density curves derived from galvanostatic charge-discharge curves at their corresponding current densities. The formulas used for calculating the energy and power density are

$$E = C_{sp} * \Delta V^2 \qquad\qquad (5.3)$$

$$P = \frac{E}{\Delta t} \qquad\qquad (5.4)$$

where C_{sp} is the specific capacitance, ΔV is the potential window and Δt is the discharge time. The energy versus power density curve has almost a similar pattern as the specific capacitance curve plotted with respect to current density. Increase or decrease in energy density was in relation with the obtained capacitance since they are directly proportional to each other as can be seen in the equation 5.3. A maximum energy density of 8.47 Wh/Kg was recorded for the AC electrode at a current of 0.5 A/g with a power density of 250 W/Kg. And by inclusion of MoS_2 along with AC, the energy density increased to more than three times by retaining the same amount of power. So, a maximum energy density of 28.8 Wh/Kg was obtained using MCG 1.9 electrode at a current density of 0.5 A/g, with the same power density of 250 W/Kg. Although power density is directly proportional to energy density, it is inversely proportional to discharge time. So as the discharge time decreases with an increasing current density, the power density also increases. Therefore, MCG 1.9 has a maximum power density of 5500 W/Kg at a current density of 11 A/g compared to 3000 W/Kg at 6 A/g for the AC electrode as shown in Table 6.

Table 6: Maximum Energy and Power density of AC and all MCG nanocomposites

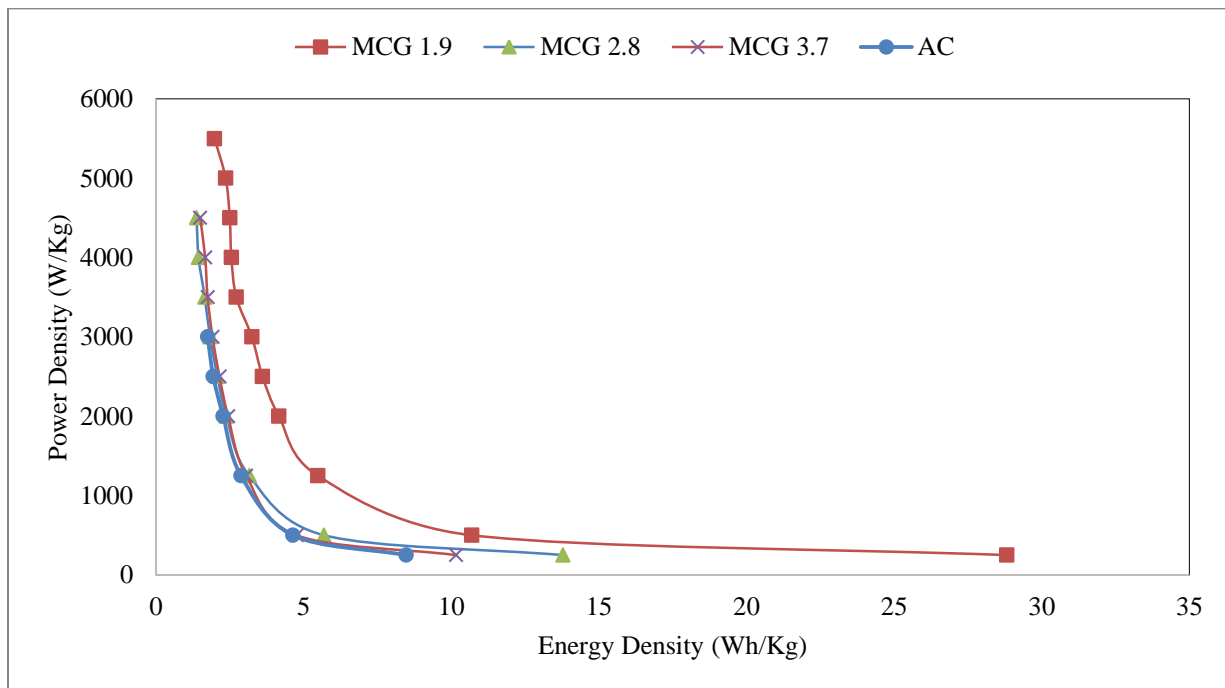|	Max. Energy density (W/Kg)	Max. Power density (W/Kg)
AC	8.47	3000
MCG 1.9	28.81	5500
MCG 2.8	13.78	4500
MCG 3.7	10.16	4500

Figure 5.8: Ragone plot of AC and all MCG nanocomposites measured from galvanostatic charge/ discharge curves

To make sure that the results obtained using the MCG 1.9 nancomposite electrode were repeatable and not just a one-time luck, the experiments were repeated. It can be seen in Figure 5.9 (a) and (b) that although the time taken to charge and discharge was different at 0.5 A/g, it was almost the same at 1 A/g. Supporting this behavior, the specific capacitance, energy and power density were also different in the newly prepared membrane only at 0.5 A/g Figure 5.10 (a) and (b) but were almost the same at every other current densities proving that the synthesized material is consistent and can be reproduced.

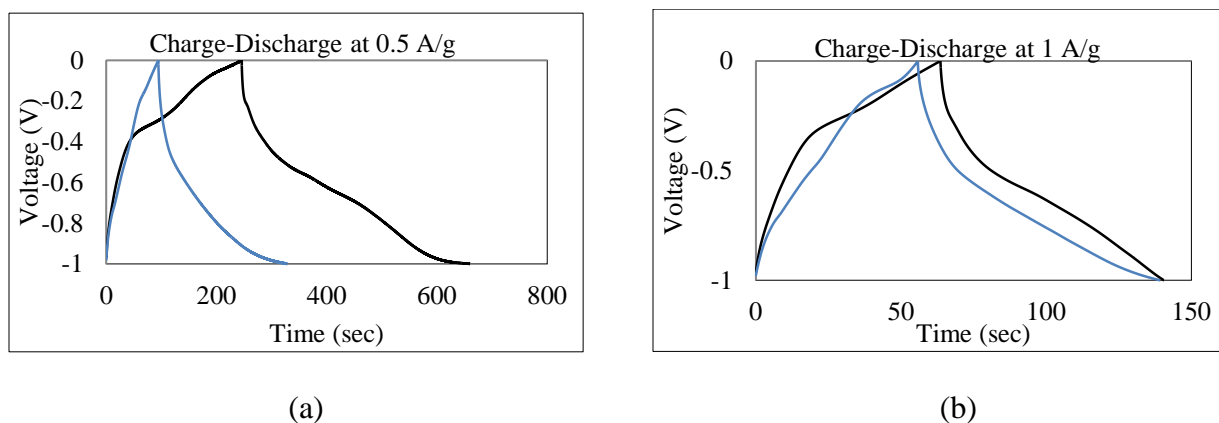(a)   (b)

Figure 5.9: Repeatability of charge/discharge curve of MCG 1.9 nanocomposite at (a) 0.5 A/g and (b) 1 A/g

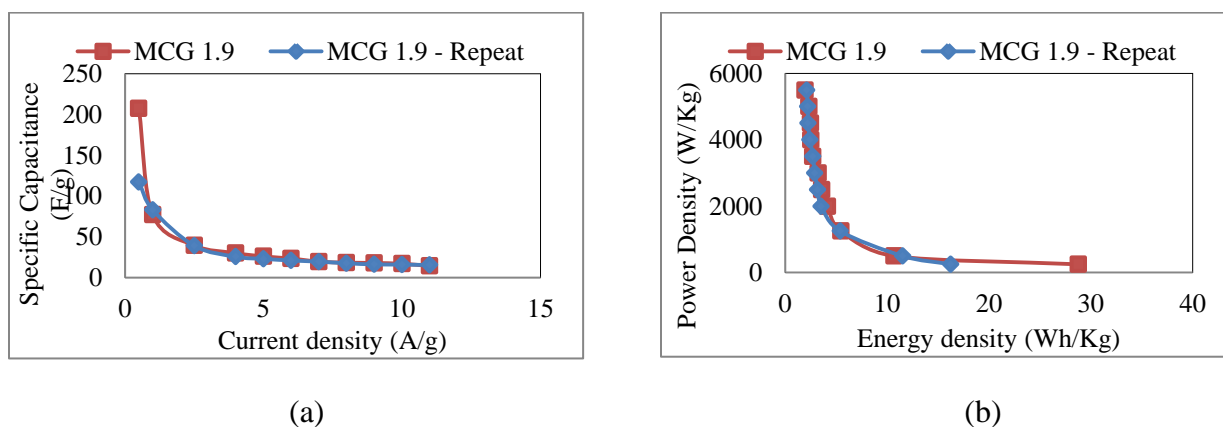(a)   (b)

Figure 5.10: Repeatability of MCG 1.9 nanocomposite in response with (a) specific capacitance and (b) energy and power density

5.4 Supercapacitor testing with various electrolytes

After testing the performance of all the materials as individual electrodes, the highest performance material (MCG 1.9) was further investigated as an electric double layer supercapacitor. So the composite material was synthesized as a stand-alone electrode by mixing 10% MoS_2 with carbon ink, coating it on a Teflon sheet, and drying at $80^{o}C$ for 30 minutes. This dried sheet was then peeled away from the Teflon surface and annealed at $350^{o}C$ for 1 hour. The stand-alone composite was treated as the positive and negative electrodes of the EDLC with Celgard membrane as the separator between them. The electrochemical performances of EDLCs are not only based on surface area of the active materials but also on the size of solvated ions in the electrolytes [5.12-5.14]. The migration speed of these ions and its effective interactions with active materials in an energy device have a deep impact on its ionic radius. As a fact, organic solvents have large ionic radius in comparison to aqueous electrolytes due to which, electrode materials with macro-pores are preferred [5.15-5.17]. Very few studies have been reported on the electrochemical performance of carbon based materials with effect to solvated ions [5.18]. In this section of the report, a similar kind of study has been carried out to explore the effect of three different electrolyte solutions namely, potassium sulfate (K_2SO_4), sodium sulfate (Na_2SO_4), and lithium sulfate (Li_2SO_4) at a concentration of 0.5 M with our high performance electrode material. Electrochemical studies were done using electrochemical impedance spectra between 0.1 Hz and 1 MHz and galvanostatic charge/ discharge method at different current densities.

Figure 5.11 shows the EIS curve of MCG 1.9 with all the three aqueous electrolytes (K_2SO_4, Na_2SO_4 and Li_2SO_4) under an open circuit voltage. As explained earlier, capacitance of a material will be high if the impedance curve is vertical at lower frequencies. It can be seen in the figure that the line keeps becoming linear in the order of $K_2SO_4 > Na_2SO_4 > Li_2SO_4$. This kind of

behavior can be attributed to the ionic radius of K^+ (3.31 Å), Na^+ (3.58 Å) and Li^+ (3.82 Å) ions which possess different migration speeds and charge densities. It is well known that all simple salts dissolve in water, producing ions, and consequently, conduct electrical current. Smaller ions migrate more easily towards cathode, and thus, conduct more than larger ions. Lithium ions are smaller, and thus, conduct higher current in comparison to sodium and potassium ions. However, the ionic mobility or conductivity measurements in aqueous solutions yield opposite results i.e., conductivity: $K^+>Na^+>Li^+$. The reason for this is that the ions are hydrated in the solution. For example, Li^+ ions are smaller and can be very heavily hydrated. This makes the radius of the hydrated Li^+ ion large, and hence, can only move slowly. Same concept applies for Na^+ ions. The capacitance of the EDLCs with their respective electrolytes also increases in the same order of $K_2SO_4>Na_2SO_4>Li_2SO_4$ due to a similar effect during charging/ discharging process at different current densities.
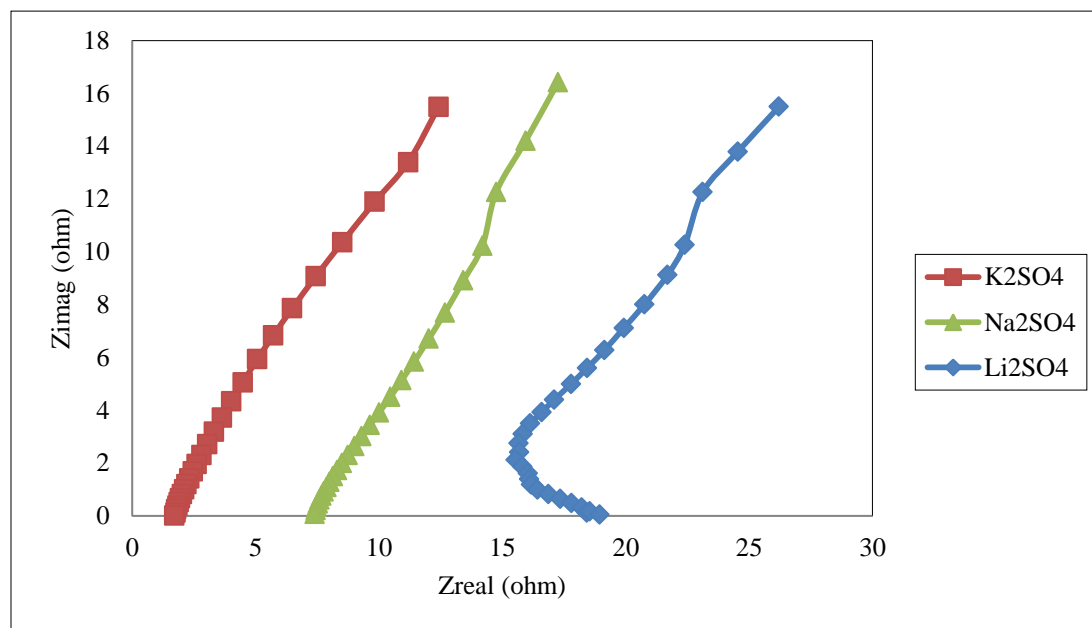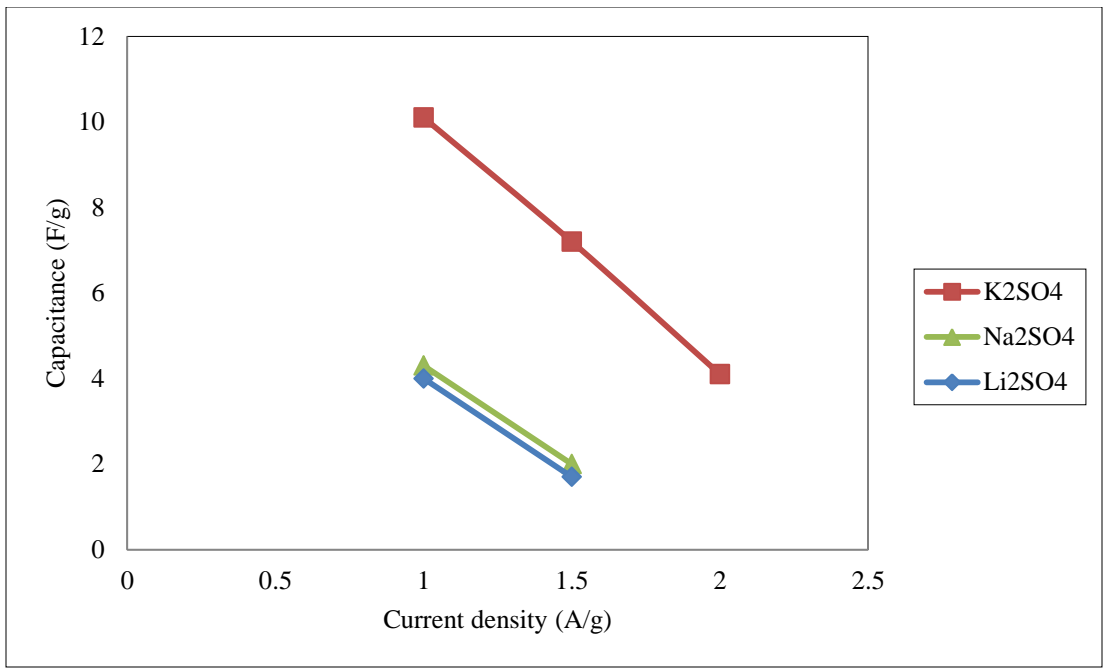

Figure 5.11: Nyquist plots of MCG 1.9 nanocomposite in 0.5 M K_2SO_4, Na_2SO_4 and Li_2SO_4 electrolytes

A maximum capacitance of 10.1, 4.3 and 4 F/g has been recorded at a current density of 1 A/g

with K_2SO_4, Na_2SO_4 and Li_2SO_4 as electrolyte solutions as shown in Figure 5.12(a). Since the

energy density is directly proportional to capacitance, the maximum energy density is calculated

to be 4.5, 1.9 and 1.8 Wh/Kg for the respective electrolyte based EDLCs as can be seen in Figure

5.12(b). From these results it is pretty clear that K_2SO_4 exhibits an undoubtedly highest

performance. And in addition, for K_2SO_4 based EDLC, the current density at which it the can be

charged/ discharged is also higher in comparison to other electrolyte based EDLCs as seen in

Table 7. Therefore, it can be determined that an aqueous electrolyte with small ionic radius will

help in improving the performance of a supercapacitor device. The solubility of K_2SO_4 salt is

limited to around 0.5M concentration. So, all the above tests were performed using the same

concentration of 0.5M for uniform comparison. But in our individual electrode tests 1M Na_2SO_4

was used as the electrolyte solution, and there are a lot of supercapacitor works reported with this

concentration of electrolyte [5.19-5.21]. So, in order to verify and compare the effects of higher

concentration solutions, EDLCs were tested with 1M Na_2SO_4 and 1M Li_2SO_4 electrolytes.

Table 7: Comparison of different parameters tested using MCG 1.9 nanocomposite in 0.5 M
K_2SO_4, Na_2SO_4 and Li_2SO_4 electrolytes

| Electrolyte	Maximum Voltage	Maximum Current density (A/g)	Maximum Capacitance (F/g)	Maximum Energy density (Wh/Kg)	Maximum Power density (W/Kg)
0.5M K_2SO_4	1.8 V	2	10.1	4.5	11070
0.5M Na_2SO_4	1.8 V	1.5	4.3	1.9	5400
0.5M Li_2SO_4	1.8 V	1.5	4	1.8	4629

(a)
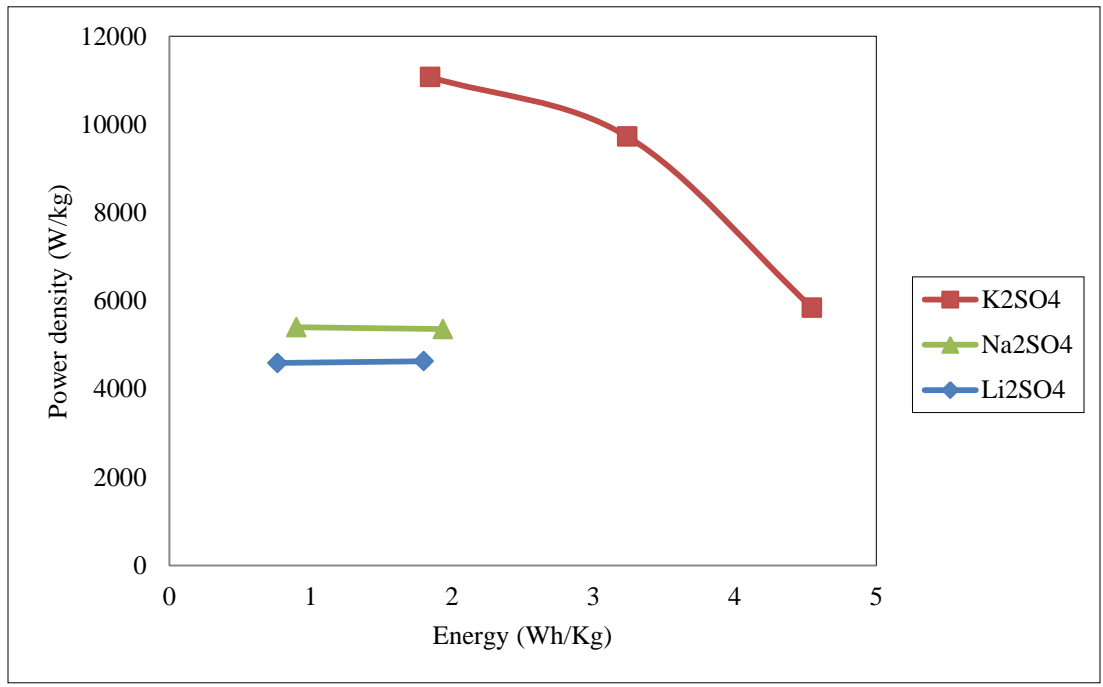
(b)

Figure 5.12: (a) Specific capacitance and (b) Ragone plot of MCG 1.9 nanocomposite in 0.5 M K_2SO_4, Na_2SO_4 and Li_2SO_4 electrolytes

From Figure 5.13a, it can be observed that a maximum capacitance of 15.2 F/g and 12.3 F/g was obtained at 1 A/g current density using 1M Na_2SO_4 and 1M Li_2SO_4 electrolyte solutions respectively. The maximum energy density of 8.4 Wh/Kg and 6.1 Wh/Kg has been calculated for the respective electrolyte solutions as can be seen in Figure 5.13b. So, more than 50% of increase in capacitance and energy density has been obtained just by increasing the concentration of the electrolyte solution. In addition, the current densities at which the EDLC can be charged/discharged also have been increased to a maximum of 3.5 A/g comparatively. In spite of an overall increase in performance for both the types of electrolytes, the Na_2SO_4 electrolyte based EDLC is still dominant over the EDLC with Li_2SO_4 electrolyte as seen in Table 8, proving again the fact that solvate ions with smaller ionic radius can migrate faster and have more affinity to the active sites of the electrodes.

Table 8: Comparison of different parameters tested using MCG 1.9 nanocomposite in 1 M Na_2SO_4 and Li_2SO_4 electrolytes

Electrolyte	Maximum Voltage	Maximum Current density (A/g)	Maximum Capacitance (F/g)	Maximum Energy density (Wh/Kg)	Maximum Power density (W/Kg)
1M Na_2SO_4	2 V	3.5	15.2	8.4	6600
1M Li_2SO_4	2 V	3.5	12.3	6.1	6153
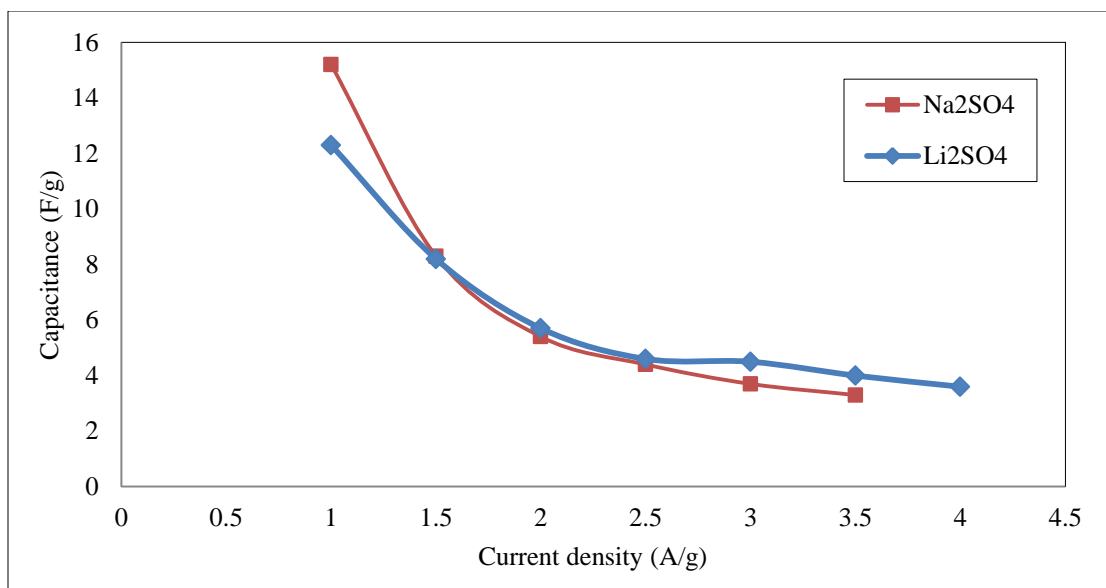
(a)
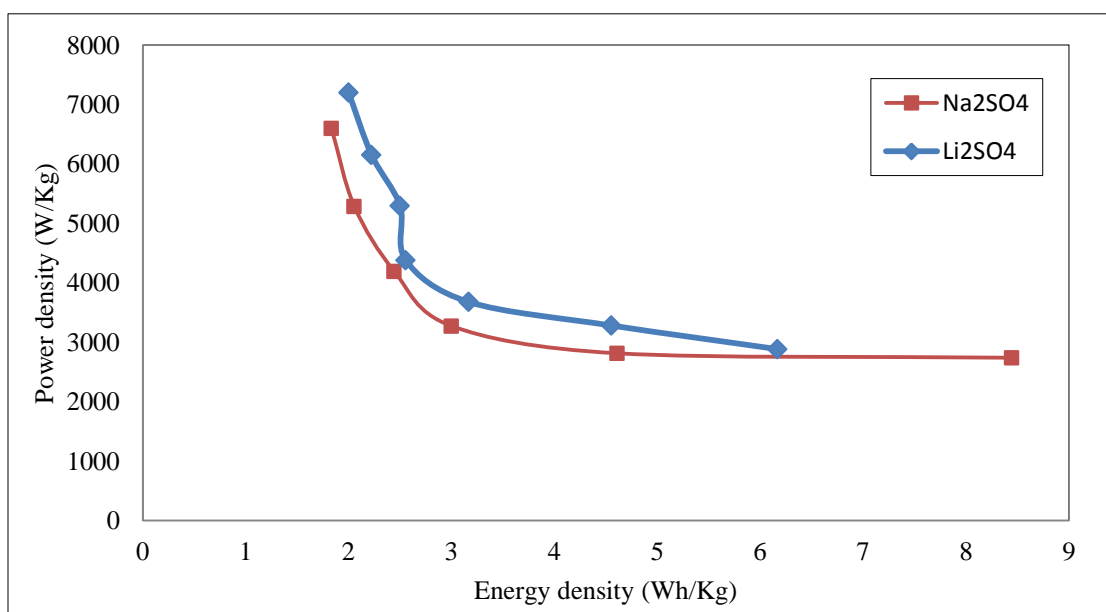
(b)

Figure 5.13: (a) Specific capacitance and (b) Ragone plot of MCG 1.9 nanocomposite in 1 M
Na$_2$SO$_4$ and Li$_2$SO$_4$ electrolytes

5.5 Summary

After thorough analysis of carbon material, different ratios of MoS_2 were mixed with AC, where the nanocomposite containing just 10% of MoS_2 exhibited the highest performance with a maximum energy density of 28.8 Wh/Kg at a current density of 0.5 A/g. This material was then assembled as an electric double layer capacitor in a button cell. To obtain maximum performance, different types of electrolyte solution were tested using the button cell. 0.5 M K_2SO_4 electrolyte which has smaller ions sizes with maximum access to the active electrode sites displayed a higher performance among all the electrolytes with a maximum capacitance and energy density of 10.1 F/g and 4.5 Wh/Kg respectively. These values were further heightened just by the usage of a higher molarity electrolyte solution. Since the solubility of K_2SO_4 was limited, the tests were performed with other two electrolyte solutions, among which Na_2SO_4 displayed up to 50% increase in capacitance and energy density.

5.6 References

5.1 Matteo Atzori, Flavia Artizzu, Elisa Sessini, Luciano Marchiò, Danilo Loche, Angela Serpe, Paola Deplano, Giorgio Concas, Flavia Pop, Narcis Avarvari, Maria Laura Mercuri, "Halogen-Bonding in a New Family of tris(haloanilato)metallate(III) Magnetic Molecular Building Blocks", J. Name., 00, 1-3 (2012).

5.2 Zhang. H, Lu. S. B, Zheng. J, Du. J, Wen. S. C, Tang. D. Y, Loh. K.P, "Molybdenum disulfide (MoS_2) as a broadband saturable absorber for ultra-fast photonics", Opt. Express, 22, 7249-7260 (2014).

5.3 Jia Mei Soon, Kian Ping Loh, "Electrochemical Double-Layer Capacitance of MoS2 Nanowall Films", Electrochem. Solid-State Lett, 10 (11), A250−A254 (2007).

5.4 Chen. J, Kuriyama. N, Yuan. H, Takeshita. H. T, Sakai. T, "Electrochemical hydrogen storage in MoS2 nanotubes", J. Am. Chem. Soc., 123, 11813-11814 (2001).

5.5 Umar Khan, Arlene O'Neill, Mustafa Lotya, Sukanta De, Jonathan N. Coleman, "High-Concentration Solvent Exfoliation of Graphene", Small, 6, 864 (2010).

5.6 Karthikeyan. K, Amaresh. S, Aravindan. V, Lee. Y. S, "Microwave assisted green synthesis of MgO–carbon nanotube composites as electrode material for high power and energy density supercapacitors", J. Mater. Chem. A, 1, 4105 (2013).

5.7 Sungjin Park, Jinho An, Richard D. Piner, Inhwa Jung, Dongxing Yang, Aruna Velamakanni, SonBinh T. Nguyen, Rodney S. Ruoff, "Aqueous Suspension and Characterization of Chemically Modified Graphene Sheets", Chem Mater., 20,6592 (2008).

5.8 Yanwu Zhu, Shanthi Murali, Meryl D. Stoller, Aruna Velamakanni, Richard D. Piner, Rodney S. Ruoff, "Microwave assisted exfoliation and reduction of graphite oxide for ultracapacitors", Carbon, 48, 2118-2122 (2010).

5.9 Manas Mandal, Debasis Ghosh, Swinderjeet Singh Kalra, Chapal Kumar Das, "High Performance Supercapacitor Electrode Material based on Flower like MoS2/Reduced Graphene Oxide Nanocomposite", International Journal of Latest Research in Science and Technology, 3 (3), 65-69 (2014).

5.10 Mukkannan Azhagurajan, Tetsuya Kajita, Takashi Itoh, Youn-Geun Kim, Kingo Itaya, "In Situ Visualization of Lithium Ion Intercalation into MoS_2 Single Crystals using Differential Optical Microscopy with Atomic Layer Resolution", J. Am. Chem. Soc., 138 (10), 3355–3361 (2016).

5.11 Jiayu Wan, Steven D. Lacey, Jiaqi Dai, Wenzhong Bao, Michael S. Fuhrer, Liangbing Hu, "Tuning two-dimensional nanomaterials by intercalation: materials, properties and applications", Chem. Soc. Rev., 45, 6742 (2016).

5.12 Hongtao Liu, Guoyi Zhu, "The electrochemical capacitance of nanoporous carbons in aqueous and ionic liquids" J. Power Sources, 171, 1054 (2007).

5.13 Bin Xu, Feng Wu, Renjie Chen, Gaoping Cao, Shi Chen, Guoqing Wang, Yusheng Yang, "Room temperature molten salt as electrolyte for carbon nanotube-based electric double layer capacitors", J. Power Sources, 158, 773 (2006).

5.14 Ping Liu, Mark Verbrugge, Souren Soukiazian, "Influence of temperature and electrolyte on the performance of activated-carbon supercapacitors", J. Power Sources, 156, 712 (2006).

5.15 Lihong Wang, Takahiro Morishita, Masahiro Toyoda, Michio Inagaki, "Asymmetric electric double layer capacitors using carbon electrodes with different pore size distributions", Electrochim. Acta, 53, 882 (2007).

5.16 Cheol-Min Yang, Yong-Jung Kim, Morinobu Endo, Hirofumi Kanoh, Masako Yudasaka, Sumio Iijima, Katsumi Kaneko, "Nanowindow-Regulated Specific Capacitance of Supercapacitor Electrodes of Single-Wall Carbon Nanohorns", J. Am. Chem. Soc., 129, 20 (2007).

5.17 Vix-Guterl. C, Saadallah. S, Jurewicz. K, Frackowiak. E, Reda. M, Parmentier. J, Patarin. J, Beguin. F, "Supercapacitor electrodes from new ordered porous carbon materials obtained by a templating procedure, Mater. Sci. Eng. B, 108, 148 (2004).

5.18 Qu. Q. T, Wang. B, Yang. L.C, Shi. Y, Tian. S, Wu. Y. P, "Study on electrochemical performance of activated carbon in aqueous Li2SO4, Na2SO4 and K2SO4 electrolytes", Electrochemistry Communications, 10, 1652–1655 (2008).

5.19 Bichat. M. P, Raymundo-Pin˜ero. E, Be´guin. F, "High voltage supercapacitor built with seaweed carbons in neutral aqueous electrolyte", Carbon, 48, 4351–4361 (2010).

5.20 Demarconnay. L, Raymundo-Pin˜ero. E, Be´guin. F, "A symmetric carbon/carbon supercapacitor operating at 1.6 V by using a neutral aqueous solution", Electrochem. Commun., 12, 1275–1278 (2010).

5.21 Siheng Li, Li Qi, Lehui Lu, Hongyu Wang, "Facile preparation and performance of mesoporous manganese oxide for supercapacitors utilizing neutral aqueous electrolytes", RSC Adv., 2, 3298–3308 (2012).

6.   Chapter 6: Assembly and Testing of Flexible Supercapacitors

6.1   Pouch Cell Supercapacitor

The necessity and need for developing wearable electronics is a high motivation to develop next generation high performance flexible energy storage devices. Because of the simple processing methods and the ease of production at large scale, supercapacitor based flexible devices is most promising. The main challenge of a flexible storage device is its low energy density. In order to explore if our materials can address this issue, annealed carbon (AC) and annealed carbon/MoS_2 nanocomposite (MCG 1.9) based flexible supercapacitors were prepared using flexible pouch cell as shown in Figure 6.1 (a) and (b).

(a)   (b)

Figure 6.1: (a), (b) MCG 1.9 composite electrode based pouch cell supercapacitor

The AC and the MCG 1.9 materials were synthesized as explained in Chapter 5. In order to fabricate supercapacitor as a flexible device, thin stainless sheets were used as current collector for the materials. So, AC and MCG 1.9 nanocomposite materials were coated on to these thin

and flexible stainless sheets using screen printing technique. Screen printing helps in attaining uniform thickness with almost the same weight and thickness each time the samples are prepared. After screen printing, the stainless steel sheets with the materials were dried at 100°C for 1 hour and later annealed at 350°C. Each pair of electrodes having the respective inks was assembled in a pouch cell with Celgard membrane acting as the separator and 1M Na_2SO_4 as the electrolyte solution.

To our knowledge this is the first time a cheap and novel carbon ink based flexible supercapacitor is proposed. Although, a maximum current density at which the MCG 1.9 and AC based supercapacitor could be charged/discharged was only 3 and 2.5 A/g respectively as seen in Table 9. But still a maximum capacitance of 19.9 F/g and 10 F/g were attained at a current density of 0.5 A/g for MCG 1.9 and AC based flexible pouch cell supercapacitor respectively as shown in Figure 6.2 (a). A calculated maximum energy density of 11.05 Wh/Kg and 8.8 Wh/Kg, respectively for MCG 1.9 and AC based flexible pouch cell supercapacitors was also obtained at a current density of 0.5 A/g as can be seen in Figure 6.2 (b). These flexible devices have an overall better performance compared to button cell based supercapacitor because of the fact that the active materials were coated as thin sheets using screen printing method. This allows the network fibers in the nancomposite material to be aligned in a linear fashion where the electrons are able to mobilize faster with strong Van Der Waals forces. Moreover, the electrolyte solution will be able to cover more active sites of the thin materials.

Table 9: Comparison of different parameters tested using MCG 1.9 nanocomposite and AC electrode flexible supercapacitor with aqueous electrolyte

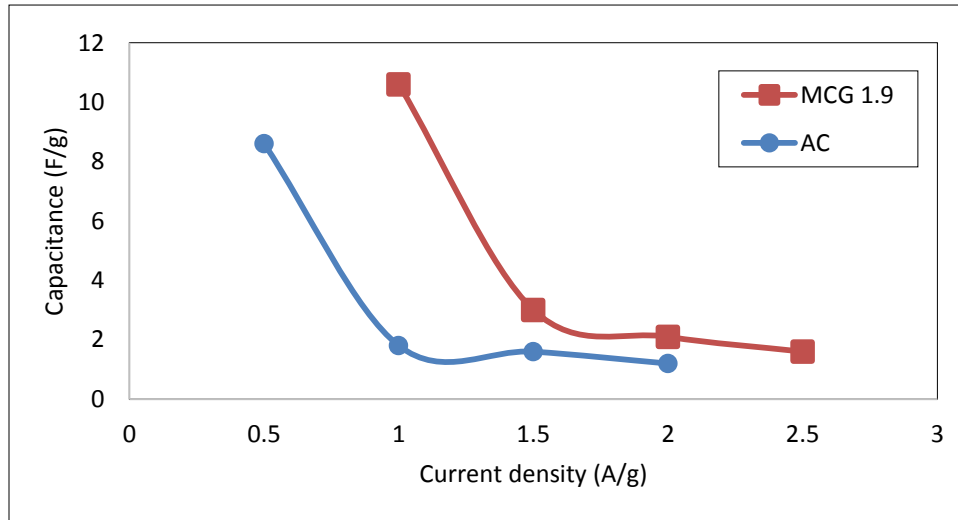|	Maximum Voltage	Maximum Current density (A/g)	Maximum Capacitance (F/g)	Maximum Energy density (Wh/Kg)	Maximum Power density (W/Kg)
MCG 1.9	2 V	3	19.9	11.05	6400
AC	2.5 V	2.5	10	8.68	3820
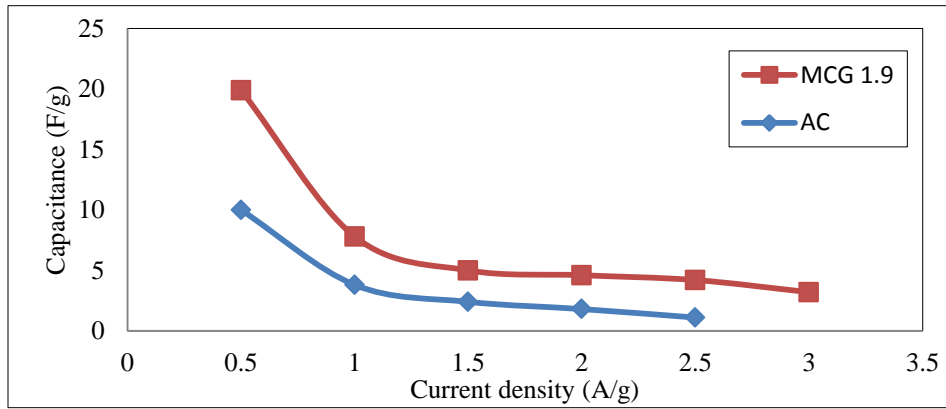
(a)
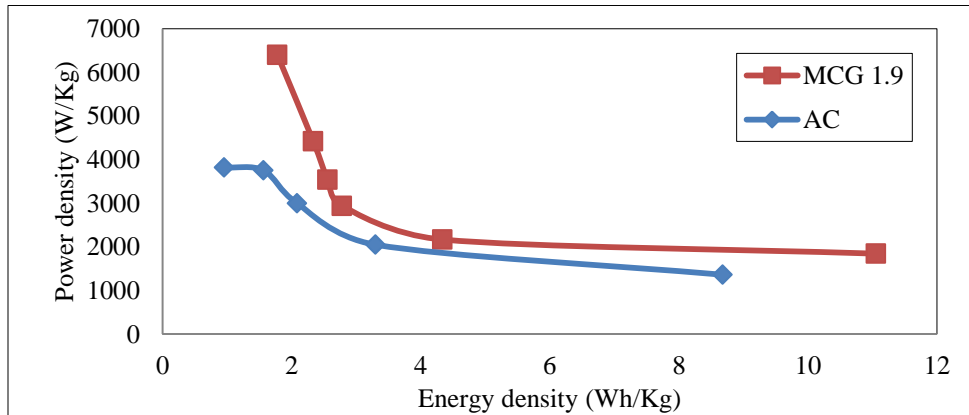
(b)

Figure 6.2: (a) Specific capacitance and (b) Ragone plot of MCG 1.9 nanocomposite and AC electrode flexible supercapacitor with aqueous electrolyte

In most of the works, performance of the supercapacitor has been mainly dependent on geometry of the electrode materials [6.1]. But, in our work here, we have proved that the electrolyte solution also plays a crucial role and helps in significant improvement in performance of the supercapacitor. Aqueous electrolytes have various advantages such as they are inexpensive, non-flammable, have higher ionic conductivity [6.2-6.4]. However, these electrolyte solutions pose the threat of leakage, crystallization, and release of hazardous byproducts into the environment. So recently, solid electrolytes have attracted a lot of attention that replaces the separator and aqueous electrolyte in the flexible supercapacitor [6.5-6.8]. Now that we were able to successfully assemble and test a flexible supercapacitor with aqueous electrolyte, the further exploration was made by synthesizing a gel electrolyte as reported by Zang et.al., [6.9] to fabricate a solid state supercapacitor. In brief, 3g of polyvinyl alcohol (PVA) was mixed in 30ml deionized (DI) water and stirred for 1 hour at 90°C. 2g of phosphoric acid (H_3PO_4) was added to the mixture and stirred for about 10minutes and then cooled down to room temperature. The solution was then poured on a Teflon surface and dried at room temperature overnight. The fabrication of the solid-state supercapacitor was done by manually pressing the pair of respective AC and MCG 1.9 electrodes with the dried gel electrolyte between them at 60°C for 3 hours.

Figure 6.3 (a) shows the comparison of MCG 1.9 and AC electrode based solid state supercapacitors with specific capacitance at different current densities. It can be seen that the MCG 1.9 nanocomposite based supercapacitor has a higher capacitance value of 10.6 F/g at 1 A/g current density. Whereas, the AC based supercapacitor exhibits only 1.8 F/g at 1 A/g current density. We know that energy density is directly proportional to capacitance. So the calculated energy density of MCG 1.9 is also higher than that of AC based supercapacitor with 10.6 and 1.8 Wh/Kg at 1 A/g, respectively, as shown in Figure 6.3 (b). Apart from an improved performance

97

of MCG 1.9 nanocomposite based supercapacitor in terms of capacitance and energy density, the current density at which it can charge/discharge is also higher (2.5 A/g) as can be seen in Table 10. The overall performance of the device has been enhanced by not compromising much on the power density and the operating voltage.
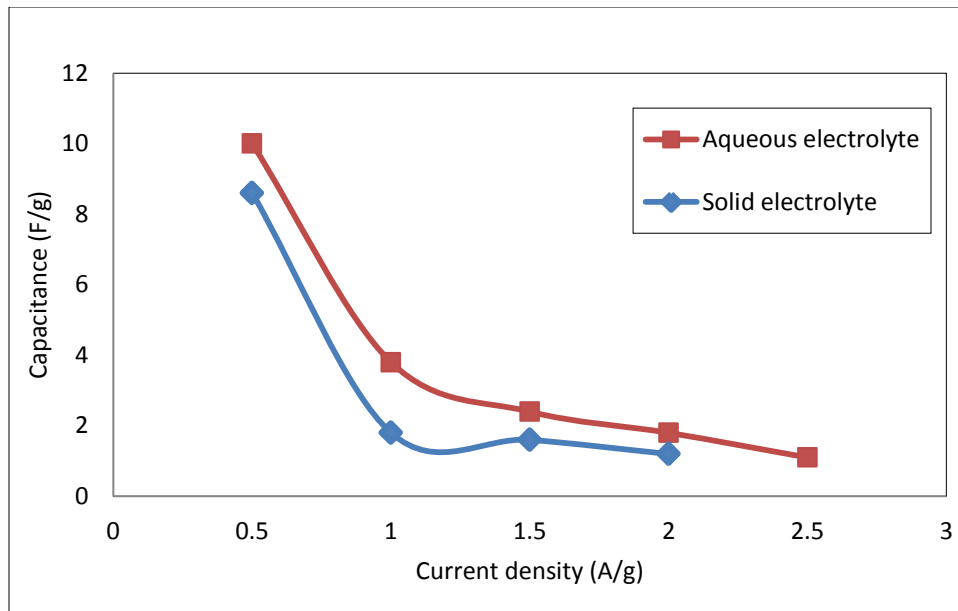

(a)
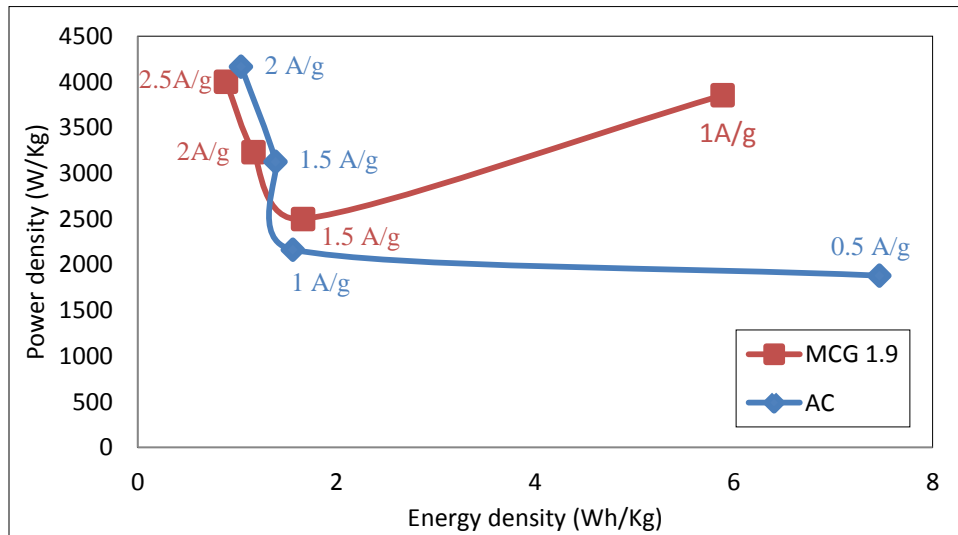
(b)

Figure 6.3: (a) Specific capacitance and (b) Ragone plot of MCG 1.9 nanocomposite and AC electrode as a solid state supercapacitor using PVA-H_3PO_4 solid electrolyte
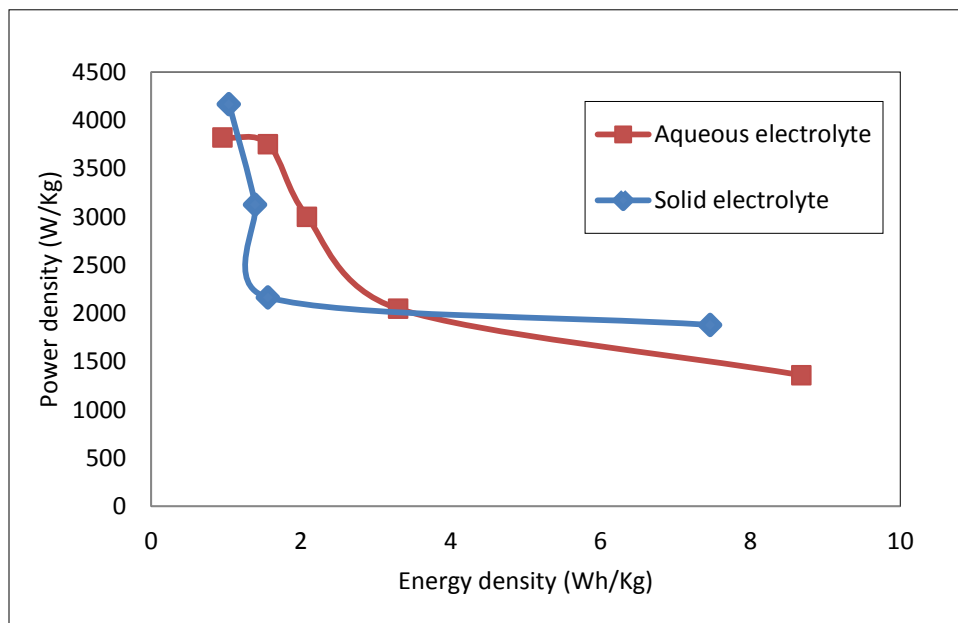
Table 10: Comparison of MCG 1.9 nanocomposite and AC electrode as a solid state supercapacitor using PVA-H$_3$PO$_4$ solid electrolyte

	Maximum Voltage	Maximum Current density (A/g)	Maximum Capacitance (F/g)	Maximum Energy density (Wh/Kg)	Maximum Power density (W/Kg)
MCG 1.9	2 V	2.5	10.6 at 1 A/g	5.9 at 1 A/g	4000
AC	2.5 V	2	1.8 at 1 A/g	1.5 at 1 A/g	4166

As mentioned earlier, there are a few advantages of using solid electrolyte by replacing the separator membrane and the aqueous electrolyte solution. But these advantages cannot be overlooked when it comes to the overall performance of the device. The following results show the comparison of MCG 1.9 nanocomposite and AC electrode based supercapacitor with aqueous and solid state electrolytes. As can be seen in Figure 6.4 (a), the capacitance of AC electrode based supercapacitor is less at all current densities. Similarly, the energy and power density are also significantly less as can be observed in Figure 6.4 (b). In addition, the current density at which the supercapacitor can be charged/discharged is also lower while using solid electrolyte. A similar kind of behavior with a significant difference in capacitance, energy and power density can also be observed while comparing the MCG 1.9 based supercapacitor with both kinds of electrolytes. Even with this electrode, the current density at which the solid electrolyte based supercapacitor can be charged/discharged is lower as shown in Figure 6.5 (a) and (b).
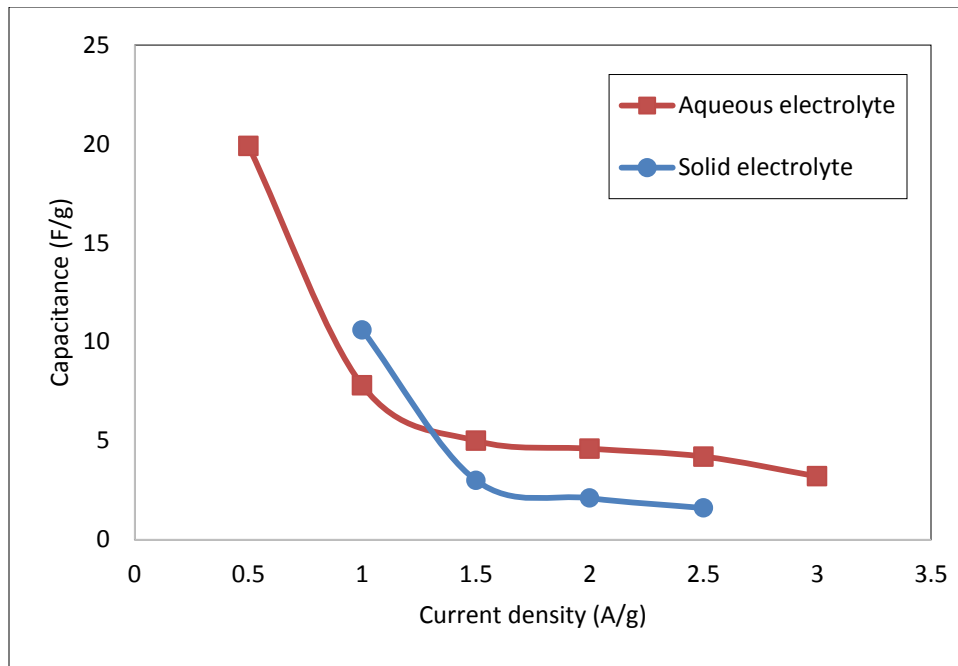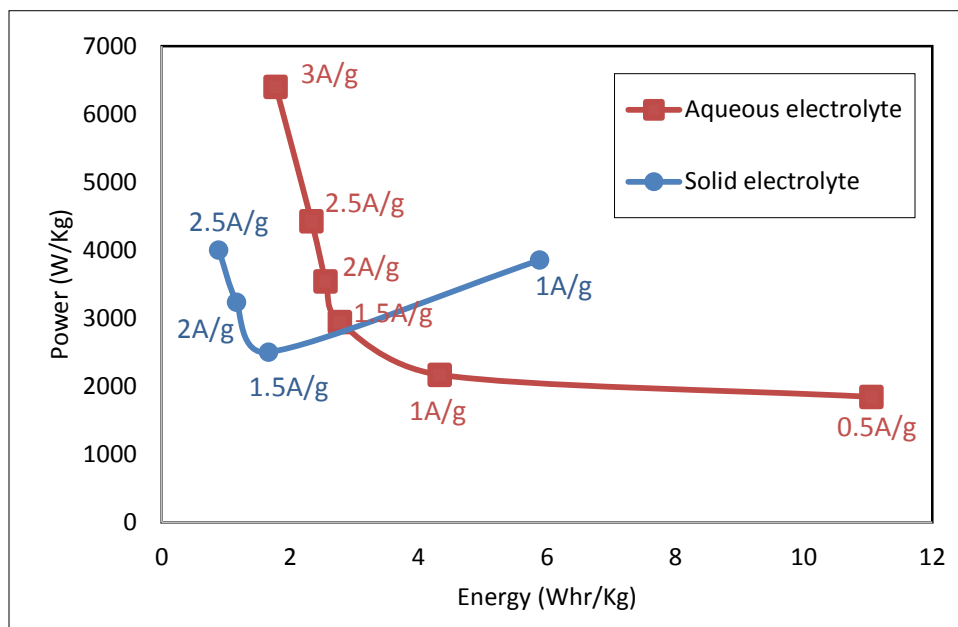
(a)

(b)

Figure 6.4: Comparison of (a) Specific capacitance and (b) Ragone plot of AC electrode between aqueous and solid electrolyte

(a)

(b)

Figure 6.5: Comparison of (a) Specific capacitance and (b) Ragone plot of MCG 1.9
nanocomposite between aqueous and solid electrolyte

6.2   Cylindrical Cell Supercapacitor

Currently, most of the primary and secondary batteries are packaged in the form of a cylindrical cell. The main advantages of using a cylindrical cell is that without deforming it can withstand high internal pressures and has good mechanical stability [6.10]. The basic design of the cell as shown in Figure 6.6 (a) has a cylindrical membrane at the bottom with a sealant cap at the top. The AC and MCG 1.9 nanocomposite based electrodes were prepared by screen printing the respective inks over a thin 12 inch stainless steel sheets. These sheets were then dried at 100°C for 1 hour and later annealed at 350°C. Pair of these 12 inch sheets was assembled with a Celgard membrane in between them and were rolled manually as shown in Figure 6.6 (b) to fit in the cylindrical cell. The positive and negative connections were made from each of the sheets and were pressure sealed with 1 M Na_2SO_4 electrolyte solution.
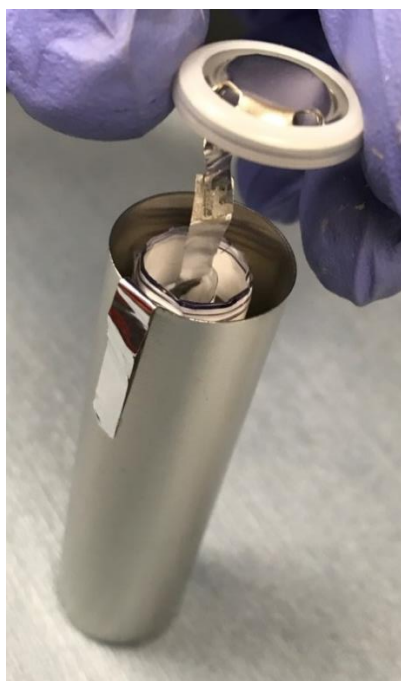

(a)   (b)

Figure 6.6: (a), (b) MCG 1.9 composite electrode based cylindrical cell supercapacitor

Observing the diminished performance of pouch cell based supercapacitor with solid electrolyte, the cylindrical cell supercapacitor was tested only with the aqueous electrolyte. A maximum capacitance of 6.7 F/g and 4.3 F/g was obtained with MCG 1.9 and AC electrode based cylindrical supercapacitor, respectively. The overall energy and power density of MCG 1.9 electrode based supercapacitor exhibits an enhanced performance with maximum values of 4.9 Wh/Kg and 5847 W/Kg, respectively. These kinds of behavior, as mentioned previously, is due to high surface area of the nanocomposite material and the synergistic effects the 10 % MoS_2 present in it.
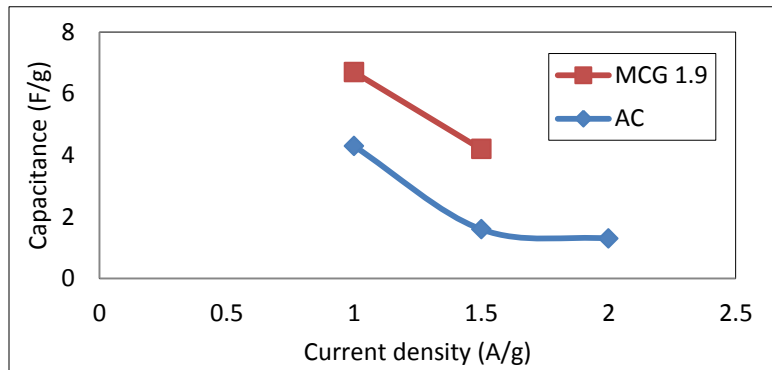
(a)
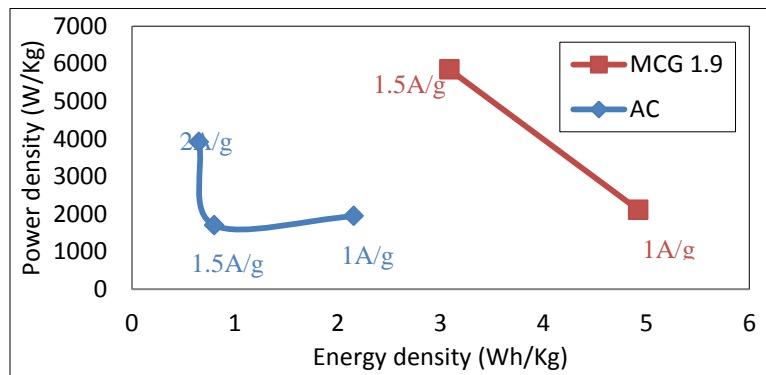
(b)

Figure 6.7: (a) Specific capacitance and (b) Ragone plot of MCG 1.9 nanocomposite and AC electrode as a flexible supercapacitor in cylindrical cell

103

6.3 Summary

In this final chapter, different kinds of flexible supercapacitors were assembled and tested in a pouch cell and cylindrical cell. In the pouch cell, both aqueous and solid electrolytes were used and compared for its performances. It was found that despite the advantages the solid electrolyte comparatively, aqueous electrolyte based supercapacitor showed the best performance with maximum capacitance and energy density of 7.8 F/g and 4.3 Wh/Kg, respectively at a current density of 1 A/g. Finally, the cylindrical cell supercapacitor was tested using the high performance nanocomposite and electrolyte solution on a rolled 12 inch stainless steel flexible sheets which exhibited a maximum capacitance and energy density of 6.7 F/g and 5 Wh/Kg respectively, at a current density of 1 A/g.

6.4 References

6.1 Yanwu Zhu, Shanthi Murali, Meryl D. Stoller, K. J. Ganesh, Weiwei Cai, Paulo J. Ferreira, Adam Pirkle, Robert M. Wallace, Katie A. Cychosz, Matthias Thommes, Dong Su, Eric A. Stach, Rodney S. Ruoff, "Carbon-Based Supercapacitors Produced by Activation of Graphene", Science, 2011, 332, 1537–1541.

6.2 Nicklas Blomquist, Thomas Wells, Britta Andres, Joakim Bäckström, Sven Forsberg, Håkan Olin, "Metal-free supercapacitor with aqueous electrolyte and low-cost carbon materials", Nature, 7:39836 (2017).

6.3 Andrew Burke, *"Ultracapacitors: why, how, and where is the technology",* Journal of power sources, 91, 37–50 (2000).

6.4 François Béguin, Volker Presser, Andrea Balducci, Elzbieta Frackowiak, *"Carbons and electrolytes for advanced supercapacitors",* Advanced Materials, 26, 2219–2251 (2014).

6.5 Chun Huang, Jin Zhang, Neil P. Young, Henry J. Snaith, Patrick S. Grant, *"Solid-state supercapacitors with rationally designed heterogeneous electrodes fabricated by large area spray processing for wearable energy storage applications",* Scientific Reports, 6, 25684 (2016).

6.6 Xihong Lu, Minghao Yu, Gongming Wang, Yexiang Tong, Yat Li, "Flexible solid-state supercapacitors: design, fabrication and applications", Energy Environ. Sci., 7, 2160–2181 (2014).

6.7 Gengzhi Sun, Xiao Zhang, Rongzhou Lin, Jian Yang, Hua Zhang, Peng Chen, "Hybrid fibers made of molybdenum disulfide, reduced graphene oxide, and multi-walled carbon nanotubes for solid-state, flexible, asymmetric supercapacitors", Angewandte Chemie Int. Ed., 127, 4734–4739 (2015).

6.8 Linlin Li, Shengjie Peng, Hao Bin Wu, Le Yu, Srinivasan Madhavi, Xiong Wen (David) Lou, "A flexible quasi-solid-state asymmetric electrochemical capacitor based on hierarchical porous V2O5 nanosheets on carbon nanofibers", Adv. Energy Mater., 5, 1500753 (2015).

6.9 Jianfeng Zang, Changyong Cao, Yaying Feng, Jie Liu, Xuanhe Zhao, "Stretchable and High-Performance Supercapacitors with Crumpled Graphene Papers", Nature, 7:6492 (2014).

6.10 http://batteryuniversity.com/learn/article/types_of_battery_cells.

7. Chapter 7: Conclusions and Future Work

7.1 Contribution of this work

The research work carried out in this dissertation focused on synthesis of nanocomposite materials and electrochemical characterization of the supercapacitor devices with these electrodes along with the effects of various electrolytes on the supercapacitor performance. Proper selection of electrode materials and electrolyte solutions are very significant for improvement in performance of the device. Also, a brief study on the usage of solid electrolyte has been explored that would help in fabrication of state-of-the art flexible solid-state supercapacitor.

One of our objectives was to simplify the fabrication of electrodes for the supercapacitors. Initially, a 2-D MoS_2/rGO nanocomposite was prepared using solution process method. MoS_2, having structure and properties similar to graphene, was exfoliated using hydrothermal process and mixed along with rGO. The inclusion of MoS_2 leads to an increase in surface area of the material therefore resulting in fast ion charge transfer within the material. A button cell based supercapacitor assembled and tested using the MoS_2/rGO nanocomposite exhibited an improved performance in terms of capacitance and energy density when compared to using just the rGO. Since this button cell supercapacitor showed some promising results, it provided motivation to further improve the performance of the device. Proceeding forward, a cheap and low resistance carbon ink based annealed carbon (AC) was mixed along with MoS_2 at different ratios of 10%, 20% and 30%. Careful testing of these materials using three-electrode method provided basic information that the nanocomposite with just 10% MoS_2 exhibited the highest capacitance and energy density among them. Further addition of MoS_2 resulted in restacking of materials and weak Van der Waals forces, hindering the fast ion transfer, thereby leading to degradation in

performance. Although the electrode materials contribute to major portion of the supercapacitor performance, the electrolyte solution also plays an important role.

So button cell based supercapacitors were assembled with the highest performance nanocomposite and tested with different neutral electrolyte solutions (0.5 M Li_2SO_4, Na_2SO_4 and K_2SO_4). The electrolytes have ionic radius increasing in the order of K+ (3.31 Å), Na+ (3.58 Å) and Li+ (3.82 Å) which contributes to different migration speeds and charge densities. The supercapacitor having the smallest ionic radius (K+) electrolyte solution and having access to most active sites of the active material showed the maximum capacitance and energy density. This result was further enhanced just by increasing the concentration of the electrolyte solution. But due to insolubility of K_2SO_4, the other two electrolytes were tested among which 1 M Na_2SO_4 exhibited the improved capacitance and energy density.

With an increasing demand for cheap, lightweight and flexible energy storage devices, pouch cell based supercapacitors were assembled with this highest performance nanocomposite and small ionic radius electrolyte solution. The electrodes were prepared by coating the nanocomposite material over 1X1 inch thin and flexible stainless steel sheets using screen printing technique. Aqueous 1 M Na_2SO_4 and PVP-H_3PO_4 solid electrolytes were used during the assembly of pouch cell supercapacitors. In spite of physical advantages of solid-state supercapacitor, aqueous electrolyte based supercapacitor produced better performances in terms of capacitance and energy density. The cylindrical cell supercapacitors were prepared by coating the active material over 6X2 inch stainless steel sheets and assembled with Celgard membrane and 1 M Na_2SO_4 aqueous electrolyte solution. The overall performance of the cylindrical cell supercapacitor was similar to that of the pouch cell supercapacitor.

The three major contributions of this work are

1. A facile method to synthesize an annealed carbon/MoS_2 nanocomposite for use as supercapacitor electrodes was successfully demonstrated. The nanocomposite electrode material yielded a capacitance and energy density of 207.5 F/g and 28.8 Wh/Kg, respectively, at a current density of 0.5 A/g using three-electrode method compared to those with just annealed carbon based electrode which yielded a capacitance and energy density of 99.25 F/g and 13.8 Wh/Kg, respectively at the same current density.

2. The overall performance of the supercapacitor was further enhanced up to 50% with a capacitance and energy density of 15.2 F/g and 8.4 Wh/Kg, respectively, at a current density of 1 A/g by increasing the concentration of the electrolyte from 0.5 M to 1 M.

3. Solid state supercapacitors using this annealed carbon/MoS_2 and solid electrolyte were demonstrated with significant performance having capacitance and energy density of 10.6 F/g and 5.9 Wh/Kg, respectively, at a current density of 1 A/g. These performance data were comparable to supercapacitor with aqueous electrolyte.

7.2   Future work

This work has been mainly dealt only with MoS_2/carbon based nanocomposite for supercapacitor application. Initially, a complex and time consuming process was followed for synthesis of the material and eventually some cheaper carbon based material was found and the process followed to synthesis the material was also greatly reduced. There are a lot other 2-D materials like ruthenium oxide, tungsten sulfide, black phosphorus that can be integrated along with carbon based material and tested for its performance as a supercapacitor.

When making thin sheets, the thickness aspect ratio of the active material is very important. So a process to create even thin films sheets can be designed which will help in improving the performance of the device and also have consistent results repeatedly. The annealed carbon/MoS_2 nanocomposite based supercapacitors have been tested using various neutral electrolyte solutions.. So it is natural for to precede the work further in this direction and explore the effects of other organic and inorganic electrolytes with even smaller ionic radius. In addition, apart from the only type of solid electrolyte reported in this work can be expanded even more. A solid state supercapacitor with different combinations of solid electrolytes can also be synthesized, tested and the capacitance and energy density of the supercapacitor can be improved.

Appendix A: Intellectual Property

1. Carbon paste based Annealed carbon
2. Annealed carbon/MoS_2 nanocomposite
3. Screen printing of carbon paste and Nanocomposite
4. Flexible nanocomposite based supercapacitor

Appendix B: All equipment used for Research purpose

1.   Equipment: Gamry Reference 600
      Location: ENRC 4607
      Owner: University of Arkansas
2.   Equipment: Dell Laptop
      Location: ENRC 4607
      Owner: Anishkumar
3.   Equipment: RIGAKU miniflex X-ray diffractometer
      Location: ENRC 4607
      Owner: University of Arkansas
4.   Equipment: FEI XL-30 ESEM
      Location: NANO 125
      Owner: University of Arknsas
5.   Equipment: RFT-6000 Raman spectrometer
      Location: ENRC 2933
      Owner: University of Arknasas